이학박사학위논문

FcγRIIb variant 2와 Lyn이 알츠하이머병의 아밀로이드 베타 신경독성에 관여하는 기전 연구

Studies on the effects of FcγRIIb variant 2 and Lyn on amyloid-beta neurotoxicity in Alzheimer's disease

2017 년 2 월

서울대학교 대학원

생명과학부

권 영 대

ABSTRCT

Studies on the effects of FcγRIIb variant 2 and Lyn on amyloid-beta neurotoxicity in Alzheimer's disease

Youngdae Gwon

School of Biological Sciences

The Graduate School

Seoul National University

Amyloid beta (Aβ) is the major component of the extracellular senile plaque, a pathological hallmark seen in the brain of Alzheimer's disease (AD) patients, and gives a toxic edge to neuron in several ways. Some membrane proteins have been suggested to be Aβ receptors sine they bind to soluble Aβ and trigger neurotoxic pathway. Fcγ-receptor IIb (FcγRIIb) serves as a receptor for soluble Aβ oligomer. Genetic deletion of FcγRIIb ameliorates neuronal death and LTP impairment induced by Aβ oligomer and rescues memory deficits seen in

PDAPP AD mouse model. Recently, it is reported that alteration of phosphoinositide metabolism elicited by Aβ-FcγRIIb interaction is responsible for the hyperphosphorylation of tau and memory impairment in 3x Tg-AD mouse model. Here, I demonstrate another mechanistic study supporting the pathogenic role of FcγRIIb in AD through neuronal internalization of Aβ. In addition, I identify the role of Lyn in mediating phosphorylation of FcγRIIb under Aβ exposure and propose the protective effect of a putative Lyn inhibitor isolated by virtual screening.

Intraneuronal Aβ is characterized in the brain of early-phase AD patients. Some AD mouse models with intensive intraneuronal Aβ even manifest memory loss without extracellular amyloid deposits. Further, the propagation of pathogenic Aβ between neurons is linked to accumulation of Aβ in neuron. However, molecular mediator to be in charge of neuronal Aβ accumulation and its propagation to adjacent neuron is unclear. In chapter I, I demonstrate the role of FcγRIIb2 variant in neuronal uptake and interneuronal spreading of pathogenic Aβ. Neuronal uptake of oligomeric $A\beta_{1-42}$ was reduced in *Fcgr2b* knockout neurons compared to WT neuron. In 3x Tg-AD mouse model, both intraneuronal and soluble $A\beta_{1-42}$ were diminished by loss-of-function of FcγRIIb. Moreover, memory deficits were alleviated by forebrain-specific expression of Aβ-uptake-defective *Fcgr2b* mutant in 3xTg-AD mice. I

also found that enriched expression of transcription variant 2 of FcγRIIb (FcγRIIb2) in neuron is associated with elevated uptake of Aβ. *Target of Myb1* (TOM1) isolated from functional screening bind to FcγRIIb2 and suppress FcγRIIb2-mediated Aβ internalization. Accelerated uptake of Aβ via FcγRIIb2 leads to cytoplasmic and mitochondrial accumulation of Aβ over endocytic compartments and causes neurotoxicity. Finally, blockade of propagation of intraneuronal Aβ to connected neuron by *Fcgr2b* KO is analyzed by using microfluidic devices. To sum up, I demonstrate a novel function of FcγRIIb2 variant in the pathogenesis of AD by regulating intraneuronal Aβ.

Lyn is originally considered to be a member of Src-family tyrosine kinase and take a role in inhibiting immune cells to phosphorylate immune complex binding proteins, including FcγRIIb. However, its association to Aβ-FcγRIIb signaling in neuron is uncertain. In Chapter II, I demonstrate that Lyn is critical for $A\beta_{1-42}$-mediated neurotoxicity by phosphorylating FcγRIIb. $A\beta_{1-42}$ oligomer activated Lyn and further induced the tyrosine phosphorylation of FcγRIIb in neuronal cells. Interestingly, both $A\beta_{1-42}$-initiated FcγRIIb phosphorylation and cell death were reduced by knockdown of Lyn in neuronal cells. A small molecule KICG2576, a putative ATP-competitive inhibitor of Lyn was isolated from virtual screening. Binding of KICG2576 to the cleft between the two lobes of Lyn kinase domain was verified by co-crystal structure.

Whereas Aβ-induced FcγRIIb phosphorylation was attenuated by KICG2576, Aβ- or FcγRIIb-induced neuronal cell death were also suppressed. $A\beta_{1-42}$-induced memory impairment determined by Y-maze and novel object recognition tests were also diminished by intracerebroventricularly injected KICG2675. Finally, I confirmed the activation of Lyn in the brain of AD patients compared to non-AD controls. Taken together, Lyn plays an essential role in Aβ–mediated neurotoxicity, providing detailed understanding of Aβ- FcγRIIb neurotoxic pathway in AD pathogenesis.

Key Words: Alzheimer's disease, Amyloid beta, Intraneuronal Aβ, Propagation of pathogenic proteins, FcγRIIb2, TOM1, Lyn

Student Number: 2009-20322

CONTENTS

LIST OF FIGURES

ABBREVIATIONS

AD	Alzheimer’s disease
Aβ	Amyloid beta
APP	Amyloid betea precursor protein
NIa	Nuclear inclusion a
RAGE	Receptor for advanced glycation endproduct
LRP1	Low-density lipoprotein receptor-related protein 1
FcγRIIb	Fcγ-receptor IIb
mAβ	Aβ monomer
oAβ	Aβ oligomer
ED	Extracellular domain
Tg	Transgenic
IHC	Immunohistochemistry
APP-CTFα	APP C-terminal fragment α
APP-CTFβ	APP C-terminal fragment β
AICD	APP intracellular domain

SYP	Synaptophysin
NSE	Neuron-specific endolase
FcγRIIb2	FcγRIIb transcription variant 2
TOM1	Target of Myb 1
RT-PCR	Reverse transcription-polymerase chain reaction
LTP	Long-term potentiation
WT	Wild-type
KO	Knockout
ITIM	Immunoreceptor tyrosine-based inhibitory motif
Tyr	Tyrosine
FBS	Fetal bovine Serum
PMSF	Phenylmethylsulfonyl fluoride
PAGE	Polyacrylamide gel electrophoresis

CHAPTER I

Aberrant role of FcγRIIb2 variant in the propagation and pathogenesis of intracellular Aβ in Alzheimer's disease

Abstract

Intraneuronal Aβ accumulation correlates with the onset of Alzheimer's disease (AD) and is potentially linked to the propagation of pathogenic Aβ through neurons. However, critical mediator associated with AD pathology needs to be clarified. Here, I report that FcγRIIb2 variant functions in neuronal uptake and interneuronal spreading of pathogenic Aβ. Accumulation of oligomeric $A\beta_{1\text{-}42}$, not monomeric $A\beta_{1\text{-}42}$ or oligomeric $A\beta_{1\text{-}40}$, was blocked by *Fcgr2b* knockout in neurons. $A\beta_{1\text{-}42}$ internalization was dependent on the di-leucine motif of FcγRIIb2 and attenuated by TOM1, a FcγRIIb2-binding protein. Cytosolic accumulation of Aβ, including mitochondria, via endocytic compartments caused neurotoxicity. Moreover, neuronal accumulation of Aβ and memory deficits were simultaneously ameliorated by interfering Aβ-FcγRIIb2 interaction and by forebrain-specific expression of Aβ-uptake-defective *Fcgr2b* mutant in 3xTg-AD mice. In addition, Aβ propagation to connected neurons occurs through FcγRIIb2. Our findings reveal a novel role of FcγRIIb2 responsible for the pathogenesis and propagation of intracellular Aβ in AD.

Introduction

Alzheimer's disease (AD) is the most frequent type of senile dementia with symptoms of cognitive decline and memory loss. Accumulation of amyloid-β (Aβ) in the forebrain is the most prominent feature of AD, and Aβ production is accelerated by familial AD mutations in amyloid-β precursor protein *(*APP) and presenilin *1* and *2* genes (Querfurth and LaFerla, 2010). Although the extracellular amyloid deposition mainly composed of Aβ was regarded as the key feature of AD in the past, mounting evidences have shown that intraneuronal Aβ plays a key role in neurotoxicity. The presence of intraneuronal Aβ precedes the build-up of extracellular amyloid plaques in individuals with mild cognitive impairment and AD (LaFerla et al., 2007). In many AD mouse models, intraneuronal Aβ strongly correlates with the onset of memory impairment, sometimes even without extracellular Aβ load (Billings et al., 2005; Eimer and Vassar, 2013; Tomiyama et al., 2010). Moreover, AD-like neuronal defects are ameliorated by the modulation of intraneuronal Aβ-degrading enzymes, such as neprilysin, endothelin-converting enzymes, and nuclear inclusion a (NIa) (Marr et al., 2003; Pacheco-Quinto and Eckman, 2013; Shin et al., 2014).

Aβ is generated by a sequential cleavage of APP by β-secretase 1 and γ-

secretase complex along the endocytic pathway (Haass et al., 2012). Most cleaved Aβ in the lumen of endocytic compartments is secreted extracellularly and this event is regulated by neuronal activity (Cirrito et al., 2008; Moghekar et al., 2011; Tampellini et al., 2009). Thus, a substantial portion of intraneuronal Aβ is from the re-uptake of secreted Aβ. Receptor for advanced glycation endproduct (RAGE) and low-density lipoprotein receptor-related protein 1 (LRP1) were reported to mediate neuronal uptake of Aβ (Kanekiyo and Bu, 2014; Takuma et al., 2009). However, pathologic impact of RAGE is controversial and is not shown in *in vivo* model (Vodopivec et al., 2009). In addition, internalized Aβ through LRP1 is linked to the clearance pathway rather than the formation of intraneuronal Aβ pool (Kanekiyo et al., 2013). Thus, there is a discrepancy in understanding the deleterious role of intraneuronal Aβ with the current view on Aβ receptors.

Cell-to-cell propagation of misfolded proteins is a common feature over many neurodegenerative diseases (Guo and Lee, 2014). In the case of Aβ, the amyloid deposition extends from the site of exogenous Aβ graft in AD mouse models (Meyer-Luehmann et al., 2006; Ye et al., 2015). Moreover, spreading of Aβ between neurons is accompanied by synaptic dysfunction and neurotoxicity (Domert et al., 2014; Harris et al., 2010). While endocytic pathway may function in interneuronal propagation of Aβ, inhibiting cellular prion protein,

NMDA receptor, or AMPA receptor does not affect Aβ propagation (Nath et al., 2012). Thus, critical mediator responsible for Aβ uptake for neurotoxicity and neuronal transmission is unknown yet. Role of Fcγ-receptor IIb (FcγRIIb) as a Aβ receptor was previously discovered (Kam et al., 2013). While FcγRIIb deficiency ameliorates memory deficits in PDAPP AD mice, the precise manner of neurotoxicity induced by FcγRIIb-Aβ interaction remains to be solved. Here, I determined that the neuronal FcγRIIb2 variant is critical in neuronal uptake of pathogenic Aβ for neurotoxicity and neuronal transmission through the synapse.

Results

FcγRIIb is an essential receptor for neuronal uptake of $A\beta_{1-42}$ oligomers

To quantify intracellular Aβ, I used a subcellular fractionation assay after extracellular Aβ treatment to primary neurons. Consistent with the previous studies (LaFerla et al., 2007; Takuma et al., 2009), Aβ was found largely in the membrane-enclosing organelles, including endocytic compartments, as well as in the cytoplasm and mitochondria (Figure I-1A). Then, monomeric $A\beta_{1-42}$ ($mA\beta_{1-42}$) and oligomeric $A\beta_{1-42}$ ($oA\beta_{1-42}$) were prepared and assessed for their internalization into primary neurons and astrocytes (Figure I-1B). Interestingly, $oA\beta_{1-42}$ was preferentially internalized into primary neurons, while $mA\beta_{1-42}$ was internalized by primary astrocytes. Consistent with this observation, confocal microscopy showed that FITC-$oA\beta_{1-42}$ and FITC-$mA\beta_{1-42}$ were found mainly inside primary neurons and astrocytes, respectively, when cells were incubated with FITC-labeled $A\beta_{1-42}$ (Figure I-2). These results illustrate that $oA\beta_{1-42}$ is preferentially internalized into primary neurons relative to $mA\beta_{1-42}$.

I then evaluated the relevance of FcγRIIb function in cellular uptake of Aβ species because of the previous report showing that FcγRIIb acts as a receptor for $oA\beta_{1-42}$ in the AD brains (Kam et al., 2013). The results revealed that $oA\beta_{1-42}$ was internalized into WT cortical neurons but not into *Fcgr2b* KO cortical

neurons (Figure I-3A). Similar pattern and level of oAβ_{1-42} uptake were also observed in WT and *Fcgr2b* KO astrocytes. Compared to oAβ_{1-42}, however, mAβ_{1-42} uptake was predominant in primary astrocytes and was not much affected by *Fcgr2b* KO. Consistently, FITC-oAβ_{1-42} internalization was also declined by *Fcgr2b* KO in MAP2b-positive hippocampal neurons, whereas FITC-mAβ_{1-42} was not significantly internalized (Figures I-3B and C). Comparison of the kinetics revealed that oAβ_{1-42} uptake over time was delayed by *Fcgr2b* KO in neurons (Figure I-4); internalized Aβ was detected at 1.5 h after treatment in WT neurons and at 12 h in *Fcgr2b* KO neurons. Moreover, among Aβ species, oligomeric Aβ_{1-40} (oAβ_{1-40}) was not internalized into primary neurons compared to oAβ_{1-42} (Figure I-5A). Furthermore, by utilizing the conditioned media of 7PA2 cells which secrete soluble Aβ oligomers (Walsh et al., 2002), I found that FcγRIIb could internalize Aβ_{1-42}, but not Aβ_{1-40} (Figures I-5B and C). The results suggest that FcγRIIb is crucial for neuronal uptake of oAβ_{1-42} over mAβ_{1-42} or oAβ_{1-40}.

In addition, neuronal uptake of Aβ was blocked by addition of purified FcγRIIb extracellular domain (FcγRIIb-ED) to the culture medium (Figure I-6A). Furthermore, Aβ internalization was enhanced by the overexpression of FcγRIIb or FcγRIIb Ig1 mutant, but not by deletion mutant of FcγRIIb Ig2 domain which was reported to be critical for the interaction with oAβ_{1-42} (Kam

et al., 2013) (Figure I-6B). I thus conducted a virtual screening based on the $A\beta_{1\text{-}42}$ N-terminal stretch that was reported to be important for binding of FcγRIIb to the Ig2 domain (Kam et al., 2013) and isolated small molecules (Figure I-7A). Among them, #1 and #6 were potent inhibitors of the loading of $oA\beta_{1\text{-}42}$ onto FcγRIIb-ED in an *in vitro* binding assay (Figure I-7B) and efficiently competed with the *in vitro* binding of FITC-$oA\beta_{1\text{-}42}$ to FcγRIIb-ED (Figure I-7C). The neuronal uptake and neurotoxicity of $oA\beta_{1\text{-}42}$ were also curtailed by the treatment with #1 or #6 (Figure I-8). Moreover, memory deficits attributed to the intracerebroventricular injection of $oA\beta_{1\text{-}42}$, such as spatial memory (Figure I-9A) and recognition memory (Figure I-9B), were mitigated by the administration of #6. Together, these results illustrate that the binding of $oA\beta_{1\text{-}42}$ to FcγRIIb is required for Aβ internalization and neurotoxicity.

Reduction of neuronal $A\beta_{1\text{-}42}$ in 3x Tg-AD mice by *Fcgr2b* gene deletion

It is known that 3x Tg-AD mouse model displays the early accumulation of intraneuronal Aβ with memory decline prior to extracellular amyloid deposition and neurofibrillary tangle formation (Oddo et al., 2003). To address the role of FcγRIIb in the accumulation of neuronal Aβ in these mice, I examined the presence of neuronal Aβ in the brains of 3x Tg-AD mice and 3x Tg-AD/*Fcgr2b* KO mice at 7 months of age in which 3x Tg-AD mice show impaired memory

function. Immunohistochemistry (IHC) using MOAB-2 antibody, which specifically recognizes Aβ but not APP (Youmans et al., 2012), revealed that Aβ signal was detected in the neurons of the hippocampal CA1 regions of 3x Tg-AD mice but not much in 3x Tg-AD/*Fcgr2b* KO mice (Figure I-10), indicating that the accumulation of neuronal Aβ in 3x Tg-AD mice requires FcγRIIb.

I further analyzed alteration of the overall Aβ levels in the AD mouse model with ELISA. The level of TBS-extracted soluble $A\beta_{1-42}$, but not $A\beta_{1-40}$, was significantly lower in the hippocampus of 3x Tg-AD/*Fcgr2b* KO mice than 3x Tg-AD mice at 7 months of age (Figure I-11A). On the contrary, there was no difference in the levels of guanidine-extracted insoluble $A\beta_{1-40}$ and $A\beta_{1-42}$ between 3x Tg-AD and 3x Tg-AD/*Fcgr2b* KO mice (Figure I-11B). Consequently, the prominent difference in the ratio of $A\beta_{1-42}$ to $A\beta_{1-40}$ between 3x Tg-AD and 3x Tg-AD/*Fcgr2b* KO mice was observed in the soluble fraction (Figure I-11C). I confirmed no differences in the levels of full-length APP, APP C-terminal fragment α (APP-CTFα), APP C-terminal fragment β (APP-CTFβ), and APP intracellular domain (AICD) between 3x Tg-AD and 3x Tg-AD/*Fcgr2b* KO mice (Figure I-12). These results indicate that FcγRIIb KO reduces soluble $A\beta_{1-42}$ in the hippocampus of 3x Tg-AD mice without altering APP processing.

Alleviation of memory deficits in 3x Tg-AD mice by neuron-specific expression of Aβ uptake-defective *Fcgr2b* mutant

Despite *in vivo* alteration in the intraneuronal Aβ by *Fcgr2b* deficiency, it was not certain yet whether Aβ uptake and memory deficits were dependent on the FcγRIIb in neurons. I thus generated transgenic mice expressing *Fcgr2b*-deletion mutant (*Fcgr2b*-CytΔ Tg) only in forebrain neurons under the control of the calcium/calmodulin-dependent protein kinase II alpha subunit (CamKIIα) promoter (Tsai et al., 2010). The *Fcgr2b*-CytΔ mutant consists of the extracellular domain and transmembrane region but lacks the cytoplasmic region of FcγRIIb and is predicted to be defective in Aβ uptake and compete with the endogenous FcγRIIb for binding to Aβ. I confirmed that oA$\beta_{1\text{-}42}$-induced neurotoxicity was reduced by the expression of *Fcgr2b*-CytΔ in HT22 hippocampal cells (Figure I-13A). As expected, the expression of *Fcgr2b*-CytΔ in the Tg mice was restricted to the forebrain regions, including cortex and hippocampus (Figure I-13B).

IHC assay showed that Aβ-specific MOAB-2 signal which was colocalized with synaptic protein *synaptophysin* and neuron-specific enolase (NSE) in the hippocampus and cortex of 3x Tg-AD mice, respectively, was weakened in 3x Tg-AD/*Fcgr2b*-CytΔ Tg mice (Figures I-14A and B). Reduction of neuronal Aβ

signal in 3x Tg-AD mice by *Fcgr2b*-CytΔ expression was more extensive in the hippocampus than in the cortex (Figures I-14C and D). Similarly, IHC using 4G8 antibody also showed decreased intraneuronal Aβ in the hippocampus of 3x Tg-AD mice by *Fcgr2b*-CytΔ expression (Figures I-15A and B). Moreover, the hippocampal synaptic dystrophy represented by *synaptophysin* was rescued in the same mice by *Fcgr2b*-CytΔ expression (Figure I-14E). As seen in *Fcgr2b* KO mice, the level of soluble $A\beta_{1-42}$, but not soluble $A\beta_{1-40}$ and insoluble $A\beta_{1-40}$ or $A\beta_{1-42}$ (Figures I-16A and B), and the ratio of $A\beta_{1-42}$ to $A\beta_{1-40}$ in the soluble fraction (Figure I-16C) were significantly reduced in the hippocampus of 3x Tg-AD mice by *Fcgr2b*-CytΔ expression. These changes were not elicited by the regulation of APP processing (Figure I-17). Thus, accumulation of soluble $A\beta_{1-42}$ in 3x Tg-AD mice was apparently suppressed by *Fcgr2b*-CytΔ expression.

Since the intraneuronal and soluble o$A\beta_{1-42}$ have long been implicated in the memory deficits of AD (Billings et al., 2005; Shankar et al., 2008), I evaluated memory function in these mice. 3x Tg-AD/*Fcgr2b*-CytΔ Tg mice exhibited better spatial recognition function than 3x Tg-AD mice in Y-maze test (Figure I-18A). Deficit in recognition memory of 3x Tg-AD mice assessed by novel object recognition test was ameliorated by the neuronal expression of *Fcgr2b*-CytΔ (Figure I-18B). In addition, defects in learning the connection between aversive foot shock and dark chamber in 3x Tg-AD mice were rescued by

Fcgr2b-CytΔ expression (Figure I-18C). Collectively, the neuronal function of FcγRIIb contributes to AD-like pathology, including learning and memory impairments, in 3x Tg-AD mice with the accumulation of neuronal $A\beta_{1-42}$.

Promotion of $oA\beta_{1-42}$ uptake via FcγRIIb2 variant is linked to neurotoxicity

Interestingly, in the mouse brain I found an alternative splicing variant of FcγRIIb, FcγRIIb2 which has high activity in the receptor-mediated endocytosis, by sequencing cDNA generated from FcγRIIb transcript (Hunziker and Fumey, 1994). FcγRIIb2 mRNA was exclusively detected in the hippocampus and cortex, whereas FcγRIIb1 mRNA was found in the spleen and thymus (Figure I-19A). In particular, FcγRIIb2 mRNA was dramatically increased in the $oA\beta_{1-42}$-treated primary neurons (Figure I-19B). Examination of the FcγRIIb2 activity revealed that cellular uptake of $oA\beta_{1-42}$ was enhanced by the stable expression of FcγRIIb2 in SH-S Y5Y cells, while $A\beta_{1-42}$ in the culture media was concomitantly reduced (Figure I-20). Notably, the ability of FcγRIIb2 to uptake $oA\beta_{1-42}$ was higher than FcγRIIb1 in HT22 and SH-SY5Y cells (Figure I-21). In accordance with the results observed in *Fcgr2b* KO neurons, internalization of $oA\beta_{1-42}$ over $oA\beta_{1-40}$ was selectively promoted by FcγRIIb2 expression in SH-SY5Y cells (Figure I-22). Thus, FcγRIIb2 functions to internalize $oA\beta_{1-42}$ into neurons efficiently.

To address how FcγRIIb2 internalizes oAβ$_{1-42}$, I first focused on the di-leucine motif, which is critical for the endocytosis of immune complex (Hunziker and Fumey, 1994), in the cytoplasmic domain of FcγRIIb2. I substituted the 274th and 275th leucine residues with alanine (L274A/L275A) and validated this mutant. Unlike FcγRIIb2 WT, oAβ$_{1-42}$ uptake was not stimulated by FcγRIIb2 L274A/L275A expression (Figure I-21B). Since *Fcgr2b* KO neurons have been shown to be resistant to Aβ neurotoxicity (Kam et al., 2013) and lack of intraneuronal Aβ (Figure I-3B), I performed an inverse analysis. While the overexpressed FcγRIIb2 WT and FcγRIIb2 L274A/L275A themselves did not affect cell viability, only FcγRIIb2 WT, but not FcγRIIb2 L274A/L275A or FcγRIIb1, decreased cell viability in the presence of oAβ$_{1-42}$ (Figure I-23A). In addition, treatment with monodansylcadaverine, an inhibitor of clathrin-mediated endocytosis (Chen et al., 2009), suppressed oAβ$_{1-42}$-induced cell death and oAβ$_{1-42}$ internalization in HT22 cells (Figure I-23B). Together, these results suggest that the di-leucine motif of FcγRIIb2 is essential for Aβ uptake and neurotoxicity.

FcγRIIb2-mediated Aβ uptake is negatively regulated by TOM1

I further characterized the FcγRIIb2-mediated Aβ uptake by isolating regulator(s) involved in this process. I established a cell-based assay for oAβ$_{1-}$

$_{42}$ neurotoxicity and screened a cDNA expression library encoding endo-lysosome-resident proteins. From the screening, *Target of Myb 1* (TOM1) was the most potent in suppressing oAβ_{1-42}-induced neurotoxicity in primary neurons and HT22 cells (Figure I-24). Ectopic expression of TOM1 also suppressed cell death triggered by ER stress which is downstream of FcγRIIb in oAβ_{1-42} neurotoxicity (Kam et al., 2013), but not by oxidative stress and TNF-α/cycloheximide (Figure I-24C). Interestingly, oAβ_{1-42} uptake into SH-SY5Y cells and FcγRIIb2-mediated oAβ_{1-42} uptake were all inhibited by TOM1 expression (Figure I-25A), whereas FcγRIIb2-mediated oAβ_{1-42} uptake was enhanced by TOM1 knockdown (Figure I-25B), indicating that TOM1 negatively regulates cellular uptake and neurotoxicity of oAβ_{1-42}.

To address the function of TOM1 in regulating the FcγRIIb-mediated Aβ uptake, I analyzed the subcellular localization of FcγRIIb dependent on the expression of TOM1 and Aβ treatment. Since endocytosed FcγRIIb2 goes through the recycling pathway to the plasma membrane (Bergtold et al., 2005), I hypothesized that TOM1 may regulate FcγRIIb2 translocation along the endocytic pathway. In SH-SY5Y cells, FcγRIIb2 located in the recycling endosome with Rab11a was increased by TOM1 knockdown (Figure I-26A). I also found that FcγRIIb2 located in the plasma membrane was markedly increased in TOM1 knockdown SH-SY5Y cells, while FcγRIIb2 was

internalized into the post-plasma membrane fraction in response to Aβ (Figure I-26B). These results argue that the increment of FcγRIIb2 recycling to the plasma membrane leads to facilitation of $oA\beta_{1-42}$ uptake.

I next assessed how TOM1 regulated Aβ uptake. Co-immunoprecipitation assay revealed that FcγRIIb2-FLAG bound to HA-TOM1 in the transfected cells and *vice versa* (Figure I-27). Besides, I found that endogenous FcγRIIb2 bound to TOM1 in HT22 cells and this interaction was weakened by $oA\beta_{1-42}$ treatment (Figure I-28A). To determine a pathophysiological relevance of this observation, I analyzed the FcγRIIb2-TOM1 interaction in AD brains. FcγRIIb2 bound to TOM1 in the hippocampal lysates of non-AD controls and this interaction was significantly diminished in the AD brains (Figure I-28B). I also found that TOM1 level was reduced in the hippocampus of patients with AD compared with non-AD controls and was reduced by $oA\beta_{1-42}$ treatment in HT22 cells (Figure I-29). To sum up, TOM1 binds to FcγRIIb2 and declined level of TOM1 might facilitate Aβ uptake during AD progression.

Massive influx of Aβ into lysosome elicits Aβ overflow to other compartments for neurotoxicity

To address how the internalized Aβ exhibits neurotoxicity, I assessed

degradation event of the internalized Aβ. As reported (Caglayan et al., 2014), the inhibition of lysosomal activity with bafilomycin A1 (Baf A1), a vacuolar-type H^+-ATPase inhibitor, resulted in the accumulation of FITC-oAβ_{1-42} in the DND-99-positive lysosomes of SH-SY5Y cells (Figure I-30A). As a comparable control, prevention of receptor-mediated endocytosis with MβCD showed accumulation of FITC-oAβ_{1-42} on the plasma membrane. Again, fractionation assay following brief exposure to oAβ_{1-42} revealed that the degradation of internalized Aβ was blocked by the treatment with Baf A1 or 3-MA, an autophagy inhibitor, but not by MG132, a proteasome inhibitor (Figure I-30B). Hence, most of the internalized Aβ is degraded in the lysosome. Actually, a low dose of intraneuronal oAβ_{1-42} was rapidly degraded at an early time without affecting cell viability. In contrast, treatment of high and neurotoxic dose of oAβ_{1-42} resulted in a drastic accumulation of oAβ_{1-42} in the lysosome (Figure I-31A). Similar accumulation was also observed by the overexpressed FcγRIIb2 which caused massive internalization of oAβ_{1-42} (Figure I-31B). Accordingly, lysosomal accumulation of oAβ_{1-42} was reduced by *Fcgr2b* KO in hippocampal neurons (Figure I-32). Collectively, excess uptake of Aβ exceeds the degrading capacity of lysosomes, causing degradation failure and accumulation in the lysosome.

As reported (Friedrich et al., 2010; Kandimalla et al., 2009), I found

significant amounts of Aβ in the mitochondria and cytoplasm (Figure I-33A). Moreover, these subcellular localizations of Aβ were greatly reduced by *Fcgr2b* KO in primary neurons. Quantitative analysis using ELISA revealed that Aβ level in the cytoplasmic fraction was reduced by FcγRIIb deficiency, while it was 50% in the membrane-enriched fraction (Figure I-33B). Furthermore, the contribution of cytosolic Aβ to neurotoxicity was assessed by utilizing NIa, a cytoplasmic Aβ protease (Shin et al., 2014). Both neuronal death initiated by the treatment with $oA\beta_{1-42}$ and intraneuronal Aβ levels found in the cytoplasmic and mitochondrial fractions were simultaneously reduced by the expression of NIa, not by NIa D81A activity-dead mutant (Figure I-34). These results indicate that the cytoplasmic and mitochondrial Aβ originating from $oA\beta_{1-42}$ uptake via FcγRIIb2 contribute to neurotoxicity.

FcγRIIb2 is essential for $oA\beta_{1-42}$ uptake and interneuronal propagation

I further evaluated whether FcγRIIb2 played a role in the propagation of Aβ into adjacent neurons at the synapse. I established a fluidic isolation of donor and recipient neurons utilizing microfluidic chambers which are widely utilized in cell-to-cell transmission experiments of other aggregation-prone proteins, including *α-synuclein* (Freundt et al., 2012) (Figure I-35A). The internalized $oA\beta_{1-42}$ in hippocampal neurons in the donor chamber was transmitted to the

recipient neurons via synaptic connection (Figure I-35B). In contrast, this propagation was remarkably reduced when *Fcgr2b* KO neurons were loaded in the donor chamber (Figure I-35B and D). Moreover, oAβ_{1-42} transmission was severely affected by placing *Fcgr2b* KO neurons in the recipient chamber or both donor and recipient chambers (Figures I-35B and D). In addition, immunostaining analysis revealed that FITC-oAβ_{1-42} was co-localized with *synaptophysin* in WT neurons, but not in *Fcgr2b* KO neurons (Figure I-35C), confirming the propagation of FITC-Aβ_{1-42} between neurons. Therefore, oAβ_{1-42} uptake through FcγRIIb2 in the presynaptic or postsynaptic neurons is critical in the interneuronal propagation of oAβ_{1-42}.

Figure I-1. Neuronal uptake of $A\beta_{1-42}$ oligomer determined by subcellular fractionation assay.

(A) Establishment of an assay determining internalized Aβ level based on subcellular fractionation. SH-SY5Y cells were treated with 2.5 μM $oA\beta_{1-42}$ for 1.5 h and then subjected to subcellular fractionation analysis. All fractions (Nu., nucleus; Cyto., cytoplasm; Mito., mitochondria; Memb., membrane) were confirmed by western blotting using CHDH (mitochondria), LC3 (autophagosome), BiP (ER), Flotilin (lipid raft), and GM130 (Golgi apparatus) antibodies. (B) Preferential uptake of $oA\beta_{1-42}$ in primary neurons. Primary mouse hippocampal neurons and astrocytes were treated with vehicle (Veh.), 1 μM $mA\beta_{1-42}$, or 1 μM $oA\beta_{1-42}$ for 12 h. The membrane-enriched fraction and conditioned media were investigated by western blotting using Aβ antibody.

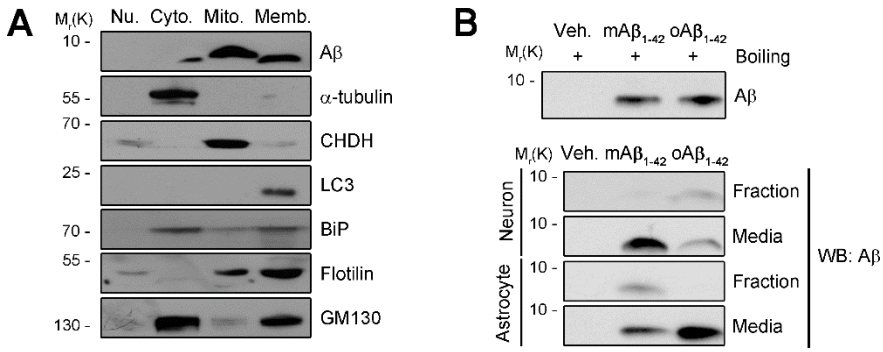
A
Mr(K)
Nu.
Cyto.
Mito.
Memb.
10 -
Aβ
55 -
α-tubulin
70 -
CHDH
25 -
LC3
70 -
BiP
55 -
Flotilin
130 -
GM130
B
Veh.
mAβ1-42
oAβ1-42
Mr(K)
+
+
+
Boiling
10 -
Aβ
Mr(K)
Veh.
mAβ1-42
oAβ1-42
Neuron
Astrocyte
10 -
Fraction
Media
Fraction
Media
WB: Aβ

Figure I-2. Preferential uptake of $A\beta_{1-42}$ oligomers over $A\beta_{1-42}$ monomer in primary neurons.

(A) Representative confocal images of internalized $mA\beta_{1-42}$ and $oA\beta_{1-42}$ in primary neurons and astrocytes. Primary murine hippocampal neurons at 10 DIV and astrocytes were incubated with 1.25 μM $mA\beta_{1-42}$ or $oA\beta_{1-42}$ for 18 h. Neurons and astrocytes were then analyzed by immunocytochemistry using MAP2b and GFAP antibodies, respectively. Scale bar, 50 μm. (B and C) Quantification of FITC-$A\beta_{1-42}$ signal intensity in primary neurons (B) and astrocytes (C). At least 25 cells per each group were scored. $^{**}p < 0.01$, $^{***}p < 0.005$. Bars represent mean ± SD ($n = 3$).

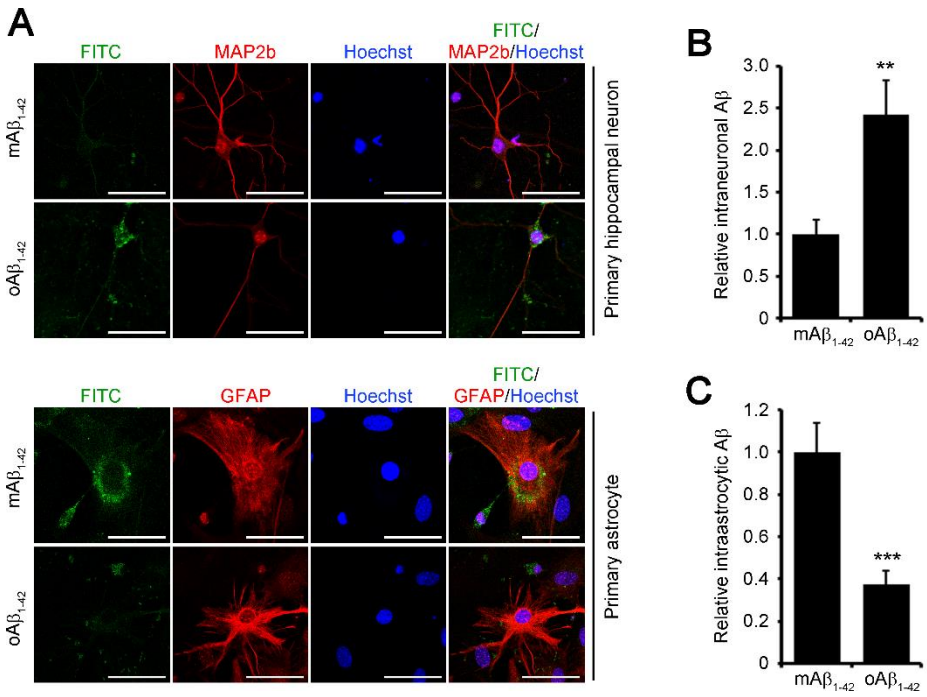
A
FITC
MAP2b
Hoechst
FITC/
MAP2b/Hoechst
mAβ1-42
oAβ1-42
Primary hippocampal neuron
FITC
GFAP
Hoechst
FITC/
GFAP/Hoechst
mAβ1-42
oAβ1-42
Primary astrocyte
B
Relative intraneuronal Aβ
3.0
2.5
2.0
1.5
1.0
0.5
0
**
mAβ1-42
oAβ1-42
C
Relative intraastrocytic Aβ
1.2
1.0
0.8
0.6
0.4
0.2
0
***
mAβ1-42
oAβ1-42

Figure I-3. FcγRIIb plays a role in the neuronal uptake of $A\beta_{1-42}$ oligomers.

(A) Involvement of FcγRIIb in the neuronal uptake of $A\beta_{1-42}$ oligomers. Cortical neurons and astrocytes were treated with 1 μM $mA\beta_{1-42}$ or $oA\beta_{1-42}$. Intracellular Aβ level in the membrane-enriched fraction was determined. (B and C) Intracellular accumulation of $oA\beta_{1-42}$ in WT MAP2B-positive neurons but not in *Fcgr2b* KO neurons. Primary neurons were incubated with 1.25 μM $mA\beta_{1-42}$ or $oA\beta_{1-42}$ for 18 h. Scale bar, 50 μm (B). Comparison of intraneuronal FITC-$A\beta_{1-42}$ signals of WT and *Fcgr2b* KO neurons ($n > 25$ cells per each group) (C). ***$p < 0.005$. Bars represent mean ± SD.

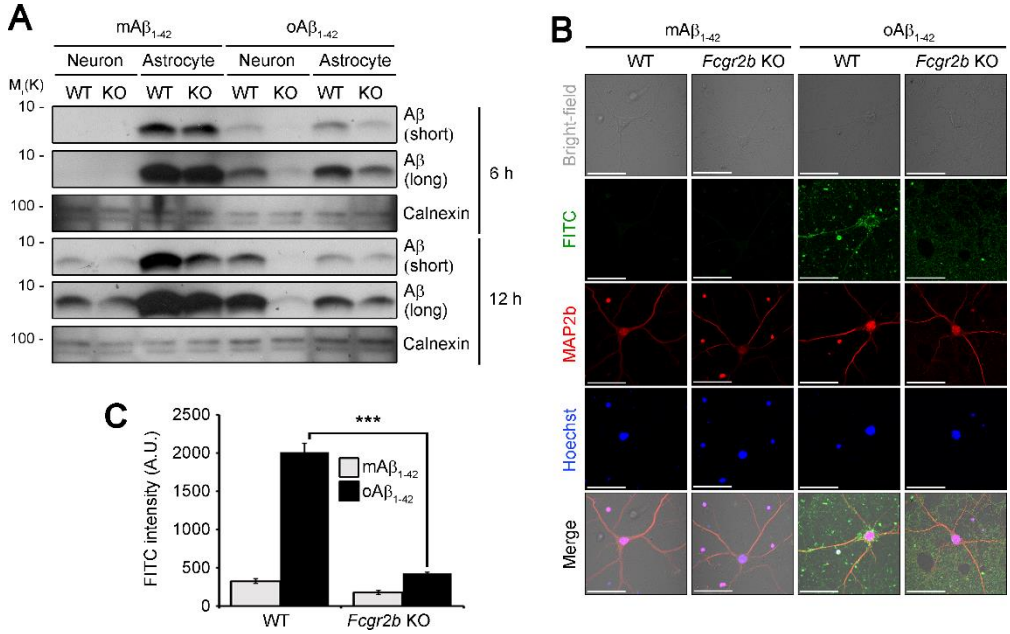
A
mAβ1-42
oAβ1-42
Neuron
Astrocyte
Neuron
Astrocyte
Mr(K)
WT KO WT KO WT KO WT KO
10 -
Aβ (short)
10 -
Aβ (long)
6 h
100 -
Calnexin
10 -
Aβ (short)
10 -
Aβ (long)
12 h
100 -
Calnexin
B
mAβ1-42
oAβ1-42
WT
Fcgr2b KO
WT
Fcgr2b KO
Bright-field
FITC
MAP2b
Hoechst
Merge
C
FITC intensity (A.U.)
2500
2000
1500
1000
500
0
***
mAβ1-42
oAβ1-42
WT
Fcgr2b KO

Figure I-4. Validation of FcγRIIb-mediated uptake of $A\beta_{1-42}$ oligomers in a time-course.

Time-dependent internalization of $oA\beta_{1-42}$ by FcγRIIb. Aβ signals on the blots in (A) were quantified (B) (n = 3). *$p < 0.05$, **$p < 0.01$, ***$p < 0.005$. Bars represent mean ± SD.

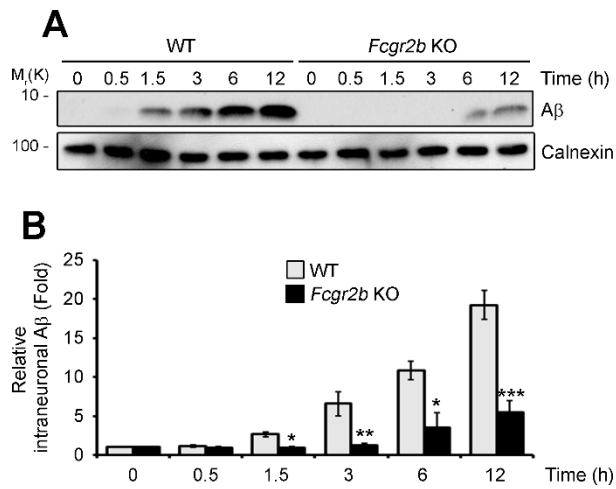
A
WT
Fcgr2b KO
M_r(K)
0 0.5 1.5 3 6 12 0 0.5 1.5 3 6 12
Time (h)
10 -
Aβ
100 -
Calnexin
B
Relative intraneuronal Aβ (Fold)
25
20
15
10
5
0
WT
Fcgr2b KO
*
**
*
***
0 0.5 1.5 3 6 12
Time (h)

Figure I-5. Accumulation of oligomeric $A\beta_{1-42}$, not $A\beta_{1-40}$, was blocked in *Fcgr2b* knockout neurons.

(A) Preferential uptake of $oA\beta_{1-42}$ over $oA\beta_{1-40}$ by FcγRIIb. Cortical neurons were treated with 1 μM $oA\beta_{1-40}$ or $oA\beta_{1-42}$ for 1.5 h. (B and C) Internalization of cell-derived $A\beta_{1-42}$ by FcγRIIb. Cortical neurons were incubated for 24 h with the conditioned media prepared from 7PA2 cells. $A\beta_{1-40}$ (B) and $A\beta_{1-42}$ (C) in lysates and conditioned media were measured by ELISA (n = 4). $^{**}p < 0.01$. Bars represent mean ± SD.

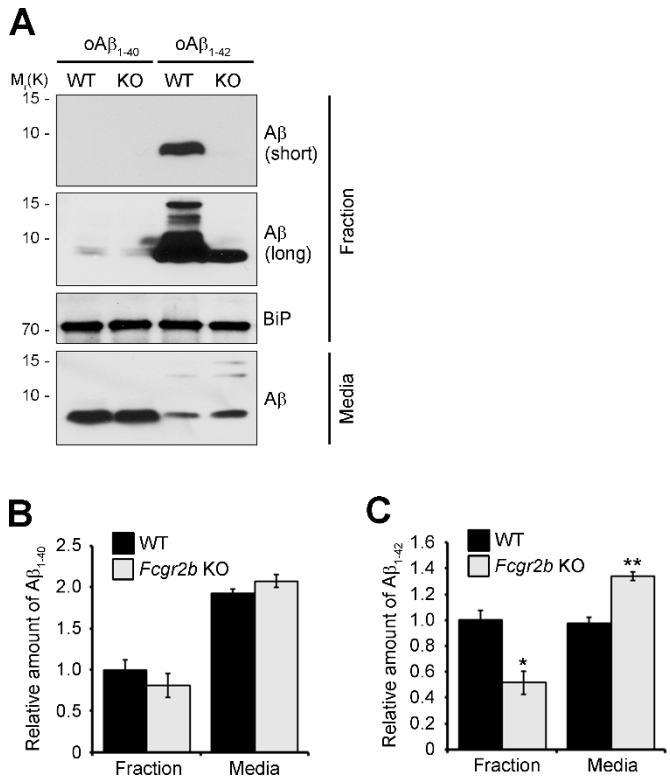
A
oAβ1-40
oAβ1-42
M.(K)
WT
KO
WT
KO
15 -
10 -
Aβ
(short)
15 -
10 -
Aβ
(long)
Fraction
70 -
BiP
15 -
10 -
Aβ
Media
B
Relative amount of Aβ1-40
2.5
2.0
1.5
1.0
0.5
0
WT
Fcgr2b KO
Fraction
Media
C
Relative amount of Aβ1-42
1.6
1.4
1.2
1.0
0.8
0.6
0.4
0.2
0
WT
Fcgr2b KO
*
**
Fraction
Media

Figure I-6. FcγRIIb-Aβ_{1-42} oligomer interaction is critical for the neuronal uptake of Aβ_{1-42} oligomer.

(A) Binding of oAβ_{1-42} to FcγRIIb is indispensable for its uptake. SH-SY5Y cells were incubated with 1 μM oAβ_{1-42} alone or together with 3 mg (1:1) or 9 mg (1:3) purified FcγRIIb–ED protein for 1.5 h. (B) Requirement of FcγRIIb immunoglobulin (Ig) 2 domain in oAβ_{1-42} internalization. SH-SY5Y cells were transfected with pEGFP-N1 (Mock), pFcγRIIb2-GFP, pFcγRIIb2 Ig1 deletion mutant-GFP (ΔIg1), or pFcγRIIb2 Ig2 deletion mutant-GFP (ΔIg2) for 24 h and then treated with 1 μM oAβ_{1-42} for 1.5 h. The membrane-enriched fractions were examined by western blotting.

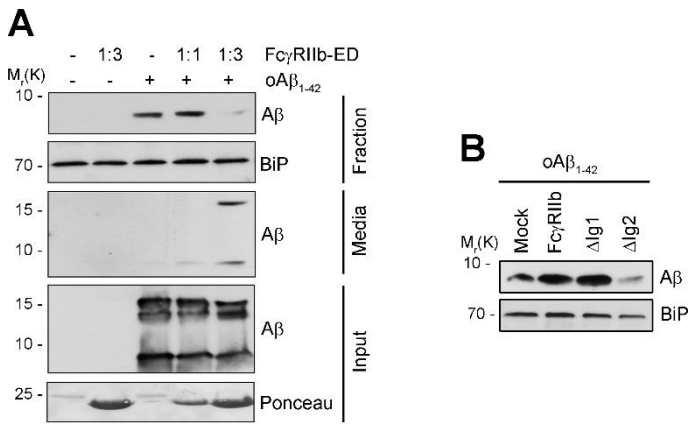
A
- 1:3 - 1:1 1:3 FcγRIIb-ED
M_r(K) - - + + + oAβ_{1-42}
10 -
Aβ
70 -
BiP
Fraction
15 -
10 -
Aβ
Media
15 -
10 -
Aβ
Input
25 -
Ponceau
B
oAβ_{1-42}
M_r(K)
Mock
FcγRIIb
ΔIg1
ΔIg2
10 -
Aβ
70 -
BiP

Figure I-7. Isolation of small molecules blocking interaction between FcγRIIb and Aβ$_{1-42}$ by virtual screening.

(A) Structural formula of #1 and #6, putative blockers of FcγRIIb2-Aβ$_{1-42}$ interaction. (B) Inhibition of FcγRIIb-ED-Aβ interaction by small molecules #1 and #6. Purified FcγRIIb-ED protein (15 μg/ml) was incubated with Aβ in the absence or presence of 100 nM small molecules and the reaction was subjected to pull-down assay. (C) Inhibition of FITC-oAβ$_{1-42}$-FcγRIIb-ED interaction by small molecules #1 and #6. Culture plate coated with 15 μg/ml FcγRIIb-ED protein was first incubated with FcγRIIb-ED, FcγRIIb antibody, or 100 nM small molecule (#1, #6, and #5) and then with 5 μM FITC-oAβ$_{1-42}$ (n = 6). After washing with PBS, the fluorescence of FITC remaining on the plate was measured with fluorometer. *$p < 0.05$, ***$p < 0.005$. Bars represent mean ± SD.

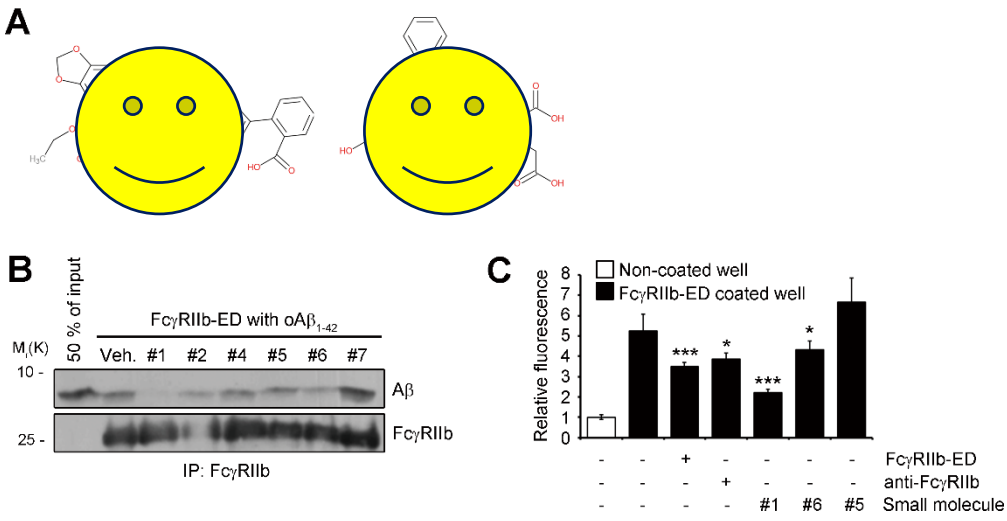
A
B
50 % of input
FcγRIIb-ED with oAβ1-42
Mr(K)
Veh. #1 #2 #4 #5 #6 #7
10 -
25 -
Aβ
FcγRIIb
IP: FcγRIIb
C
Non-coated well
FcγRIIb-ED coated well
Relative fluorescence
8
7
6
5
4
3
2
1
0
***
*
***
*
FcγRIIb-ED
anti-FcγRIIb
#1 #6 #5 Small molecule

Figure I-8. Aβ internalization and neurotoxicity are suppressed by putative FcγRIIb2-Aβ$_{1-42}$ interaction blocker.

(A) Inhibition of Aβ internalization by small molecules #1 and #6. Primary neurons were pre-treated with small molecules #1, #4 or #6 for 1.5 h, and then incubated with 1 μM oAβ$_{1-42}$ for 1.5 h. Intraneuronal Aβ in the membrane-enriched fraction (Fraction) and residual Aβ in the conditioned media (Media) were determined by western blotting. (B) Inhibition of Aβ neurotoxicity by small molecules #1 and #6. HT22 cells were pre-treated with the indicated concentrations of small molecules for 1.5 h, and then incubated with 5 μM oAβ$_{1-42}$ for 36 h (n = 3). *$p < 0.05$, **$p < 0.01$, ***$p < 0.005$. Bars represent mean ± SD.

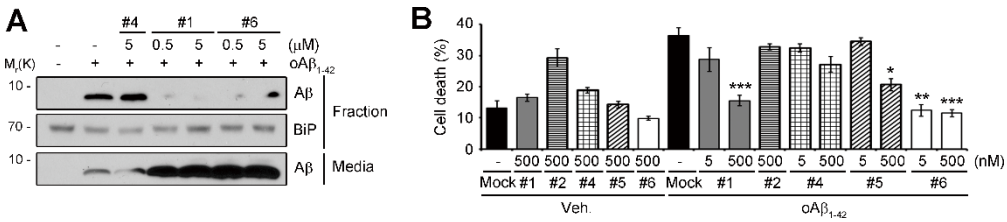
A
#4
#1
#6
(μM)
Mr(K)
oAβ1-42
10 -
Aβ
70 -
BiP
Fraction
10 -
Aβ
Media
B
Cell death (%)
40
30
20
10
0
(nM)
Mock
#1
#2
#4
#5
#6
Veh.
oAβ1-42
***
*
**
***

Figure I-9. Amelioration of cognitive impairment in Aβ-injected mice by small molecule #6.

Five week-old WT mice were i.c.v. injected with vehicle (Veh.) or 2 μg oAβ_{1-42} in the presence of 0.615 μg small molecule #6 and analyzed by Y maze (A) and novel object recognition (B) tests (n = 6 per each group).

*$p < 0.05$, **$p < 0.01$. Bars represent mean ± SEM.

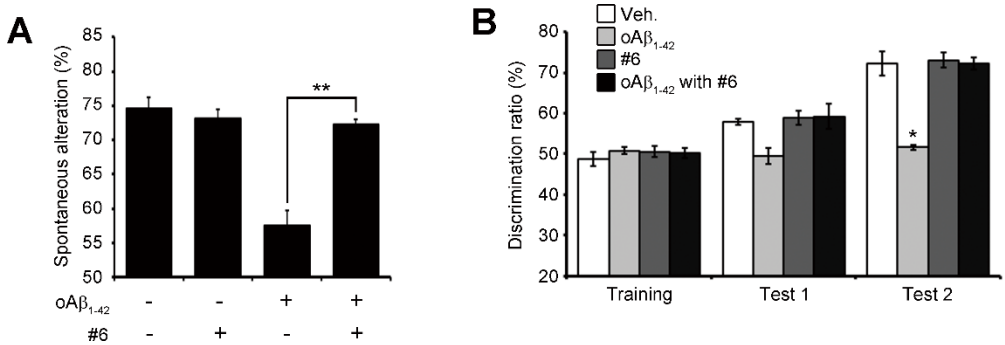
A
Spontaneous alteration (%)
85
80
75
70
65
60
55
50
**
oAβ1-42 - - + +
#6 - + - +
B
Veh.
oAβ1-42
#6
oAβ1-42 with #6
Discrimination ratio (%)
80
70
60
50
40
30
20
*
Training
Test 1
Test 2

Figure I-10. Reduction of intraneuronal $A\beta_{1-42}$ in 3x Tg-AD mice by *Fcgr2b* gene deletion.

Intraneuronal Aβ in the CA1 of the hippocampus of 7 month-old 3x Tg-AD and 3x Tg-AD/*Fcgr2b* KO mice were detected using MOAB-2 antibody with 200x (A) and 400x (B) and quantified (C) (n = 6). Scale bar, 50 μm (A) and 20 μm (B). ***$p < 0.005$. Bars represent mean ± SEM.

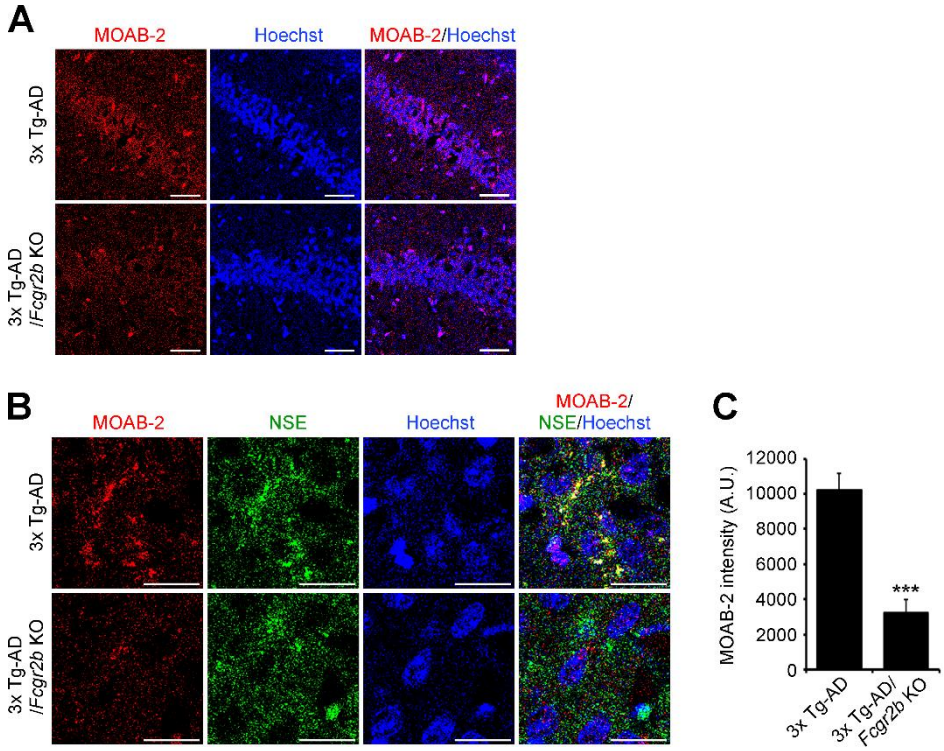
A
MOAB-2
Hoechst
MOAB-2/Hoechst
3x Tg-AD
3x Tg-AD /Fcgr2b KO
B
MOAB-2
NSE
Hoechst
MOAB-2/ NSE/Hoechst
3x Tg-AD
3x Tg-AD /Fcgr2b KO
C
MOAB-2 intensity (A.U.)
12000
10000
8000
6000
4000
2000
0
***
3x Tg-AD
3x Tg-AD/ Fcgr2b KO

Figure I-11. Soluble $A\beta_{1-42}$ in the hippocampus of 3x Tg-AD mice is reduced by genetic deletion of *Fcgr2b*.

Reduction of soluble $A\beta_{1-42}$, not insoluble $A\beta_{1-42}$, by *Fcgr2b* KO in 3x Tg-AD. The hippocampal extracts of 7 month-old 3x Tg-AD and 3x Tg-AD/*Fcgr2b* KO mice were prepared in TBS (A) or 5 M guanidine hydrochloride (GDN) (B), and the concentrations of $A\beta_{1-40}$ and $A\beta_{1-42}$ were then measured (n = 4). $A\beta_{1-42}/A\beta_{1-40}$ ratios were calculated in (C). $*p < 0.05$. Bars represent mean ± SEM.

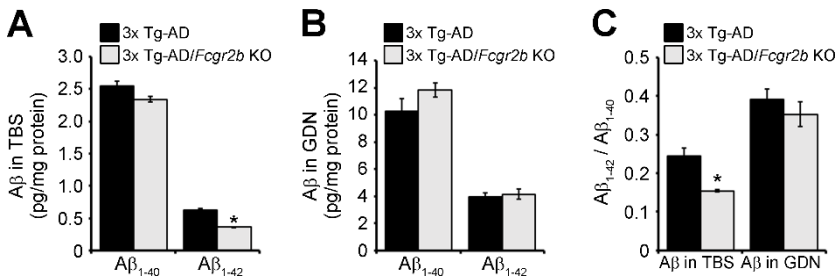
A
3x Tg-AD
3x Tg-AD/Fcgr2b KO
Aβ in TBS (pg/mg protein)
3.0
2.5
2.0
1.5
1.0
0.5
0
*
Aβ1-40
Aβ1-42
B
3x Tg-AD
3x Tg-AD/Fcgr2b KO
Aβ in GDN (pg/mg protein)
14
12
10
8
6
4
2
0
Aβ1-40
Aβ1-42
C
3x Tg-AD
3x Tg-AD/Fcgr2b KO
Aβ1-42 / Aβ1-40
0.5
0.4
0.3
0.2
0.1
0
*
Aβ in TBS
Aβ in GDN

Figure I-12. No differences in APP processing between 3x Tg-AD and 3x Tg-AD/*Fcgr2b* KO mice.

Levels of APP, APP-CTFα (CTFα), APP-CTFβ (CTFβ) and AICD in the hippocampus of both 3x Tg-AD and 3x Tg-AD/*Fcgr2b* KO mice at the age of 7 months (n = 3). Bars represent mean ± SEM.

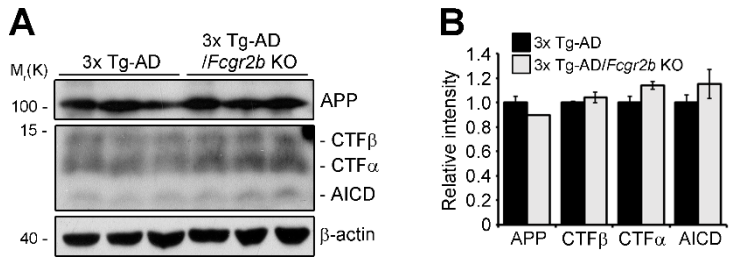
A
3x Tg-AD
3x Tg-AD
/Fcgr2b KO
M_r(K)
100 -
15 -
40 -
APP
- CTFβ
- CTFα
- AICD
β-actin
B
3x Tg-AD
3x Tg-AD/Fcgr2b KO
Relative intensity
1.4
1.2
1.0
0.8
0.6
0.4
0.2
0
APP
CTFβ
CTFα
AICD

Figure I-13. Generation of forebrain neuron-specific *Fcgr2b*-CytΔ Tg mice.

(A) Inhibition of oAβ_{1-42}-elicited cell death by the expression of *Fcgr2b*-CytΔ. HT22 cells were transfected with pEGFP-N1 (GFP) or pFcγRIIb-CytΔ-GFP (*Fcgr2b*-CytΔ) for 12 h and then treated with 5 μM oAβ_{1-42} (n = 3). (B) Forebrain neuron-specific expression of *Fcgr2b*-CytΔ transgene by CamKIIα promoter. Cortex, hippocampus, and cerebellum of WT and *Fcgr2b*-CytΔ Tg mice at the age of 3 months were analyzed by western blotting. *$p < 0.05$. Bars represent mean ± SD.

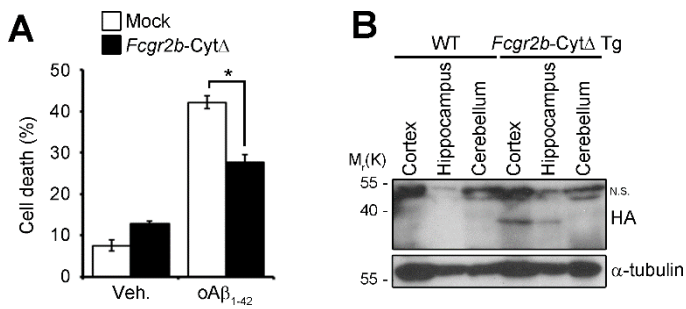
A
Mock
Fcgr2b-CytΔ
Cell death (%)
50
40
30
20
10
0
*
Veh.
oAβ1-42
B
WT
Fcgr2b-CytΔ Tg
Cortex
Hippocampus
Cerebellum
Cortex
Hippocampus
Cerebellum
Mr(K)
55 -
40 -
N.S.
HA
55 -
α-tubulin

Figure I-14. Neuronal expression of *Fcgr2b*-CytΔ in 3x Tg-AD mice decreases MOAB-2-positive intraneuronal accumulation of $A\beta_{1-42}$.

Intraneuronal Aβ in the CA1 of the hippocampus (A) and cortex (B) of 8 month-old 3x Tg-AD and 3x Tg-AD/*Fcgr2b*-CytΔ Tg mice were detected using MOAB-2 (Representative confocal images, 200x, Scale bar, 50 μm). Reactivities of the MOAB-2 in the hippocampal CA1 (C) and cortex (D) and of the *synaptophysin* in the hippocampal CA1 (E) were quantified. $^{**}p < 0.01$, $^{***}p < 0.005$. Bars represent mean ± SEM.

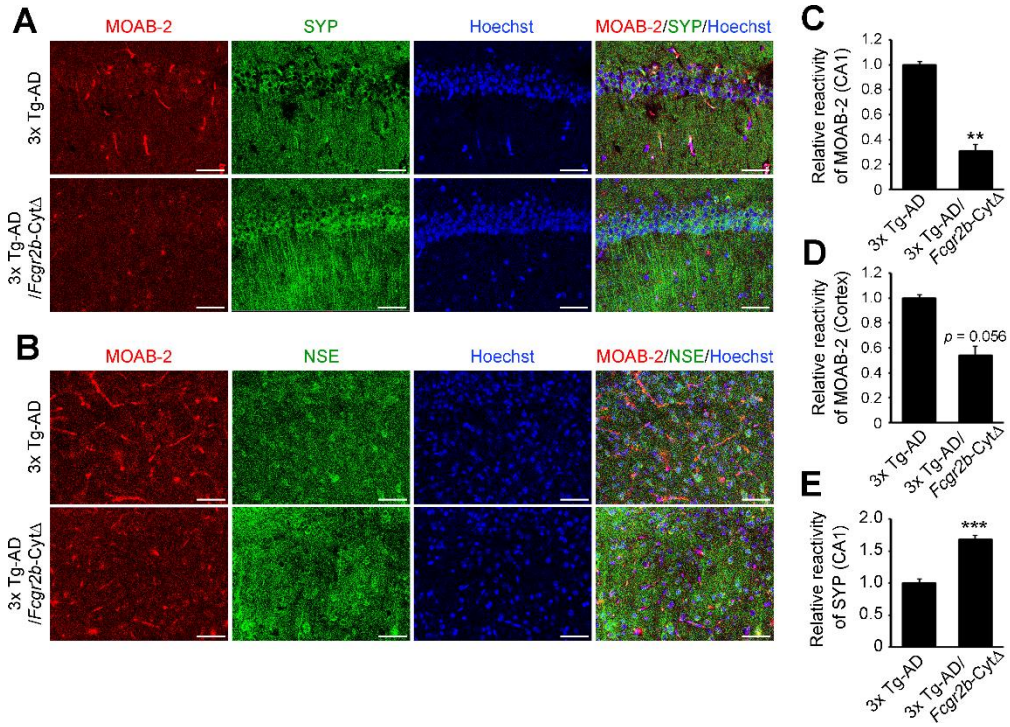
A
MOAB-2
SYP
Hoechst
MOAB-2/SYP/Hoechst
3x Tg-AD
3x Tg-AD /Fcgr2b-CytΔ
B
MOAB-2
NSE
Hoechst
MOAB-2/NSE/Hoechst
3x Tg-AD
3x Tg-AD /Fcgr2b-CytΔ
C
Relative reactivity of MOAB-2 (CA1)
1.2
1.0
0.8
0.6
0.4
0.2
0
**
3x Tg-AD
3x Tg-AD/ Fcgr2b-CytΔ
D
Relative reactivity of MOAB-2 (Cortex)
1.2
1.0
0.8
0.6
0.4
0.2
0
p = 0.056
3x Tg-AD
3x Tg-AD/ Fcgr2b-CytΔ
E
Relative reactivity of SYP (CA1)
2.0
1.5
1.0
0.5
0
***
3x Tg-AD
3x Tg-AD/ Fcgr2b-CytΔ

Figure I-15. Neuronal expression of *Fcgr2b*-CytΔ in 3x Tg-AD mice decreases 4G8-positive intraneuronal accumulation of $A\beta_{1-42}$.

Immunofluorescent detection of intraneuronal Aβ in the CA1 region of the hippocampus of 8 month-old 3x Tg-AD and 3x Tg-AD/*Fcgr2b*-CytΔ Tg mice using 4G8 antibody with magnifying power 50x (A) and 200x (B).

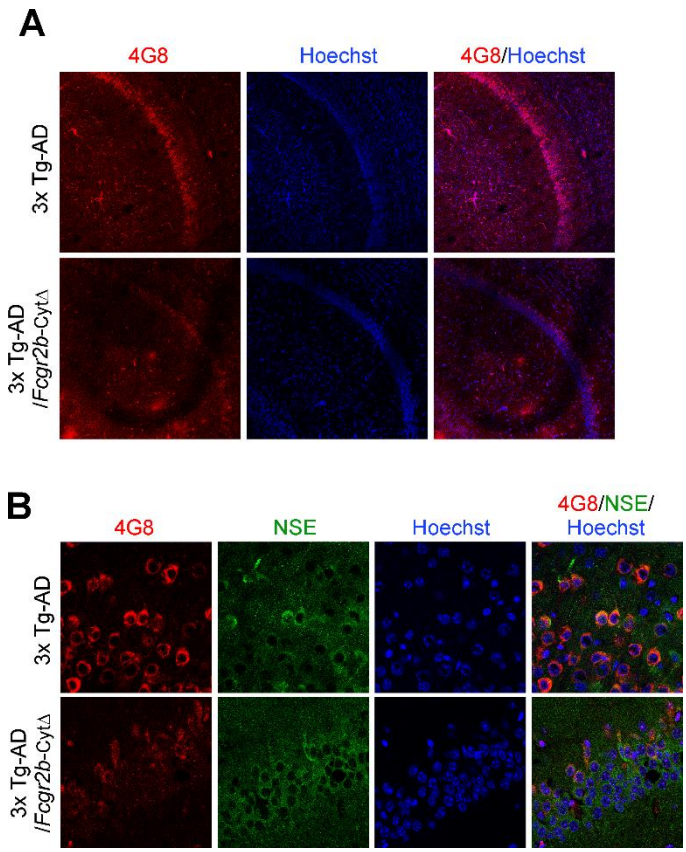
A
4G8
Hoechst
4G8/Hoechst
3x Tg-AD
3x Tg-AD
/Fcgr2b-CytΔ
B
4G8
NSE
Hoechst
4G8/NSE/
Hoechst
3x Tg-AD
3x Tg-AD
/Fcgr2b-CytΔ

Figure I-16. Soluble $A\beta_{1-42}$ in the hippocampus of 3x Tg-AD mice is reduced by neuronal expression of *Fcgr2b*-CytΔ.

The concentrations of $A\beta_{1-40}$ and $A\beta_{1-42}$ in the hippocampal extracts prepared in TBS (A) and 5 M guanidine hydrochloride (GDN) (B) from 3x Tg-AD and 3x Tg-AD/*Fcgr2b*-CytΔ mice at 8 months of age (n = 4) were measured. $A\beta_{1-42}/A\beta_{1-40}$ ratios in (A) and (B) were calculated (C). $*p < 0.05$. Bars represent mean ± SEM.

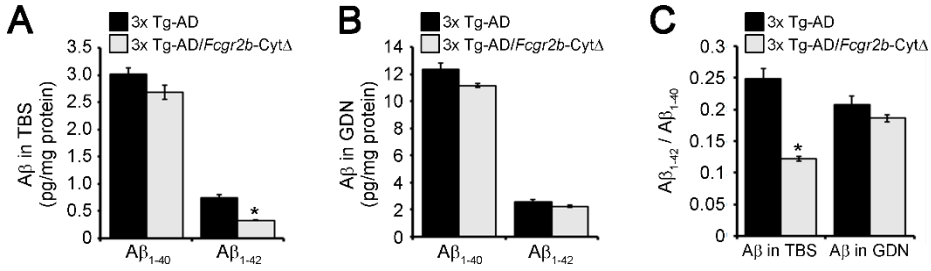
A
3x Tg-AD
3x Tg-AD/Fcgr2b-CytΔ
Aβ in TBS (pg/mg protein)
3.5
3.0
2.5
2.0
1.5
1.0
0.5
0
*
Aβ1-40
Aβ1-42
B
3x Tg-AD
3x Tg-AD/Fcgr2b-CytΔ
Aβ in GDN (pg/mg protein)
14
12
10
8
6
4
2
0
Aβ1-40
Aβ1-42
C
3x Tg-AD
3x Tg-AD/Fcgr2b-CytΔ
Aβ1-42 / Aβ1-40
0.3
0.25
0.2
0.15
0.1
0.05
0
*
Aβ in TBS
Aβ in GDN

Figure I-17. No differences in APP processing between 3x Tg-AD and 3x Tg-AD/*Fcgr2b*-CytΔ mice.

Levels of APP, APP-CTFα (CTFα), APP-CTFβ (CTFβ), and AICD in the hippocampus of both 3x Tg-AD and 3x Tg-AD/*Fcgr2b*-CytΔ mice at the age of 8 months (n = 3). Bars represent mean ± SEM.

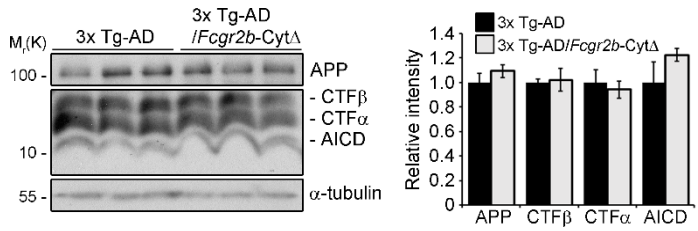
3x Tg-AD
3x Tg-AD /Fcgr2b-CytΔ
M$_r$(K)
100 -
10 -
55 -
APP
- CTFβ
- CTFα
- AICD
α-tubulin
3x Tg-AD
3x Tg-AD/Fcgr2b-CytΔ
Relative intensity
1.4
1.2
1.0
0.8
0.6
0.4
0.2
0
APP
CTFβ
CTFα
AICD

Figure I-18. Alleviation of memory deficits in 3x Tg-AD mice by neuron-specific expression of Aβ uptake-defective *Fcgr2b* mutant.

Alleviation of cognitive impairment in 3x Tg-AD mice by neuronal expression of *Fcgr2b*-CytΔ. The Y-maze (A), novel object recognition (B), and passive avoidance (C) tests were performed in 7 month-old mice (n = 9-11 male mice per group). *$p < 0.05$, **$p < 0.01$, ***$p < 0.005$. Bars represent mean ± SEM.

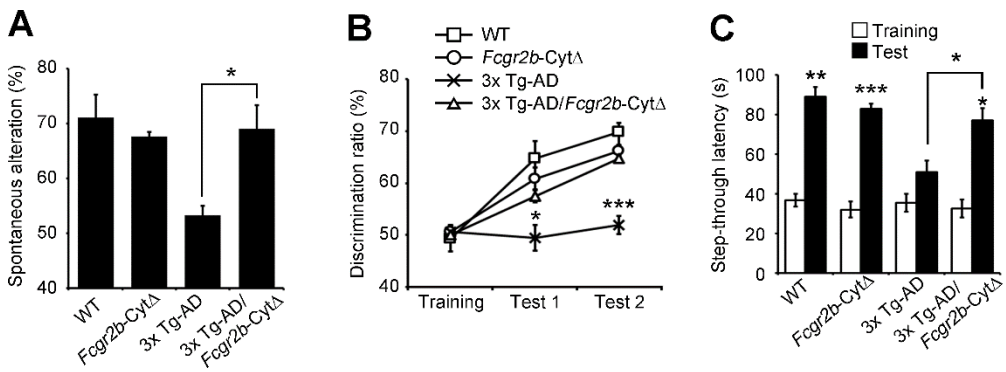
A
Spontaneous alteration (%)
80
70
60
50
40
*
WT
Fcgr2b-CytΔ
3x Tg-AD
3x Tg-AD/
Fcgr2b-CytΔ
B
WT
Fcgr2b-CytΔ
3x Tg-AD
3x Tg-AD/Fcgr2b-CytΔ
Discrimination ratio (%)
80
70
60
50
40
*
***
Training
Test 1
Test 2
C
Training
Test
Step-through latency (s)
100
80
60
40
20
0
**
***
*
*
WT
Fcgr2b-CytΔ
3x Tg-AD
3x Tg-AD/
Fcgr2b-CytΔ

Figure I-19. Enriched transcription of FcγRIIb variant 2 in neurons.

(A) Expression pattern of FcγRIIb2 in the brain tissues. Total RNAs isolated from the hippocampus (Hippo.), cortex, spleen, and thymus of WT and *Fcgr2b* KO mice were analyzed by RT-PCR. (B) Neuronal expression of the FcγRIIb2 variant revealed by RT-PCR. Cortical neurons were treated with 1 μM m$A\beta_{1\text{-}42}$ or o$A\beta_{1\text{-}42}$ for 24 h.

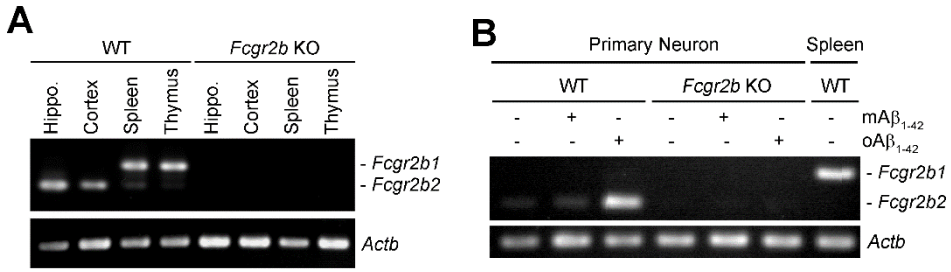
A
WT
Fcgr2b KO
Hippo.
Cortex
Spleen
Thymus
Hippo.
Cortex
Spleen
Thymus
- Fcgr2b1
- Fcgr2b2
Actb
B
Primary Neuron
Spleen
WT
Fcgr2b KO
WT
mAβ1-42
oAβ1-42
- Fcgr2b1
- Fcgr2b2
Actb

Figure I-20. Increased internalization of oAβ_{1-42} by FcγRIIb2 stable expression.

The amounts of Aβ in the membrane-enriched fraction (Fraction) and conditioned media (Media) were examined (A) and the signals on the blots were quantified (n = 3) (B, C). *$p < 0.05$, **$p < 0.0$. Bars represent mean ± SD. *N.S*, not significant.

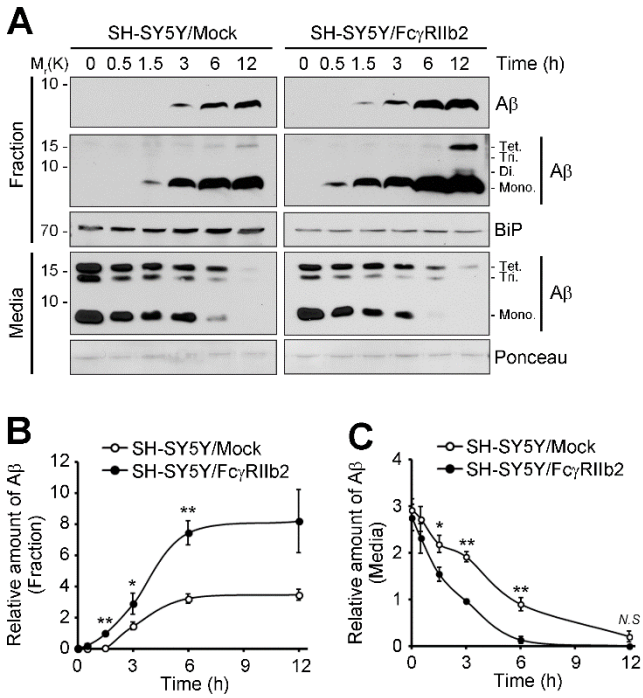
A
SH-SY5Y/Mock
SH-SY5Y/FcγRIIb2
M.(K)
0 0.5 1.5 3 6 12
0 0.5 1.5 3 6 12
Time (h)
Fraction
Media
10
15
10
70
15
10
Aβ
Tet.
Tri.
Di.
Mono.
Aβ
BiP
Tet.
Tri.
Mono.
Aβ
Ponceau
B
SH-SY5Y/Mock
SH-SY5Y/FcγRIIb2
Relative amount of Aβ (Fraction)
Time (h)
C
SH-SY5Y/Mock
SH-SY5Y/FcγRIIb2
Relative amount of Aβ (Media)
N.S
Time (h)

Figure I-21. Enhanced internalization of oAβ_{1-42} by the expression of FcγRIIb2 is dependent on its di-leucine motif.

(A) FcγRIIb2-mediated cellular uptake of oAβ_{1-42}. HT22 and SH-SY5Y cells were transfected with pEGFP-N1, pFcγRIIb1-EGFP or pFcγRIIb2-EGFP for 36 h, and treated with 1 μM oAβ_{1-42} for 1.5 h. The Aβ levels in the membrane-enriched fraction (Fraction) and conditioned media (Media) were determined by western blotting. (B) FcγRIIb2 di-leucine residues critical in Aβ uptake. SH-SY5Y cells were transfected with the indicated constructs for 24 h and then treated with 1 μM oAβ_{1-42} for 6 h.

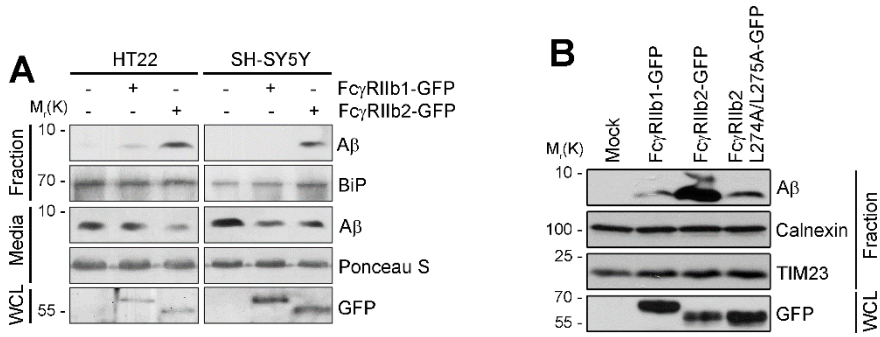
A
HT22
SH-SY5Y
FcγRIIb1-GFP
FcγRIIb2-GFP
Mr(K)
Fraction
Media
WCL
10
70
55
Aβ
BiP
Ponceau S
GFP
B
Mock
FcγRIIb1-GFP
FcγRIIb2-GFP
FcγRIIb2 L274A/L275A-GFP
100
25
Calnexin
TIM23

Figure I-22. Internalization of oAβ_{1-42}, not oAβ_{1-40}, is promoted by FcγRIIb2.

Distinct uptake of oAβ_{1-42} and oAβ_{1-40} via FcγRIIb2. SH-SY5Y cells were transfected with pEGFP-N1 or pFcγRIIb2 for 36 h, and treated with 1 μM oAβ_{1-42} for 1.5 h.

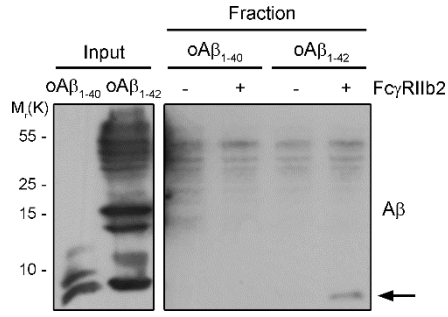
Fraction
Input
oAβ1-40
oAβ1-42
oAβ1-40 oAβ1-42
-
+
-
+
FcγRIIb2
Mr(K)
55 -
25 -
15 -
10 -
Aβ

Figure I-23. Di-leucine motif of FcγRIIb2 required for Aβ uptake is critical for neurotoxicity.

(A) Enhanced Aβ internalization by FcγRIIb2 induces neuronal death. Cortical neurons were transfected with the constructs for 24 h and incubated with vehicle (Veh.), 1 μM $mA\beta_{1-42}$, or 1 μM $oA\beta_{1-42}$ for 36 h (n = 3). (B) Suppression of $oA\beta_{1-42}$–induced neurotoxicity by the inhibition of clathrin-mediated endocytosis. SH-SY5Y cells were preincubated with 100 μM monodansylcadaverine (MDC) for 1 h and then treated with 1 μM $oA\beta_{1-42}$ for 36 h (left panel) or 12 h (right panel). Cell death rates (left panel, n = 4; $p < 0.001$ by ANOVA) and the Aβ levels in the membrane-enriched fraction (Fraction) and conditioned media (Media) were determined. $*p < 0.05$, $**p < 0.01$. Bars represent mean ± SD. *N.S*, not significant.

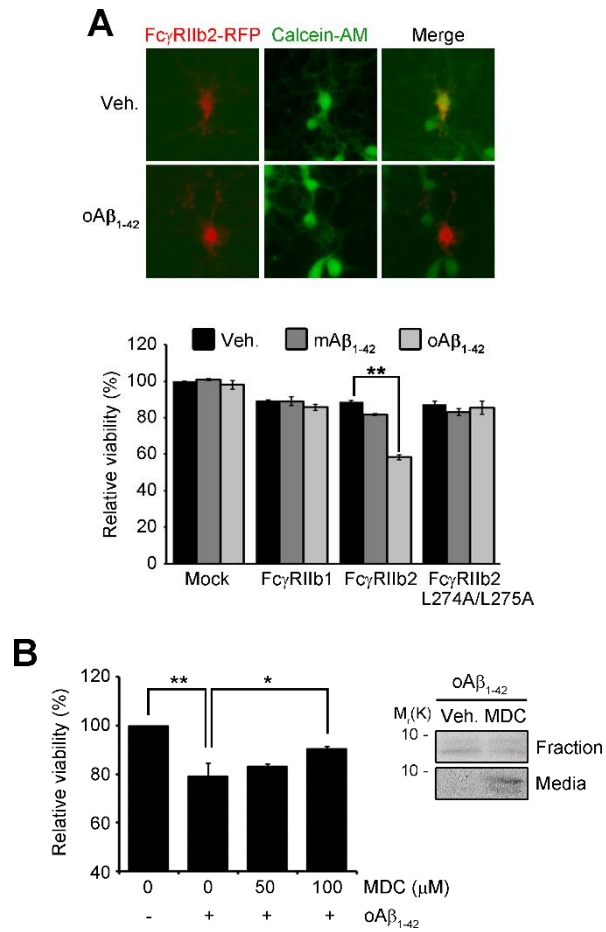
A
FcγRIIb2-RFP
Calcein-AM
Merge
Veh.
oAβ1-42
Veh.
mAβ1-42
oAβ1-42
Relative viability (%)
120
100
80
60
40
20
0
**
Mock
FcγRIIb1
FcγRIIb2
FcγRIIb2 L274A/L275A
B
Relative viability (%)
120
100
80
60
40
**
*
0
0
50
100
MDC (μM)
-
+
+
+
oAβ1-42
oAβ1-42
Mr(K)
Veh.
MDC
10 -
10 -
Fraction
Media

Figure I-24. Isolation of TOM1 as a genetic reliever of Aβ neurotoxicity by functional screening.

(A) Dot plot describing cell-based functional screening to isolate the modulators of oAβ_{1-42}–induced neurotoxicity in HT22 cells. (B) Inhibition of Aβ_{1-42} oligomer-induced neuronal death by TOM1. The pEGFP-C1 (Mock) or pEGFP-TOM1-transfected hippocampal neurons were incubated with 5 μM oAβ_{1-42} for 36 h (n = 3). (C) Inhibition of oAβ_{1-42}- and ER stress-induced neuronal death by TOM1. HT22 cells were transfected with pEGFP-C1 (Mock) or pEGFP-TOM1 for 16 h and treated with 5 μM oAβ_{1-42} for 36 h (left panel) or thapsigargin (Tg) for 12 h, 300 μM H_2O_2 for 18 h or both 30 ng/ml TNF-α and 10 μg/ml cycloheximide (CHX) for 18 h (right panel) (n = 3). *$p < 0.05$, ***$p < 0.005$. Bars represent mean ± SD. (In collaboration with Tae-In Kam, Ph.D.)

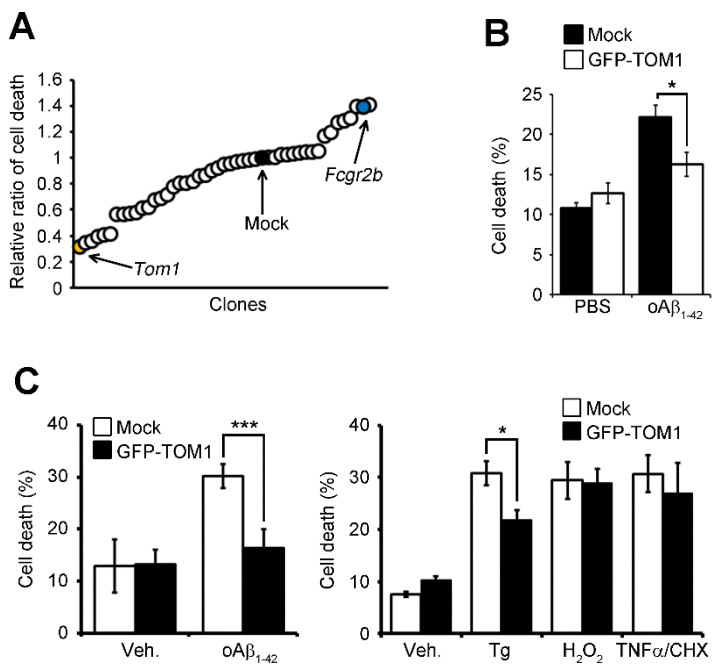
A
Relative ratio of cell death
1.6
1.4
1.2
1
0.8
0.6
0.4
0.2
0
Fcgr2b
Mock
Tom1
Clones
B
Mock
GFP-TOM1
Cell death (%)
25
20
15
10
5
0
*
PBS
oAβ1-42
C
Mock
GFP-TOM1
Cell death (%)
40
30
20
10
0
***
Veh.
oAβ1-42
Mock
GFP-TOM1
Cell death (%)
40
30
20
10
0
*
Veh.
Tg
H2O2
TNFα/CHX

Figure I-25. FcγRIIb2-mediated Aβ uptake is negatively regulated by TOM1.

(A) Inhibition of FcγRIIb2-mediated Aβ uptake by TOM1. SH-SY5Y cells were transfected with indicated plasmids and treated with 1 μM $A\beta_{1-42}$ for 1.5 h. (B) Enhancement of FcγRIIb2-mediated Aβ uptake by TOM1 knockdown. SH-SY5Y stable cells expressing pSUPER-neo (Mock) or pTOM1 shRNA (shTOM1) were transfected with pFcγRIIb2-GFP for 48 h and treated with $oA\beta_{1-42}$ for additional 3 h.

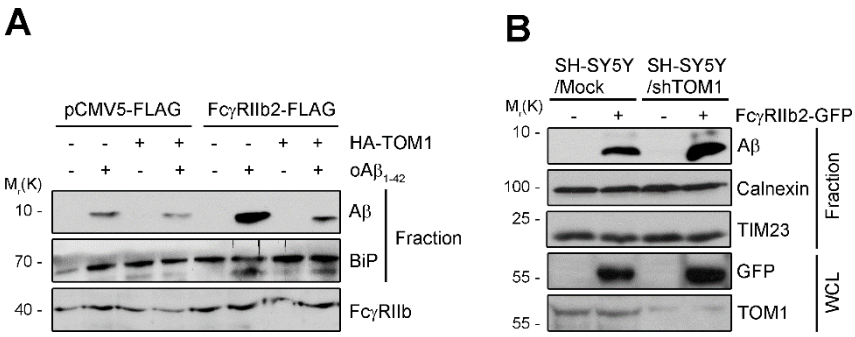
A
pCMV5-FLAG
FcγRIIb2-FLAG
HA-TOM1
oAβ1-42
Mr(K)
10 -
70 -
40 -
Aβ
BiP
FcγRIIb
Fraction
B
SH-SY5Y /Mock
SH-SY5Y /shTOM1
FcγRIIb2-GFP
10 -
100 -
25 -
55 -
55 -
Aβ
Calnexin
TIM23
GFP
TOM1
Fraction
WCL

Figure I-26. FcγRIIb2 recycling to plasma membrane is attenuated by TOM1.

(A) Membrane-retargeting of endocytosed FcγRIIb2 via recycling endosome is enhanced by TOM1 knockdown. pFcγRIIb2-RFP and pRab11a-GFP transfected SH-SY5Y/Mock and SH-SY5Y/shTOM1 were incubated with 1 μM oAβ_{1-42} for 6 h. Scale bar, 20 μm. (B) Localization of FcγRIIb2 to the plasma membrane is elevated by TOM1 knockdown. SH-SY5Y/Mock and SH-SY5Y/shTOM1 cells were treated with PBS or 1 μM oAβ_{1-42} for 12 h. Lysates were subjected to fractionation assay to prepare plasma membrane (PM) and post-plasma membrane (Post-PM).

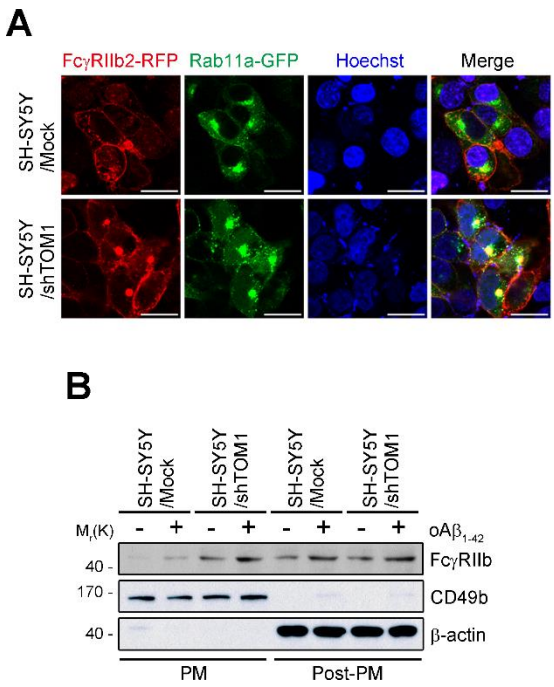
A
FcγRIIb2-RFP
Rab11a-GFP
Hoechst
Merge
SH-SY5Y /Mock
SH-SY5Y /shTOM1
B
SH-SY5Y /Mock
SH-SY5Y /shTOM1
SH-SY5Y /Mock
SH-SY5Y /shTOM1
Mr(K)
- + - + - + - +
oAβ1-42
40 -
FcγRIIb
170 -
CD49b
40 -
β-actin
PM
Post-PM

Figure I-27. Interaction between overexpressed FcγRIIb2 and TOM1.

HEK293T cells were transfected with pFcγRIIb2-FLAG and pHA-TOM1 for 24 h and subjected to immunoprecipitation (IP) assay using FLAG (C) or HA (D) antibody. (In collaboration with Tae-In Kam, Ph.D.)

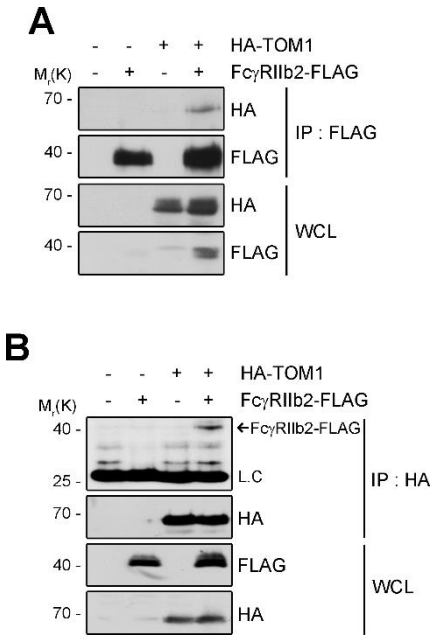
A
- - + + HA-TOM1
Mr(K) - + - + FcγRIIb2-FLAG
70 -
40 -
HA
FLAG
IP : FLAG
70 -
40 -
HA
FLAG
WCL
B
- - + + HA-TOM1
Mr(K) - + - + FcγRIIb2-FLAG
40 -
25 -
←FcγRIIb2-FLAG
L.C
IP : HA
70 -
HA
40 -
70 -
FLAG
HA
WCL

Figure I-28. Endogenous interaction between FcγRIIb2 and TOM1 is decreased in neurons by $A\beta_{1-42}$ oligomer and in AD brain.

(A) Blockade of the FcγRIIb-TOM1 interaction by $oA\beta_{1-42}$. Whole cell lysates (WCL) of HT22 cells were immunoprecipitated (IP) using IgG or FcγRIIb antibody. (B) Decreased interaction between FcγRIIb2 and TOM1 in the hippocampus of AD patients. Hippocampal lysates were subjected to immunoprecipitation (*left panel*). Level of TOM1-interacting FcγRIIb on the blots were quantified (*right panel*; n = 3). $*p < 0.05$. Bars represent mean ± SEM.

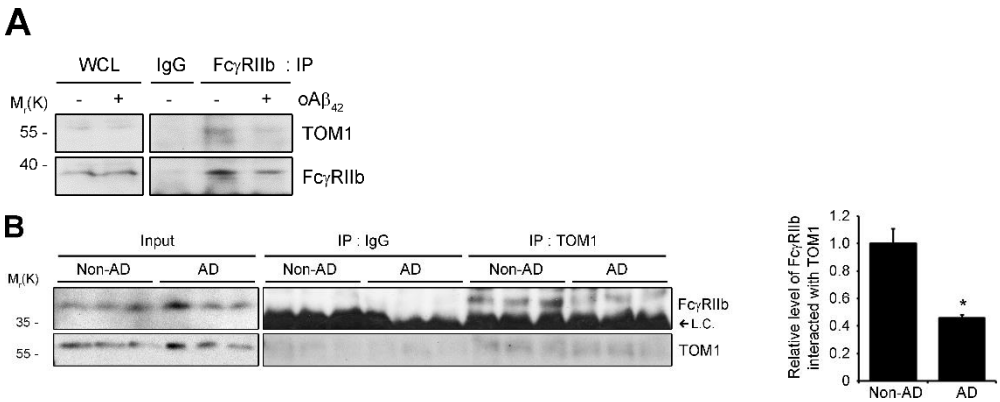
A
WCL
IgG
FcγRIIb : IP
M_r(K)
- + - - + oAβ42
55 -
TOM1
40 -
FcγRIIb
B
Input
IP : IgG
IP : TOM1
Non-AD AD Non-AD AD Non-AD AD
M_r(K)
35 -
FcγRIIb
←L.C.
55 -
TOM1
Relative level of FcγRIIb interacted with TOM1
1.2
1.0
0.8
0.6
0.4
0.2
0
*
Non-AD
AD

Figure I-29. Protein level of TOM1 is decreased by $A\beta_{1-42}$ oligomer and in AD brain.

(A) Decrease of TOM1 expression by $oA\beta_{1-42}$. SH-SY5Y cells were treated with 1 μM $oA\beta_{1-42}$ for 24 h (n = 3). (B) Decreased expression of TOM1 in the hippocampus of AD patients. Hippocampal homogenates were analyzed by western blotting (*left panel*) and quantified (r*ight panel*; n = 9 for Non-AD controls and n = 15 for AD patients). **p* < 0.05, ****p* < 0.005. Bars represent mean ± SD. (In collaboration with Tae-In Kam, Ph.D.)

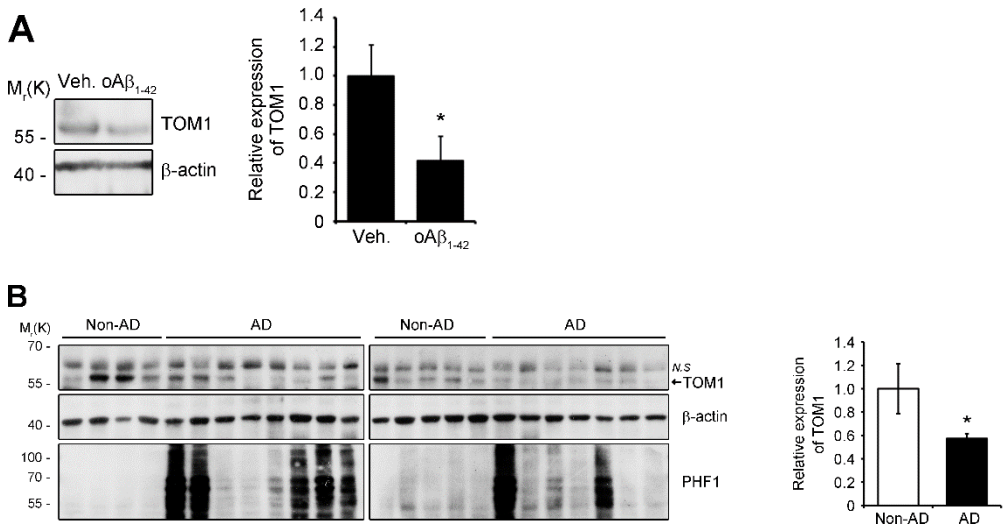
A
M_r(K)
Veh.
oAβ1-42
55 -
40 -
TOM1
β-actin
Relative expression of TOM1
1.4
1.2
1.0
0.8
0.6
0.4
0.2
0
*
Veh.
oAβ1-42
B
M_r(K)
Non-AD
AD
Non-AD
AD
70 -
55 -
40 -
100 -
70 -
55 -
N.S
←TOM1
β-actin
PHF1
Relative expression of TOM1
1.4
1.2
1.0
0.8
0.6
0.4
0.2
0
*
Non-AD
AD

Figure I-30. Internalized $A\beta_{1-42}$ is degraded in the lysosome.

(A) Inhibition of lysosome leads to accumulation of $A\beta_{1-42}$ in the lysosome. SH-SY5Y cells were incubated with 250 nM FITC-o$A\beta_{1-42}$ and vehicle (Veh.), 0.5 mM methyl-β-cyclodextrin (MβCD), or 10 nM Baf.A1 for 2 h and then treated with 50 nM Lysotracker Red (DND-99) for 1 h. Arrow indicates stacked Aβ in activity prevents degradation of the internalized Aβ. SH-SY5Y cells were treated with 1 μM o$A\beta_{1-42}$ for 12 h and further incubated with $A\beta_{1-42}$-free medium and vehicle (Veh.), 10 nM Baf. A1, 2.5 μM MG132, or 5 mM 3-MA for the indicated times.

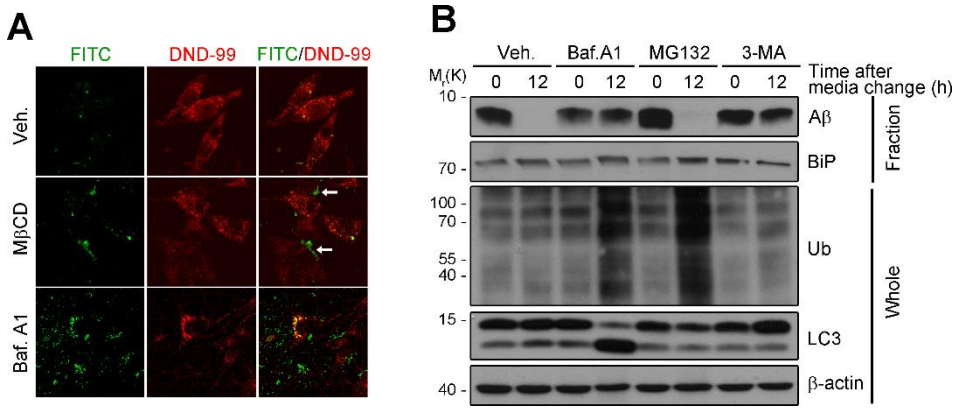
A
FITC
DND-99
FITC/DND-99
Veh.
MβCD
Baf. A1
B
Veh.
Baf.A1
MG132
3-MA
Time after media change (h)
0 12 0 12 0 12 0 12
Mr(K)
10 -
70 -
100 -
70 -
55 -
40 -
15 -
40 -
Aβ
BiP
Ub
LC3
β-actin
Fraction
Whole

Figure I-31. Promoted internalization of oAβ_{1-42} by FcγRIIb2 is linked to its cellular accumulation.

(A) Accumulation pattern of high or low-dose of oAβ_{1-42}. SH-SY5Y cells were treated with 1 or 5 μM oAβ_{1-42} for 12 h, and then incubated with Aβ_{1-42}-free medium for the indicated times in the presence of vehicle (Veh.) or 10 nM bafilomycin A1 (Baf. A1). The Aβ levels in the membrane-enriched fraction (Fraction) and conditioned media (Media) were determined. (B) Increase of internalized Aβ in FcγRIIb2-expressing neuronal cells. SH-SY5Y/Mock and SH-SY5Y/FcγRIIb2 cells were treated with 1 μM oAβ_{1-42} for 12 h and incubated with Aβ_{1-42}-free medium. (In collaboration with Tae-In Kam, Ph.D.)

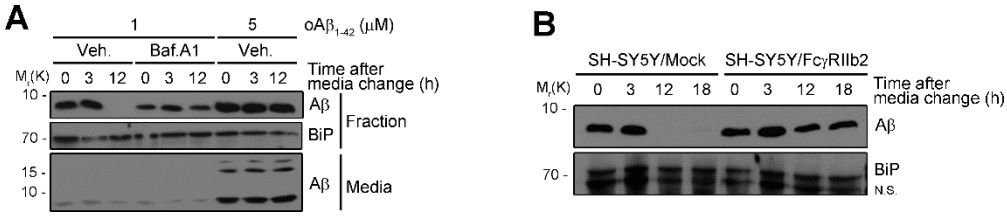
A
1
5
oAβ1-42 (μM)
Veh.
Baf.A1
Veh.
Mr(K)
0 3 12 0 3 12 0 3 12
Time after media change (h)
10 -
Aβ
Fraction
70 -
BiP
15 -
10 -
Aβ
Media
B
SH-SY5Y/Mock
SH-SY5Y/FcγRIIb2
Mr(K)
0 3 12 18 0 3 12 18
Time after media change (h)
10 -
Aβ
70 -
BiP
N.S.

Figure I-32. Excessive uptake of Aβ mediated by FcγRIIb2 causes degradation failure and accumulation in the lysosome.

(A) Accelerated degradation of internalized Aβ in *Fcgr2b* KO neurons. Cortical neurons were treated with 1 μM mAβ_{1-42} or oAβ_{1-42} for 12 h and incubated with Aβ_{1-42}-free media. (B) Internalized Aβ_{1-42} accumulates in the lysosome through FcγRIIb. Hippocampal neurons were incubated with 1.25 μM mAβ_{1-42} or oAβ_{1-42} for 18 h and incubated with 100 nM Lysotracker Red (DND-99) for 1 h.

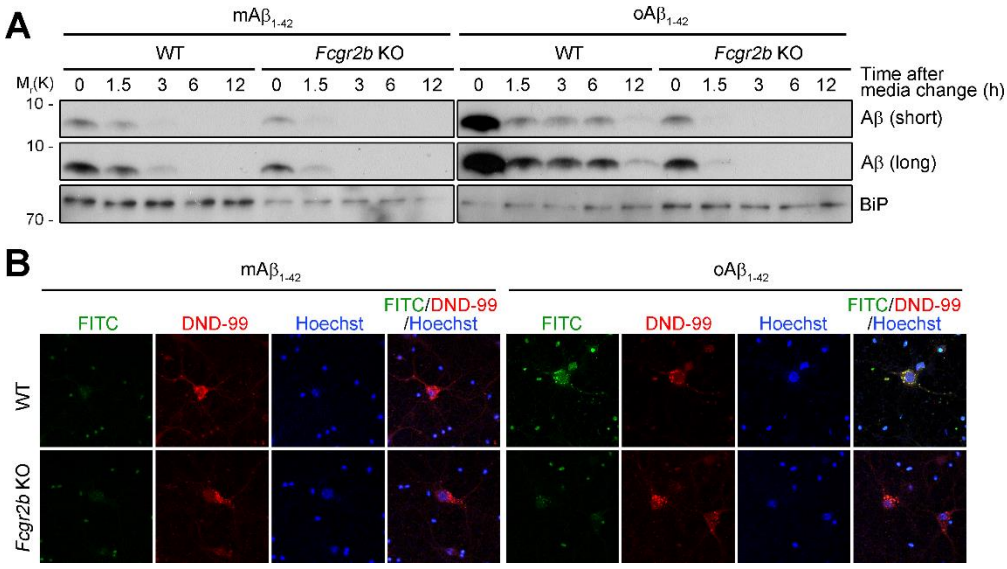
A
mAβ1-42
oAβ1-42
WT
Fcgr2b KO
WT
Fcgr2b KO
Mr(K)
0 1.5 3 6 12 0 1.5 3 6 12 0 1.5 3 6 12 0 1.5 3 6 12
Time after media change (h)
10 -
Aβ (short)
10 -
Aβ (long)
70 -
BiP
B
mAβ1-42
oAβ1-42
FITC
DND-99
Hoechst
FITC/DND-99 /Hoechst
FITC
DND-99
Hoechst
FITC/DND-99 /Hoechst
WT
Fcgr2b KO

Figure I-33. Reduction of Aβ in other cellular compartments by FcγRIIb deficiency.

Cortical neurons were treated with 1 μM mA$\beta_{1\text{-}42}$ or oA$\beta_{1\text{-}42}$ for 18 h. The Aβ in the membrane-enriched (Memb.), mitochondrial (Mito.), and cytoplasmic (Cyto.) fractions were determined by western blotting (A) and ELISA (n = 3; $p < 0.001$ by ANOVA) (B). *$p < 0.05$, ***$p < 0.005$. Bars represent mean ± SD.

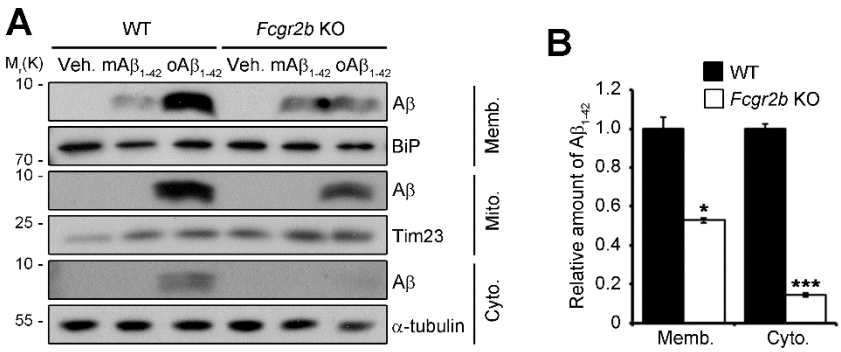
A
WT
Fcgr2b KO
Mr(K)
Veh. mAβ1-42 oAβ1-42 Veh. mAβ1-42 oAβ1-42
10 -
70 -
10 -
25 -
10 -
55 -
Aβ
BiP
Aβ
Tim23
Aβ
α-tubulin
Memb.
Mito.
Cyto.
B
WT
Fcgr2b KO
Relative amount of Aβ1-42
1.2
1.0
0.8
0.6
0.4
0.2
0
*
***
Memb.
Cyto.

Figure I-34. Rescue of neuronal death by the degradation of cytoplasmic and mitochondrial Aβ.

pcDNA3-HA (Mock), pNIa-HA (NIa), or pNIa D81A-HA (D81A) transfected cortical neurons were incubated with 1 μM oA$\beta_{1\text{-}42}$ for 12 h (*left panel*) or 36 h (*right panel*). The Aβ level in each fraction was measured as in (E) (*left panel*). Calcein-AM-positive viable cells were counted (*right panel*; n = 3; $p < 0.01$ by ANOVA). $^{**}p < 0.01$. Bars represent mean ± SD

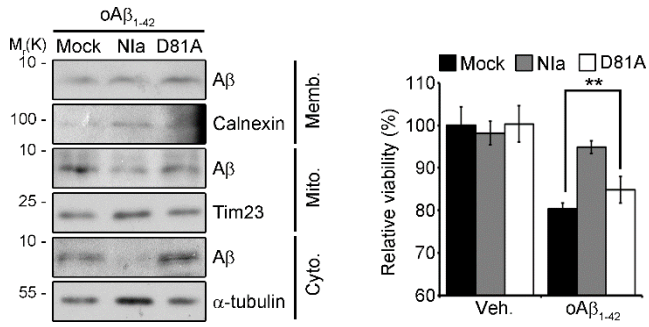
oAβ1-42
M.(K)
Mock
Nla
D81A
10 -
Aβ
Calnexin
Memb.
100 -
10 -
Aβ
Mito.
25 -
Tim23
10 -
Aβ
Cyto.
55 -
α-tubulin
Mock
Nla
D81A
Relative viability (%)
110
100
90
80
70
60
**
Veh.
oAβ1-42

Figure I-35. FcγRIIb2 is critical for neuron-to-neuron spreading of oAβ_{1-42}.

(A) Schematic picture of a microfluidic chamber. (B and C) Deterred spreading of Aβ in neurons by FcγRIIb deficiency. FITC-oAβ_{1-42} signals in microfluidic chambers were detected with 50x (B) and 200x (C). Scale bars in (B) and (C) represent 200 μm and 5 μm, respectively. (D) Comparison of fluorescent intensities in the chambers plated with WT-to-WT and WT-to-*Fcgr2b* KO neurons (n = 4). *$p < 0.05$, ***$p < 0.005$. Bars represent mean ± SD.

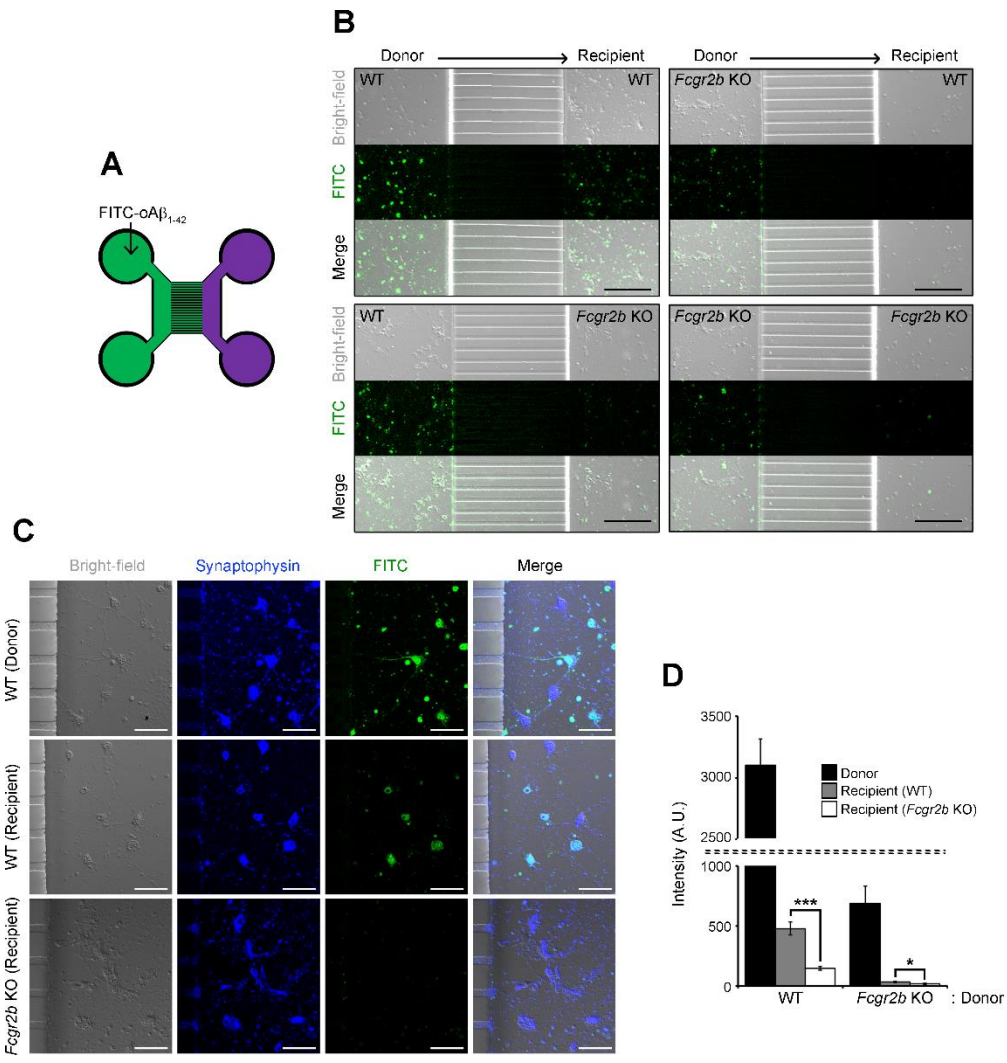
A
FITC-oAβ1-42
B
Donor
Recipient
Donor
Recipient
Bright-field
FITC
Merge
WT
WT
Fcgr2b KO
WT
WT
Fcgr2b KO
Fcgr2b KO
Fcgr2b KO
C
Bright-field
Synaptophysin
FITC
Merge
WT (Donor)
WT (Recipient)
Fcgr2b KO (Recipient)
D
Intensity (A.U.)
3500
3000
2500
1000
500
0
Donor
Recipient (WT)
Recipient (Fcgr2b KO)
***
*
WT
Fcgr2b KO
: Donor

Discussion

Increasing evidence showed that Aβ is internalized into various types of cells in the brain, including neurons, astrocytes, microglia, brain microvascular endothelia, and cerebrovascular smooth muscle cells (Kandimalla et al., 2009; LaFerla et al., 2007; Urmoneit et al., 1997). Nonetheless, the selectivity of Aβ species for cellular uptake into different cell types, the fate of internalized Aβ, and the pathophysiologic relevance of this process were not evaluated. The characteristics of Aβ species or strains differ from each other according to peptide length ($A\beta_{1-40}$ or $A\beta_{1-42}$), oligomeric states (monomer, low-n oligomer, high-n oligomer, or fibril), and source (synthetic Aβ, naturally secreted Aβ, or purified Aβ from pathogenic samples) (Benilova and De Strooper, 2013; Haass and Selkoe, 2007). Whether internalized Aβ is subjected to either degradation or exhibits neurotoxicity is also determined by its characteristics of above and cellular capacity to defense against it. Our findings that neuron has both high capacity to internalize $oA\beta_{1-42}$ and more propensity to internalize neurotoxic $oA\beta_{1-42}$ than nontoxic $mA\beta_{1-42}$ or $oA\beta_{1-40}$ provide an intriguing model that neuron itself could be a determinant for Aβ neurotoxicity. Regarding that astrocyte prefers $mA\beta_{1-42}$ to $oA\beta_{1-42}$, non-neuronal cells might degrade mAβ for the clearance.

The detrimental role of intraneuronal Aβ in AD progression was previously shown in 3x Tg-AD mice in which the accumulation of intraneuronal Aβ is temporally correlated with synaptic dysfunction and memory loss (Billings et al., 2005). In the same mice, I found that intraneuronal Aβ was remarkably decreased by *Fcgr2b* KO or neuron-specific expression of *Fcgr2b*-CytΔ at 7-8 months of age. Parallel to the reduction in intraneuronal Aβ, synaptic density and memory decline were restored by *Fcgr2b*-CytΔ expression. Because amyloid plaques and tangles are not developed but both synaptic transmission and plasticity are impaired in 3x Tg-AD mice at 7 months of age (Oddo et al., 2003), I propose that the reduction in intraneuronal Aβ in 3x Tg-AD/*Fcgr2b* KO mice and 3x Tg-AD/*Fcgr2b*-CytΔ Tg mice is mainly responsible for these improvements. Additionally, I also found that expression of Iba1, a microglia marker, and mRNA transcripts of pro-inflammatory genes, such as interleukin-1 β (IL1β), inducible nitric oxide synthase (iNOS), and tumor necrosis factor-α (TNFα), were more or less reduced by *Fcgr2b* KO in the cortex and hippocampus of 3x Tg-AD mice (data not shown). At this moment, I do not have an evidence showing that the non-neuronal activity of FcγRIIb is not solely responsible for the memory impairment. But I believe that the neuroinflammation via microglial FcγRIIb might also contribute to the aggravation of memory impairment in AD mice. Further, the notion that soluble

$A\beta_{1\text{-}42}$, but not insoluble $A\beta_{1\text{-}42}$, was reduced in 3x Tg-AD mice by *Fcgr2b* KO or *Fcgr2b*-CytΔ expression suggests that intraneuronal Aβ exists as the oligomeric state or is involved in the Aβ oligomerization, consistent with the previous reports (Oddo et al., 2006; Takahashi et al., 2013). It will be interesting to evaluate the role of FcγRIIb2 in other AD mouse models, such as APP E693Δ mice that show extensive intraneuronal Aβ phenotype and AD-like memory defect without extracellular Aβ load (Tomiyama et al., 2010).

The important question is how the internalized $oA\beta_{1\text{-}42}$ by FcγRIIb2 exhibits neurotoxicity. The process of FcγRIIb2-mediated $oA\beta_{1\text{-}42}$ uptake overlaps with or utilizes the di-leucine-dependent receptor-mediated endocytosis, leading to the accumulation of excess $oA\beta_{1\text{-}42}$ mainly in the lysosome and in the other cellular compartments as well. Although lysosome is an organelle for Aβ catabolism, massive influx of Aβ exceeding its capacity to degrade Aβ exhibited neurotoxicity, as shown in our assays, and caused the deregulation of lysosomal activity, as reported previously (Ling et al., 2009; Song et al., 2011). Furthermore, impairment of lysosomal activity by other factors, such as *presenilin* mutations (Lee et al., 2010), may further lower the catabolic activity against Aβ and thus increase the lysosome-associated neurotoxicity. Although I do not know the mechanism by which the internalized Aβ deregulates lysosome activity, I believe that the Aβ-induced lysosomal rupture leads to the leakage of

its contents and Aβ into multivesicular body and cytoplasm (Friedrich et al., 2010; Umeda et al., 2011). Thus, cytoplasmic Aβ found in the neurons of AD patients and model mice might reflect this distribution of Aβ.

Furthermore, our assays using microfluidic devices show that the neuronal uptake of oAβ_{1-42} also occurs at the synapse through FcγRIIb2 for its propagation. In this case, the internalized Aβ_{1-42} in the donor neurons bypasses lysosomal degradation, as previously evidenced by the report showing that failure in the removal of intraneuronal Aβ in the lysosome is related to the propagation of Aβ to connected neurons (Domert et al., 2014). Similarly, propagation of *α-synuclein* is promoted by insufficient clearance by autophagic inhibition, suggesting that the stereotypical spreading of aggregation-prone proteins is caused by common failures in the cellular degradative system (Lee et al., 2013). While endocytosis and synaptic activity were reported to be required for presynaptic release of Aβ in donor neurons (Cirrito et al., 2008; Tampellini et al., 2009), I propose that post-synaptic FcγRIIb2 is crucial for neuronal uptake of Aβ for synaptic transmission. Moreover, our previous observation that FcγRIIb2 is crucial for synaptic function, such as LTP, might associate with the proposed role of FcγRIIb2 in neuronal transmission of pathogenic Aβ. Whether FcγRIIb2 also plays a role in the propagation of other pathogenic proteins like *α-synuclein* (Choi et al., 2015) needs to be validated.

In conclusion, I found that the FcγRIIb2 variant is indispensable for Aβ neurotoxicity by mediating the neuronal uptake and intraneuronal accumulation of oA$\beta_{1\text{-}42}$, which affects AD neuropathology through its neuron-to-neuron propagation and memory impairment.

Materials and methods

Mice

CaMKIIα-driven transgene of *Fcgr2b*-CytΔ was produced as previously described (Kasahara et al., 2006). *Fcgr2b*-CytΔ that lacks cytoplasmic region of intact *Fcgr2b* was amplified by PCR and ligated into *Eco*RV site of pNN265. The *Not*I cleavage product (2.2 kb) of the resulting construct contains *Fcgr2b*-CytΔ flanked by 5′-UTR with SV40 small-T antigen intron and 3′-UTR with early polyadenylation sequence was ligated into pMM403 with CaMKIIα promoter. Injection of *Sfi*I-linearized construct into fertilized eggs of C57BL/6J was performed by Macrogen (Korea). *Fcgr2b* KO and 3x Tg-AD mice were previously described (Oddo et al., 2003; Takai et al., 1996). Suitable numbers of samples were adapted from the previous reports using 3x Tg-AD mice (Castello et al., 2012; Sykora et al., 2015). Since female mice were responsive to behaviors dealing with novelty and anxiety due to higher corticosterone levels (Aoki et al., 2010), only male mice were utilized in memory tests. Data were collected and quantified by investigators with blindness. All animal experiments were performed under the guidelines of Seoul National University Institutional Animal Care and Use Committee.

Human brain samples and ethical statement

Hippocampal tissues from non-AD and AD (BraakV-VI) patients were obtained from the Harvard Brain Tissue Resource Center of McLean Hospital (Belmont, MA, USA). This study was approved by the Institutional Review Board of Seoul National University (SNUIRB No. E1212/001-006).

Cell culture and DNA transfection

Primary cortical and hippocampal neurons were prepared from embryonic day 16 (E16) of mouse as described (Kam et al., 2013). Primary astrocytes were prepared form postnatal day 1 of mouse as described (Kim et al., 2013). Primary neurons were transfected using Lipofectamine 2000 reagent (Invitrogen), and SH-SY5Y, HT22 and HEK293T cells were transfected using Polyfect reagent (Qiagen) according to the manufacturer's instructions.

ELISA

Mouse hippocampus was homogenized in TBS buffer (50 mM Tris pH 7.5, 150 mM NaCl). The insoluble pellet was reconstituted in GDN buffer (50 mM Tris pH 8.0, 5 M guanidine hydrochloride). Hippocampal levels of $A\beta_{1-40}$ and $A\beta_{1-42}$

were measured by ELISA kit (IBL) according to the manufacturer's instructions.

Behavior tests

Y maze - Y maze contains 3 equal arms (32.5 cm long x 15 cm high) made of black plastic with 120° interval. Mice were laid to the end of one arm and subjected to roam freely in the apparatus for 7 min. Arm entry was regarded as valid when whole body including tail is completely entered into each arm. Effective alteration was counted when mouse entered three different arms consecutively. Spontaneous alteration was assessed as the ratio of the number of effective alteration to the number of total arm entry.

Novel object recognition - Novel object recognition was composed of 2 day habituation, 1 day training and 2 day test session. All sessions were performed at identical time in each days. In order to become familiar with the chamber (22 cm wide x 27 cm long x 30 cm high), mice was allowed to freely roam in there for 10 min. At training phase, two objects were placed to upper right and lower left sides of the chamber and mice were subjected to recognize them for 7 min. During test phases, object located in the upper right side was replaced with the novel object once a day. During training and test phase, time spent with each object was measured. Discrimination ratio was calculated by dividing T_{UR} by

sum of T_{UR} and T_{LL}, where T_{UR} and T_{LL} indicate the time spent with the object located in the upper right and lower left side of chamber, respectively.

Passive avoidance - Passive avoidance was composed of 1 day habituation, 1 day training and 1 day test session. All sessions were performed at identical time in each days. The apparatus (40 cm wide x 20 cm long x 20 cm high) consists of bright compartment which is lightened by overhead 8 W lamp and dark compartment whose floor is made of electrical grids. Two compartments are divided by a sliding door. At habitation session, mice were subjected to freely explore both compartment for 5 min. At training session, mice initially placed into the bright compartment was shocked by foot grid (0.25 mA, 1 s) shortly after entering into the dark compartment. At test session, the latency to enter the dark compartment was recorded.

DNA construction

Mouse *Fcgr2b1* and *Fcgr2b2* cDNA were amplified by PCR and ligated into pEGFP-N1 and pDsRed-N1. Human FCGR2B2 cDNA was amplified by PCR and ligated into pCMV5c-FLAG. The following nucleotide sequences were used as the primers: *Fcgr2b-Nhe*I-Sense (5′-CTA GCT AGC CAT GGA GAG CAA CTG GAC TGT-3′), *Fcgr2b-Kpn*I-Antisense (5′-GGG GTA CCC CAA

TGT GGT TCT GGT AAT C-3′), FCGR2B2-*Bgl*II-Sense (5′-GGA AGA TCT TCC ATG GGA ATC CTG TCA TTC TT-3′), and FCGR2B2-*Kpn*I-Antisense (5′-GGG GTA CCC AAT ACG GTT CTG GTC ATC A-3′). Mouse *Fcgr2b2* L274A/L275A mutant was generated by site-directed mutagenesis using following primers: *Fcgr2b2* L274A/L275A-Sense (5′-CAC CTA CTC AGC TGC CAA GCA TCC CG-3′) and *Fcgr2b2* L274A/L275A-Antisense (5′-CGG GAT GCT TGG CAG CTG AGT AGG TG-3′). Expression vectors of NIa WT and its activity dead mutant NIa D81A were provided by Dr. WJ Park (GIST, Korea).

RT-PCR

Total RNA was extracted from primary neurons or mouse tissues using TRI reagent (MRC) and cDNA was generated using M-MLV reverse transcriptase (Enzynomics, Korea). To discriminate *Fcgr2b1* and *Fcgr2b2*, a pair of primers for *Fcgr2b* were designed to encompass the sixth exons. The following nucleotide sequences were used as the primers for RT-PCR: *Fcgr2b*-RT-Sense (5′-CAG CGA CCT GTA GAT CTG GGA G-3′), *Fcgr2b*-RT-Antisense (5′-CTT CAT CCA GGG CTT CGG GAT GC-3′), *Actb*-RT-Sense (5′-GAG CTG CCT G AC GGC CAG G-3′), and *Actb*-RT-Antisense (5′-CAT CTG GAA GGT GGA C-3′).

Subcellular fractionation

Prior to subcellular fractionation, cells were briefly treated with trypsin-EDTA for 5 min to remove non-specific Aβ from the plasma membrane. Cell lysates were homogenized in hypotonic buffer (250 mM Sucrose, 20 mM HEPES pH 7.4, 10 mM KCl, 1.5 mM $MgCl_2$, 1 mM EDTA) by passing through 25 gauge needle. Nuclei and cell debris were excluded as pellets by centrifugation at 1,000xg for 10 min at 4℃. Mitochondria fraction was isolated as a pellet by centrifugation of post-nucleus supernatants at 10,000 *g* for 10 min at 4℃. The resulting supernatants were divided into the membrane-enriched fraction (pellet) and the cytoplasmic fraction (supernatant) by centrifugation at 100,000 *g* for 2 h at 4℃. Segregation of plasma membrane fraction was performed as described (Oh et al., 2012). CD49b serves as a plasma membrane marker in western blotting.

In vitro pulldown assay

In vitro interaction between o$A\beta_{1-42}$ and FcγRIIb-ED and its inhibition by small molecules were analyzed as described (Kam et al., 2013). Briefly, FcγRIIb-ED protein (15 μg/ml) was preloaded with 100 nM small molecules for 1 h in

binding buffer (50 mM Tris pH 7.4, 1 mM DTT, 0.5 mM EDTA, 0.01% Triton X-100, 10% glycerol). Then, oAβ_{1-42} (5 μg) was added to these mixtures for 2 h and subjected to the precipitation assay with FcγRIIb antibody preconjugated with protein G sepharose^{TM} (GE Healthcare). The precipitates were analyzed by western blotting.

Western blotting and immunoprecipitation

The following antibodies were used for western blotting and immunoprecipitation: Aβ (4G8 and 6E10, both Covance); BiP, Calnexin, CHDH, GFP, mouse FcγRIIb, TOM1, Ubiquitin, (Santa Cruz); Flotilin, GM130, TIM23, CD49b (BD biosciences); human FcγRIIb, LC3 (Novus); α-tubulin, β-actin, APP, FLAG (Sigma Aldrich); PHF1 (Courtesy of Dr. Peter Davies, Albert Einstein College of Medicine). Human hippocampal tissues for immunoprecipitation were solubilized in CHAPS lysis buffer (150 mM NaCl, 1 % CHAPS, 2 mM EDTA, 25 mM HEPES pH 7.4). HT22 and HEK293T cell extracts for immunoprecipitation were solubilized in RIPA lysis buffer (150 mM NaCl, 0.1 % SDS, 1 % TX-100, 50 mM Tris pH 7.5, 1 % Sodium deoxycholate).

Immunocytochemistry (ICC)

Primary neurons and astrocytes were treated with 1.25 μM mAβ_{1-42} (1 μM non-labeled mAβ_{1-42} mixed with 0.25 μM FITC-mAβ_{1-42}) or oAβ_{1-42} (1 μM non-labeled oAβ_{1-42} mixed with 0.25 μM FITC-oAβ_{1-42}) for 18 h. Cells were treated with 500 μg/ml Trypan blue in PBS before paraformaldehyde fixation to prevent background fluorescence outside the cells (Dementhon et al., 2012). Antibodies for MAP2b (BD Biosciences) and GFAP (Millipore) were used to stain primary neurons and astrocytes, respectively.

Assessment of cell viability and cell death

Viable cells were stained with 0.5 μM Calcein-AM (Molecular Probes) which is originally non-fluorescent but converted to fluorescent form under hydrolysis by intracellular esterases in live cells. Otherwise, cell viability was assessed using EZ-CyTox cell viability kit (Daeil Lab Service, South Korea). Cell death in HT22 cells were assessed by counting GFP-positive cells showing apoptotic fractured nuclei characterized by ethidium homodimer-1 (Molecular Probe).

Cell-based functional screening

HT22 cells were transfected with each of 120 cDNAs encoding endo-lysosomal proteins for 24 h and further treated with 5 μM oAβ_{1-42} for 36 h. Alteration in

cell death according to each cDNA clones were determined to isolate the putative positive clones.

Preparation of synthetic and cell-derived oAβ

Synthetic oAβ were generated as described (Kam et al., 2013). Briefly, $Aβ_{1-40}$, $Aβ_{1-42}$, and FITC-$Aβ_{1-42}$ peptides lyophilized from 1,1,1,3,3,3,-hexafluoroisopropanol (rPeptide) were solubilized in DMSO at 2 mM and then diluted in PBS to final 125 μM. The Aβ freshly diluted was used as Aβ monomer. Aβ incubated at 4℃ for 24 h was centrifuged at 12,000 *g* for 10 min and the resulting supernatant was used as Aβ oligomers. Prepared synthetic oAβ was composed of low-n (1-4) Aβ oligomer with globular shape characterized by SDS-PAGE and atomic force microscope (Kam et al., 2013). Cell-derived Aβ was prepared from the conditioned media of CHO cells stably expressing V717F mutant APP (7PA2 cells) (Courtesy of Dr. D.J. Selkoe, Harvard Medical School, MA) as described (Walsh et al., 2002). Cell debris were removed by the centrifugation at 230 *g* for 10 min and proteins in subsequent supernatants were enriched by using YM-3 centriprep centrifugal filter units (Millipore).

Immunohistochemistry (IHC)

IHC analysis of mouse brains were accomplished as described (Youmans et al., 2012). Brains were fixed with 4 % paraformaldehyde for 48 h and dehydrated with 30 % sucrose in PBS for 48 h. The 40-μm-thick floating sections were sliced on a CM1950 cryostat (Leica) and each section was allowed for antigen retrieval by incubating in 88 % formic acid for 8 min. For DAB staining, each section was treated with 0.3 % H2O2 for 5 min to inhibit endogenous peroxidase activity. The following antibodies were used: 4G8 for Aβ (Covance), MOAB-2 for Aβ (Novus), NSE (Zymed), SYP (Santa Cruz), and Iba1 (Wako).

Propagation of oAβ_{1-42} in microfluidic chamber

Master mold was fabricated on the wafer using soft lithography technique as described (Park et al., 2006). PDMS base and curing agent (Dow Corning) were mixed thoroughly and solidified on the mold at 80℃ for 1 h. Resulting microfluidic chambers contain two compartments connected by 400 μm-length ippocampal neurons were plated into donor compartment at the density of 1.0 x 10^6 cells/ml and recipient compartment at the density of 0.2 x 10^6 cells/ml. Cells in donor compartment at 3 days in vitro were incubated with 1 μM FITC-oAβ_{1-42} when axons did not stretch into the opposite side yet for 24 h and then

incubated with $A\beta_{1-42}$-free medium for 3 more days. At that point, axons from donor neurons traverse the microgrooves. Propagation of green signal representing internalized $A\beta_{1-42}$ in the neurons of left compartment to right side was observed.

Statistics

All statistical analyses were performed with GraphPad Prism Software. Comparisons between two means were performed by unpaired two-tailed *t* test. Comparisons among multiple means were performed by one-way ANOVA.

References

Aoki, M., Shimozuru, M., Kikusui, T., Takeuchi, Y., and Mori, Y. (2010). Sex differences in behavioral and corticosterone responses to mild stressors in ICR mice are altered by ovariectomy in peripubertal period. Zoolog Sci *27*, 783-789.

Benilova, I., and De Strooper, B. (2013). Neuroscience. Promiscuous Alzheimer's amyloid: yet another partner. Science *341*, 1354-1355.

Bergtold, A., Desai, D.D., Gavhane, A., and Clynes, R. (2005). Cell surface recycling of internalized antigen permits dendritic cell priming of B cells. Immunity *23*, 503-514.

Billings, L.M., Oddo, S., Green, K.N., McGaugh, J.L., and LaFerla, F.M. (2005). Intraneuronal Abeta causes the onset of early Alzheimer's disease-related cognitive deficits in transgenic mice. Neuron *45*, 675-688.

Caglayan, S., Takagi-Niidome, S., Liao, F., Carlo, A.S., Schmidt, V., Burgert, T., Kitago, Y., Fuchtbauer, E.M., Fuchtbauer, A., Holtzman, D.M.*, et al.* (2014). Lysosomal sorting of amyloid-beta by the SORLA receptor is impaired by a familial Alzheimer's disease mutation. Sci Transl Med *6*, 223ra220.

Castello, N.A., Green, K.N., and LaFerla, F.M. (2012). Genetic knockdown of brain-derived neurotrophic factor in 3xTg-AD mice does not alter Abeta or tau pathology. PLoS One *7*, e39566.

Chen, C.L., Hou, W.H., Liu, I.H., Hsiao, G., Huang, S.S., and Huang, J.S. (2009).

Inhibitors of clathrin-dependent endocytosis enhance TGFbeta signaling and responses. J Cell Sci *122*, 1863-1871.

Choi, Y.R., Kang, S.J., Kim, J.M., Lee, S.J., Jou, I., Joe, E.H., and Park, S.M. (2015). FcgammaRIIB mediates the inhibitory effect of aggregated alpha-synuclein on microglial phagocytosis. Neurobiol Dis *83*, 90-99.

Cirrito, J.R., Kang, J.E., Lee, J., Stewart, F.R., Verges, D.K., Silverio, L.M., Bu, G., Mennerick, S., and Holtzman, D.M. (2008). Endocytosis is required for synaptic activity-dependent release of amyloid-beta in vivo. Neuron *58*, 42-51.

Dementhon, K., El-Kirat-Chatel, S., and Noel, T. (2012). Development of an in vitro model for the multi-parametric quantification of the cellular interactions between Candida yeasts and phagocytes. PLoS One *7*, e32621.

Domert, J., Rao, S.B., Agholme, L., Brorsson, A.C., Marcusson, J., Hallbeck, M., and Nath, S. (2014). Spreading of amyloid-beta peptides via neuritic cell-to-cell transfer is dependent on insufficient cellular clearance. Neurobiol Dis *65*, 82-92.

Eimer, W.A., and Vassar, R. (2013). Neuron loss in the 5XFAD mouse model of Alzheimer's disease correlates with intraneuronal Abeta42 accumulation and Caspase-3 activation. Mol Neurodegener *8*, 2.

Freundt, E.C., Maynard, N., Clancy, E.K., Roy, S., Bousset, L., Sourigues, Y., Covert, M., Melki, R., Kirkegaard, K., and Brahic, M. (2012). Neuron-to-neuron

transmission of alpha-synuclein fibrils through axonal transport. Ann Neurol *72*, 517-524.

Friedrich, R.P., Tepper, K., Ronicke, R., Soom, M., Westermann, M., Reymann, K., Kaether, C., and Fandrich, M. (2010). Mechanism of amyloid plaque formation suggests an intracellular basis of Abeta pathogenicity. Proc Natl Acad Sci U S A *107*, 1942-1947.

Guo, J.L., and Lee, V.M. (2014). Cell-to-cell transmission of pathogenic proteins in neurodegenerative diseases. Nat Med *20*, 130-138.

Haass, C., Kaether, C., Thinakaran, G., and Sisodia, S. (2012). Trafficking and proteolytic processing of APP. Cold Spring Harb Perspect Med *2*, a006270.

Haass, C., and Selkoe, D.J. (2007). Soluble protein oligomers in neurodegeneration: lessons from the Alzheimer's amyloid beta-peptide. Nat Rev Mol Cell Biol *8*, 101-112.

Harris, J.A., Devidze, N., Verret, L., Ho, K., Halabisky, B., Thwin, M.T., Kim, D., Hamto, P., Lo, I., Yu, G.Q.*, et al.* (2010). Transsynaptic progression of amyloid-beta-induced neuronal dysfunction within the entorhinal-hippocampal network. Neuron *68*, 428-441.

Hunziker, W., and Fumey, C. (1994). A di-leucine motif mediates endocytosis and basolateral sorting of macrophage IgG Fc receptors in MDCK cells. EMBO J *13*, 2963-2969.

Kam, T.I., Song, S., Gwon, Y., Park, H., Yan, J.J., Im, I., Choi, J.W., Choi, T.Y., Kim, J., Song, D.K.*, et al.* (2013). FcgammaRIIb mediates amyloid-beta neurotoxicity and memory impairment in Alzheimer's disease. J Clin Invest *123*, 2791-2802.

Kandimalla, K.K., Scott, O.G., Fulzele, S., Davidson, M.W., and Poduslo, J.F. (2009). Mechanism of neuronal versus endothelial cell uptake of Alzheimer's disease amyloid beta protein. PLoS One *4*, e4627.

Kanekiyo, T., and Bu, G. (2014). The low-density lipoprotein receptor-related protein 1 and amyloid-beta clearance in Alzheimer's disease. Front Aging Neurosci *6*, 93.

Kanekiyo, T., Cirrito, J.R., Liu, C.C., Shinohara, M., Li, J., Schuler, D.R., Shinohara, M., Holtzman, D.M., and Bu, G. (2013). Neuronal clearance of amyloid-beta by endocytic receptor LRP1. J Neurosci *33*, 19276-19283.

Kasahara, T., Kubota, M., Miyauchi, T., Noda, Y., Mouri, A., Nabeshima, T., and Kato, T. (2006). Mice with neuron-specific accumulation of mitochondrial DNA mutations show mood disorder-like phenotypes. Mol Psychiatry *11*, 577-593, 523.

Kim, J.H., Choi, D.J., Jeong, H.K., Kim, J., Kim, D.W., Choi, S.Y., Park, S.M., Suh, Y.H., Jou, I., and Joe, E.H. (2013). DJ-1 facilitates the interaction between STAT1 and its phosphatase, SHP-1, in brain microglia and astrocytes: A novel

anti-inflammatory function of DJ-1. Neurobiol Dis *60*, 1-10.

LaFerla, F.M., Green, K.N., and Oddo, S. (2007). Intracellular amyloid-beta in Alzheimer's disease. Nat Rev Neurosci *8*, 499-509.

Lee, H.J., Cho, E.D., Lee, K.W., Kim, J.H., Cho, S.G., and Lee, S.J. (2013). Autophagic failure promotes the exocytosis and intercellular transfer of alpha-synuclein. Exp Mol Med *45*, e22.

Lee, J.H., Yu, W.H., Kumar, A., Lee, S., Mohan, P.S., Peterhoff, C.M., Wolfe, D.M., Martinez-Vicente, M., Massey, A.C., Sovak, G.*, et al.* (2010). Lysosomal proteolysis and autophagy require presenilin 1 and are disrupted by Alzheimer-related PS1 mutations. Cell *141*, 1146-1158.

Ling, D., Song, H.J., Garza, D., Neufeld, T.P., and Salvaterra, P.M. (2009). Abeta42-induced neurodegeneration via an age-dependent autophagic-lysosomal injury in Drosophila. PLoS One *4*, e4201.

Marr, R.A., Rockenstein, E., Mukherjee, A., Kindy, M.S., Hersh, L.B., Gage, F.H., Verma, I.M., and Masliah, E. (2003). Neprilysin gene transfer reduces human amyloid pathology in transgenic mice. J Neurosci *23*, 1992-1996.

Meyer-Luehmann, M., Coomaraswamy, J., Bolmont, T., Kaeser, S., Schaefer, C., Kilger, E., Neuenschwander, A., Abramowski, D., Frey, P., Jaton, A.L.*, et al.* (2006). Exogenous induction of cerebral beta-amyloidogenesis is governed by agent and host. Science *313*, 1781-1784.

Moghekar, A., Rao, S., Li, M., Ruben, D., Mammen, A., Tang, X., and O'Brien, R.J. (2011). Large quantities of Abeta peptide are constitutively released during amyloid precursor protein metabolism in vivo and in vitro. J Biol Chem *286*, 15989-15997.

Nath, S., Agholme, L., Kurudenkandy, F.R., Granseth, B., Marcusson, J., and Hallbeck, M. (2012). Spreading of neurodegenerative pathology via neuron-to-neuron transmission of beta-amyloid. J Neurosci *32*, 8767-8777.

Oddo, S., Caccamo, A., Shepherd, J.D., Murphy, M.P., Golde, T.E., Kayed, R., Metherate, R., Mattson, M.P., Akbari, Y., and LaFerla, F.M. (2003). Triple-transgenic model of Alzheimer's disease with plaques and tangles: intracellular Abeta and synaptic dysfunction. Neuron *39*, 409-421.

Oddo, S., Caccamo, A., Tran, L., Lambert, M.P., Glabe, C.G., Klein, W.L., and LaFerla, F.M. (2006). Temporal profile of amyloid-beta (Abeta) oligomerization in an in vivo model of Alzheimer disease. A link between Abeta and tau pathology. J Biol Chem *281*, 1599-1604.

Oh, Y., Jeon, Y.J., Hong, G.S., Kim, I., Woo, H.N., and Jung, Y.K. (2012). Regulation in the targeting of TRAIL receptor 1 to cell surface via GODZ for TRAIL sensitivity in tumor cells. Cell Death Differ *19*, 1196-1207.

Pacheco-Quinto, J., and Eckman, E.A. (2013). Endothelin-converting enzymes degrade intracellular beta-amyloid produced within the endosomal/lysosomal

pathway and autophagosomes. J Biol Chem *288*, 5606-5615.

Park, J.W., Vahidi, B., Taylor, A.M., Rhee, S.W., and Jeon, N.L. (2006). Microfluidic culture platform for neuroscience research. Nat Protoc *1*, 2128-2136.

Querfurth, H.W., and LaFerla, F.M. (2010). Alzheimer's disease. N Engl J Med *362*, 329-344.

Shankar, G.M., Li, S., Mehta, T.H., Garcia-Munoz, A., Shepardson, N.E., Smith, I., Brett, F.M., Farrell, M.A., Rowan, M.J., Lemere, C.A.*, et al.* (2008). Amyloid-beta protein dimers isolated directly from Alzheimer's brains impair synaptic plasticity and memory. Nat Med *14*, 837-842.

Shin, B., Oh, H., Park, S.M., Han, H.E., Ye, M., Song, W.K., and Park, W.J. (2014). Intracellular cleavage of amyloid beta by a viral protease NIa prevents amyloid beta-mediated cytotoxicity. PLoS One *9*, e98650.

Song, M.S., Baker, G.B., Todd, K.G., and Kar, S. (2011). Inhibition of beta-amyloid1-42 internalization attenuates neuronal death by stabilizing the endosomal-lysosomal system in rat cortical cultured neurons. Neuroscience *178*, 181-188.

Sykora, P., Misiak, M., Wang, Y., Ghosh, S., Leandro, G.S., Liu, D., Tian, J., Baptiste, B.A., Cong, W.N., Brenerman, B.M.*, et al.* (2015). DNA polymerase beta deficiency leads to neurodegeneration and exacerbates Alzheimer disease

phenotypes. Nucleic Acids Res *43*, 943-959.

Takahashi, R.H., Capetillo-Zarate, E., Lin, M.T., Milner, T.A., and Gouras, G.K. (2013). Accumulation of intraneuronal beta-amyloid 42 peptides is associated with early changes in microtubule-associated protein 2 in neurites and synapses. PLoS One *8*, e51965.

Takai, T., Ono, M., Hikida, M., Ohmori, H., and Ravetch, J.V. (1996). Augmented humoral and anaphylactic responses in Fc gamma RII-deficient mice. Nature *379*, 346-349.

Takuma, K., Fang, F., Zhang, W., Yan, S., Fukuzaki, E., Du, H., Sosunov, A., McKhann, G., Funatsu, Y., Nakamichi, N.*, et al.* (2009). RAGE-mediated signaling contributes to intraneuronal transport of amyloid-beta and neuronal dysfunction. Proc Natl Acad Sci U S A *106*, 20021-20026.

Tampellini, D., Rahman, N., Gallo, E.F., Huang, Z., Dumont, M., Capetillo-Zarate, E., Ma, T., Zheng, R., Lu, B., Nanus, D.M.*, et al.* (2009). Synaptic activity reduces intraneuronal Abeta, promotes APP transport to synapses, and protects against Abeta-related synaptic alterations. J Neurosci *29*, 9704-9713.

Tomiyama, T., Matsuyama, S., Iso, H., Umeda, T., Takuma, H., Ohnishi, K., Ishibashi, K., Teraoka, R., Sakama, N., Yamashita, T.*, et al.* (2010). A mouse model of amyloid beta oligomers: their contribution to synaptic alteration, abnormal tau phosphorylation, glial activation, and neuronal loss in vivo. J

Neurosci *30*, 4845-4856.

Tsai, K.J., Yang, C.H., Fang, Y.H., Cho, K.H., Chien, W.L., Wang, W.T., Wu, T.W., Lin, C.P., Fu, W.M., and Shen, C.K. (2010). Elevated expression of TDP-43 in the forebrain of mice is sufficient to cause neurological and pathological phenotypes mimicking FTLD-U. J Exp Med *207*, 1661-1673.

Umeda, T., Tomiyama, T., Sakama, N., Tanaka, S., Lambert, M.P., Klein, W.L., and Mori, H. (2011). Intraneuronal amyloid beta oligomers cause cell death via endoplasmic reticulum stress, endosomal/lysosomal leakage, and mitochondrial dysfunction in vivo. J Neurosci Res *89*, 1031-1042.

Urmoneit, B., Prikulis, I., Wihl, G., D'Urso, D., Frank, R., Heeren, J., Beisiegel, U., and Prior, R. (1997). Cerebrovascular smooth muscle cells internalize Alzheimer amyloid beta protein via a lipoprotein pathway: implications for cerebral amyloid angiopathy. Lab Invest *77*, 157-166.

Vodopivec, I., Galichet, A., Knobloch, M., Bierhaus, A., Heizmann, C.W., and Nitsch, R.M. (2009). RAGE does not affect amyloid pathology in transgenic ArcAbeta mice. Neurodegener Dis *6*, 270-280.

Walsh, D.M., Klyubin, I., Fadeeva, J.V., Cullen, W.K., Anwyl, R., Wolfe, M.S., Rowan, M.J., and Selkoe, D.J. (2002). Naturally secreted oligomers of amyloid beta protein potently inhibit hippocampal long-term potentiation in vivo. Nature *416*, 535-539.

Ye, L., Hamaguchi, T., Fritschi, S.K., Eisele, Y.S., Obermuller, U., Jucker, M., and Walker, L.C. (2015). Progression of Seed-Induced Abeta Deposition within the Limbic Connectome. Brain Pathol *25*, 743-752.

Youmans, K.L., Tai, L.M., Kanekiyo, T., Stine, W.B., Jr., Michon, S.C., Nwabuisi-Heath, E., Manelli, A.M., Fu, Y., Riordan, S., Eimer, W.A.*, et al.* (2012). Intraneuronal Abeta detection in 5xFAD mice by a new Abeta-specific antibody. Mol Neurodegener *7*, 8.

CHAPTER II

Role of Lyn in the Aβ-FcγRIIb neurotoxic pathway

Abstract

Amyloid-β_{1-42} ($A\beta_{1-42}$) is a critical factor of neuronal cell death and is associated with the pathogenesis of Alzheimer's disease (AD) (Hardy and Selkoe, 2002). The neurotoxic cascades initiated by extracellular $A\beta_{1-42}$ are mediated by membrane receptors. Recently, FcγRIIb is identified to be implicated in $A\beta_{1-42}$ neurotoxicity *in vitro* and memory impairment in AD model mice via interaction with $A\beta_{1-42}$ (Kam et al., 2013). However, downstream events initiated by FcγRIIb in neuronal cells are unknown. Here, I show that Lyn contributes to $A\beta_{1-42}$ and FcγRIIb-mediated neurotoxicity. I found that exposure of neuronal cells to $A\beta_{1-42}$ activated Lyn and induced the phosphorylation of FcγRIIb at Tyr273. Interestingly, knockdown of Lyn expression with shRNA decreased the phosphorylation of FcγRIIb following $A\beta_{1-42}$ exposure. In addition, down-regulation of Lyn also reduced neuronal cell death induced by $A\beta_{1-42}$. From the virtual screening, I isolated a small molecule KICG2576, an ATP-competitive inhibitor of Lyn. KICG2576 bound to Lyn in the cleft between the two lobes of the kinase domain in determination of co-crystal structure and inhibited Lyn activation. Consistently, KICG2576 inhibited Aβ- or FcγRIIb-induced neuronal cell death at sub-micromolar range. Further, intracerebroventricular-injection of KICG2675 into mice ameliorated Aβ-induced memory impairment in Y-maze and novel object recognition tests.

These results suggest that Lyn plays an essential role in $A\beta_{1-42}$–mediated neurotoxicity, providing Lyn as a target for AD therapeutics.

Introduction

Alzheimer's disease (AD) is the most common form of dementia and represents impaired cognition and loss of memory (Hardy and Selkoe, 2002). Amyloid-beta (Aβ) is the major component of senile plaque which is a remarkable hallmark in the brain of AD patients (O'Brien and Wong, 2010). $A\beta_{1-42}$ is the proteolytic product composed of 42 amino acids from amyloid precursor protein (APP) and is self-aggregated to form stable fibril and plaque, eventually (Roychaudhuri et al., 2009). $A\beta_{1-42}$ is considered as a key toxic mediator in AD, and some mutations in APP, which induce the overproduction of $A\beta_{1-42}$, trigger familial type of AD (Bertram et al., 2010; Reinhard et al., 2005). Recently, soluble oligomeric forms of $A\beta_{1-42}$ are regarded as potent species of toxicity (Haass and Selkoe, 2007). Several $A\beta_{1-42}$ oligomer species derived from AD patient or AD mice model have been reported to mediate memory impairment and loss of long-term potentiation (LTP) (Lesne et al., 2006; Shankar et al., 2008; Walsh et al., 2002). However, the acting mode of $A\beta_{1-42}$ oligomer on the pathogenesis of AD is unclear.

Recently, immune inhibitory receptor FcγRIIb was validated to be a receptor of $A\beta_{1-42}$ oligomer (Kam et al., 2013). Physical interaction between $A\beta_{1-42}$ and FcγRIIb was largely increased in the brains of AD patients. FcγRIIb knockout

(KO) neuron is less vulnerable to $A\beta_{1-42}$-induced neuronal death than wild-type (WT) neuron. In addition, genetic ablation of FcγRIIb in PDAPP mice reverses the cognitive deficit observed in these mice. Despite these effects, cellular mechanism caused by the interaction between $A\beta_{1-42}$ and FcγRIIb is uncertain.

FcγRIIb functions mainly in immune system, especially in B cell. Inhibitory signaling initiated by FcγRIIb is dependent on its immunoreceptor tyrosine-based inhibitory motif (ITIM) located in the cytosolic region (Nimmerjahn and Ravetch, 2008). This phosphorylation serves as a binding site with SH2-containing inositol phosphatase-1 (SHIP-1) (Ono et al., 1996). SHIP-1 blocks the recruitment of several pleckstrin homology (PH) domain-containing kinases, such as Btk and Akt, to plasma membrane, eventually leading to inhibition of calcium flux and proliferation of B cells (Carter et al., 1991; Jacob et al., 1999; Ono et al., 1996). Lyn, a member of Src-family tyrosine kinase (SFK), is focused on its role in the phosphorylation of several immune inhibitory receptors, including FcγRIIb (Xu et al., 2005). Importantly, Tyrosine phosphorylation of FcγRIIb within its ITIM was mostly reduced in B cells isolated from Lyn KO mice (Chan et al., 1998). Moreover, phenotype of Lyn KO mice is similar with that of FcγRIIb KO mice in that both of them succumb to autoimmune response (Bolland and Ravetch 2000; Hibbs et al., 1995). Thus, while the function of Lyn in FcγRIIb-mediated B cell inhibition is critical, its role in $A\beta_{1-42}$–induced

neuropathology remains elusive.

Here I show that Lyn plays an essential role in Aβ neurotoxicity in which Lyn is responsible for the phosphorylation at Tyr273 within ITIM of FcγRIIb. I isolated an inhibitor of Lyn (KICG2576) and found that KICG2576 attenuated $A\beta_{1\text{-}42}$ and FcγRIIb-mediated neurotoxicity. Further, intracerebroventricular (*i.c.v.*)-administration of KICG2576 suppresses $A\beta_{1\text{-}42}$-induced memory impairment. These findings suggest a neuronal role of Lyn in Aβ neurotoxicity and Aβ-associated neuropathology.

Results

$A\beta_{1-42}$ stimulates Lyn kinase to phosphorylate FcγRIIb

Since it is known that tyrosine 273 within FcγRIIb ITIM is phosphorylated by Lyn to inhibit B cell proliferation (Nimmerjahn and Ravetch, 2008), I attempted to identify whether Lyn was activated in neuronal cells by Aβ. Western blot analysis using phospho-specific antibody showed that treatment of $A\beta_{1-42}$ to both primary cortical neurons and SH-SY5Y neuroblastoma cells enhanced the phosphorylation at tyrosine 397 (Figure II-1A), an activatory phosphorylation of Lyn (Hirao et al., 1997). The mode of Lyn activation by Aβ was dose-dependent and maximal activity was acquired by over 2 μM (Figure II-1B). Unlike its dose-dependency, tracking the activity of $A\beta_{1-42}$-stimulated Lyn by time-course revealed that Lyn was rapidly activated about tenfold and gradually lost its activity for over 36 hours (Figure II-1C).

I also found that Aβ treatment increased the phosphorylation of FcγRIIb at tyrosine 273 in SH-SY5Y cells as well as the phosphorylation of Lyn at tyrosine 397 (Figure II-2A). Thus, I assessed whether Lyn is responsible for the Aβ-induced phosphorylation of FcγRIIb in neuronal cells. I reduced the level of Lyn expression using shRNA in SH-SY5Y cells (Figure II-2A). Unlike in control cells, $A\beta_{1-42}$ treatment did not induce the activatory phosphorylation of FcγRIIb

at tyrosine 273 as well as that of Lyn in Lyn knockdown cells. In addition, increased association of Lyn with FcγRIIb triggered by $A\beta_{1-42}$ is verified by immunoprecipitation assay (Figure II-2B). Conditioned media from Chinese hamster ovary cells which stably express Val717Phe mutation of APP_{751} (7PA2 cells) were characterized to secrete soluble oligomer of $A\beta_{1-42}$ (Podlisny et al., 1998 and Walsh et al., 2002). Treatment of conditioned media from 7PA2 cells enhanced endogenous interaction between Lyn and FcγRIIb in SH-SY5Y cells. These results suggest that Lyn is required for the phosphorylation of FcγRIIb at tyrosine 273 in neuronal cells after exposure to $A\beta_{1-42}$.

Lyn is associated with $A\beta_{1-42}$-evoked neuronal cell death

Since tyrosine 273 in ITIM of FcγRIIb is phosphorylated by Aβ via Lyn and this region is important in FcγRIIb-mediated neuronal cell death, I attempted to discover the role of Lyn in $A\beta_{1-42}$-evoked neuronal cell death. I utilized two neuronal cell lines, B103 rat neuroblastoma cells and HT22, which are vulnerable to $A\beta_{1-42}$ to evaluate the cell death (Song et al., 2008). Compared to untreated control cells, $A\beta_{1-42}$ treatment induced 45% of cell death in B103 cells. On the other hand, knockdown of Lyn expression effectively reduced the neuronal cell death to 27% (Figure II-3A). Amelioration of $A\beta_{1-42}$-induced neuronal cell death by silencing Lyn expression was also observed in HT22 cells

(Figure II-3B). In both cases, both Lyn expression and Lyn phosphorylation at tyrosine 397 were reduced by expression of Lyn shRNA (Figure II-3). These results indicate that stimulation of Lyn contributes to Aβ neurotoxicity.

Overall structure of Lyn kinase domain in complex with the inhibitor, KICG2576

To provide a concept of Lyn inhibition in Aβ-neurotoxicity, I attempted to generate a novel Lyn inhibitor through virtual screening. The overall structure of Lyn kinase domain is similar to the structures of well known kinase proteins which contain two lobes such as N-lobe and C-lobe. As shown in Figure II-4A, the N-lobe consists of five anti-parallel β sheets and a regulatory αC helix. The C-lobe is predominantly α-helical and serves as a docking site for substrates. ATP-binding pocket lies at the interface between the N- and C-lobes (Figure II-4A). Region of the activation loop (residues 392-400), including the phosphorylation residue Tyr397, is disordered and does not show a clear electron density. Western blot analysis showed that the purified Lyn kinase is unphosphorylated at Tyr397 in the activation loop.

Based on this structure, I isolated small molecule, KICG2576, as a novel inhibitor of Lyn and identified the mode of interaction of them. KICG2576, an

ATP-competitive inhibitor, binds with the Lyn kinase in the cleft between the two lobes of the kinase domain (Figure II-4B). There are two hydrogen bonds identified between the inhibitor and the proteins. The aminoquinazoline moiety of KICG2576 makes two hydrogen bonds with backbone NH and carbonyl oxygen of Met322 in the hinge region. In addition to the hydrogen bonds, several hydrophobic interactions are found. The planar quinazoline and immidazole rings of KICG2576 are sandwiched between the hydrophobic residues of the N-lobe (Leu253, Val261, and Ala273), the hinge region (Phe321), and the C-lobe (Leu374). Furthermore, deep hydrophobic pocket is occupied by propyl moiety of the inhibitor, forming extensive van der Waals contacts with Glu290, Met294, A384, and T319.

Next, I conducted *in vitro* kinase assay to confirm whether KICG2576 inhibits Lyn activity (Figure II-5A). In this assay, dephosphorylated casein served as an exogenous substrate for the immunoprecipitated Lyn (Young et al., 2003). Incubation of HT22 cells with KICG2576 diminished immunoreactivity against the phosphorylated α-casein compared to DMSO control or LynK-in#25, a negative-control small molecule which does not interact with Lyn. Enzymatic activity of Lyn was inhibited at 0.5 μM concentration of KICG2576. Then, I assessed the effects of KICG2576 on the phosphorylation of Lyn. Incubation of SH-SY5Y cells with 0.5 μM KICG2576 prevented $A\beta_{1\text{-}42}$-induced

phosphorylation of Lyn at tyrosine 397 to control level (Figure II-5B). These results indicate that KICG2576 is a potent inhibitor of Lyn and inhibits $A\beta_{1-42}$-triggered Lyn activation.

KICG2576 inhibits $A\beta_{1-42}$- and FcγRIIb-induced neuronal cell death

I then examined the effects of KICG2576 on $A\beta_{1-42}$–induced neurotoxicity. Incubation of HT22 cells with 0.5 μM KICG2576 completely suppressed $A\beta_{1-42}$ neurotoxicity to control level (Figure II-6A). $A\beta_{1-42}$–induced neurotoxicity was even significantly inhibited by 0.01 μM KICG2576, while LynK-in#25 did not affect on the cell death. Further, I compared KICG2576 to PP1, a widely used inhibitor of Src-family kinases including Lyn, with regard to neuroprotective effect against $A\beta_{1-42}$ (Figure II-6B). Interestingly, effect of KICG2576 in rescuing $A\beta_{1-42}$-neurotoxicity was better than that of PP1. While PP1 prevented $A\beta_{1-42}$-cytotoxicity over 1 μM, neuroprotection against $A\beta_{1-42}$ was fulfilled by treatment of at least 0.1 μM KICG2576. Similarly, KICG2576 exhibited an inhibitory activity against $A\beta_{1-42}$–neurotoxicity in primary cortical neurons; 0.5 μM KICG2576 was most effective than 0.1 μM (Figure II-7). Western blot analysis also revealed that KICG2576 inhibited proteolytic activation of caspase-3 in a dose-dependent manner as well as activatory phosphorylation of Lyn (Figure II-7). However, KICG2576 did not affect cell

death induced by other insults, including TNF-α and etoposide in HT22 cells (Figure II-8).

Since FcγRIIb is a key mediator of $A\beta_{1-42}$–mediated cell death and Lyn phosphorylates FcγRIIb under $A\beta_{1-42}$ stimulus, I investigated the ability of KICG2576 to affect FcγRIIb-mediated cell death. Consistently, KICG2576 inhibited cell death elicited by ectopic expression of FcγRIIb in HT22 cells (Figure II-9A). In addition, KICG2576 also inhibited the phosphorylation of FcγRIIb at tyrosine 273 (Figure II-9B). All these results are consistent with our earlier observation showing the role of Lyn in $A\beta_{1-42}$- and FcγRIIb-mediated cell death. Thus, it appears that KICG2576 abrogates $A\beta_{1-42}$ neurotoxicity by prohibiting Lyn.

KICG2576 rescues memory impairment triggered by *i.c.v.* injection of $A\beta_{1-42}$

Because Aβ neurotoxicity provides cellular basis for memory deficits and neuropathological features of dementia in AD (Haass and Selkoe, 2007 and Selkoe, 2002), I investigated effect of KICG2576 on learning and memory deficits in mice using intracerebroventricular(*i.c.v.*) injection model of $A\beta_{1-42}$. I found that spatial memory measured with Y maze test was impaired for 10 days

in $A\beta_{1-42}$-injected mice (Figure II-10A). On the other hand, co-injection of KICG2576 with $A\beta_{1-42}$ rescued the memory impairment. The decline of spontaneous alteration was completely restored at 22 day after injection (Figure II-10B). In addition, objective memory measured with novel object recognition task was impaired by $A\beta_{1-42}$ injection but discrimination of the novel object from familiar object was obtained by co-injection of KICG2576 (Figure II-10C). These results indicate that KICG2576 can rescue the memory impairment induced by $A\beta_{1-42}$ injection in mice.

Lyn is activated in the brain of AD patients

In order to examine *in vivo* relevance of Lyn, I analyzed the kinase activity of Lyn in the brain extracts of normal individuals and AD patients. Interestingly, I found that, the activatory phosphorylation of Lyn was increased in AD patients compared to healthy controls, whereas there was no significant change in the level of total Lyn (Figure II-11). In summary, I confirmed the pathologic correlation of Lyn activity in AD patients.

Figure II-1. Lyn is activated by $A\beta_{1-42}$ oligomer in neuronal cells.

(A) Phosphorylation of Lyn at Tyr397 by $A\beta_{1-42}$. Primary cortical neurons (DIV 5) and SH-SY5Y neuroblastoma cells were treated with PBS or 5 μM $A\beta_{1-42}$ oligomer for 24 h. Cell lysates were prepared and subjected to western blotting with the phospho-Lyn tyrosine 397 (Y397) antibody. (B and C) Increase of Lyn phosphorylation at Tyr397 by $A\beta_{1-42}$ in a dose- and time-dependent manner. SH-SY5Y cells were treated with PBS or the indicated concentrations of $A\beta_{1-42}$ for 12 h (B) or 2 μM $A\beta_{1-42}$ for the indicated times (C). Cell lysates were immunoblotted with phospho-Lyn tyrosine 397 (Y397) antibody. Graphs represent the relative ratios of p-Lyn (Y397) levels to Lyn in upper panels with mean ± SD (n = 3). *P < 0.05, **P < 0.005.

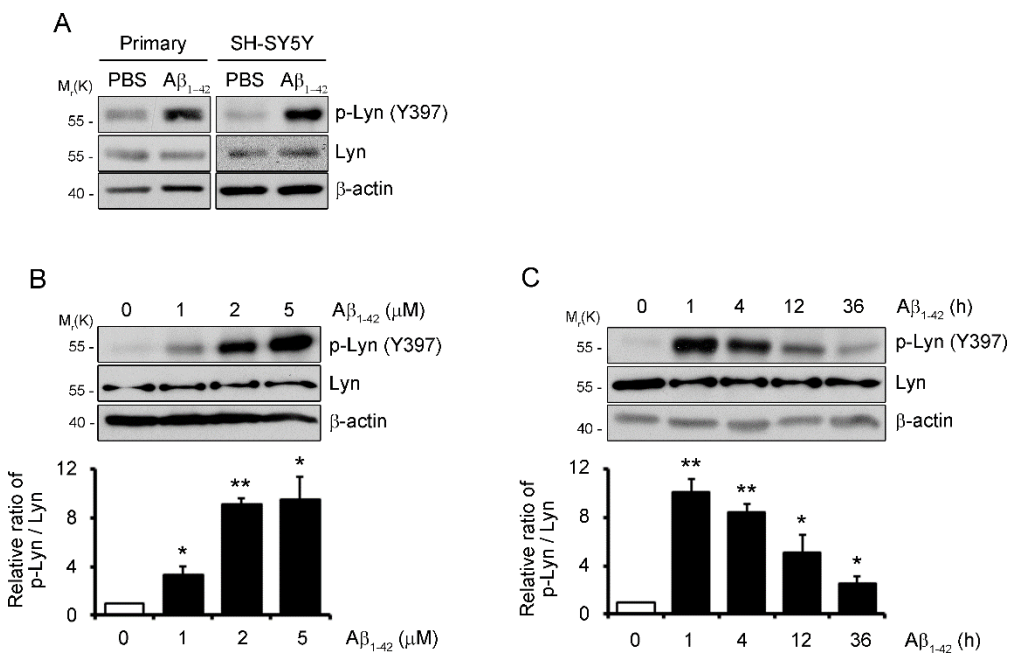
A
Primary
SH-SY5Y
M_r(K)
PBS
Aβ1–42
PBS
Aβ1–42
55 -
55 -
40 -
p-Lyn (Y397)
Lyn
β-actin
B
M_r(K)
0
1
2
5
Aβ1-42 (μM)
55 -
55 -
40 -
p-Lyn (Y397)
Lyn
β-actin
Relative ratio of p-Lyn / Lyn
12
8
4
0
*
**
*
0
1
2
5
Aβ1-42 (μM)
C
M_r(K)
0
1
4
12
36
Aβ1-42 (h)
55 -
55 -
40 -
p-Lyn (Y397)
Lyn
β-actin
Relative ratio of p-Lyn / Lyn
12
8
4
0
**
**
*
*
0
1
4
12
36
Aβ1-42 (h)

Figure II-2. Lyn is required for the phosphorylation and activation of FcγRIIb by $A\beta_{1-42}$.

(A) Abrogation of $A\beta_{1-42}$-induced phosphorylation of FcγRIIb by Lyn knockdown. SH-SY5Y cells were transfected with pSUPER-neo (Mock) or pLyn shRNA (shLyn) for 48 h and then incubated with PBS or 2 μM $A\beta_{1-42}$ for additional 12 h. Cell lysates were immunoblotted using p-FcγRIIb, FcγRIIb, p-Lyn (Y397), Lyn and β-actin antibodies. (B) Enhanced interaction between Lyn and FcγRIIb owing to $A\beta_{1-42}$. SH-SY5Y cells were treated with conditioned medium of either CHO cell or 7PA2 cell, stably expressing APP V717F mutant, for 24 h. Cell lysates were subjected to immunoprecipitation assay with normal mouse IgG (IgG) or Lyn antibody (Lyn). The immunoprecipitates were then immunoblotted with FcγRIIb and Lyn antibodies.

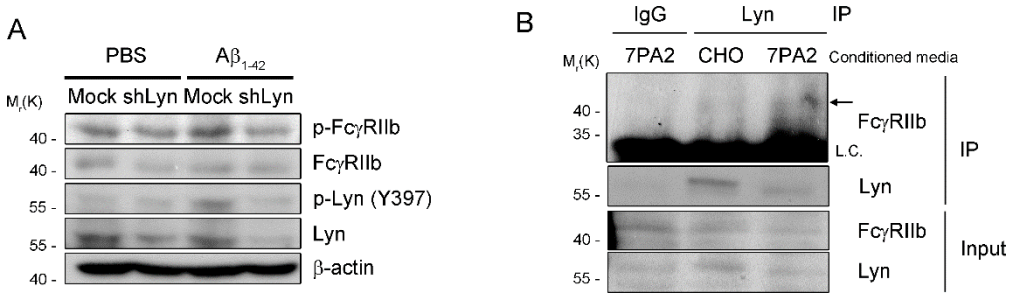
A
PBS
Aβ1-42
Mock shLyn Mock shLyn
Mr(K)
40 -
40 -
55 -
55 -
40 -
p-FcγRIIb
FcγRIIb
p-Lyn (Y397)
Lyn
β-actin
B
IgG
Lyn
IP
Mr(K)
7PA2
CHO
7PA2
Conditioned media
40 -
35 -
55 -
40 -
55 -
FcγRIIb
L.C.
Lyn
FcγRIIb
Lyn
IP
Input

Figure II-3. Reduced expression of Lyn suppresses $A\beta_{1-42}$-induced neuronal cell death.

Inhibition of $A\beta_{1-42}$-induced cell death by silencing Lyn expression. B103 cells (A) and HT22 cells (B) were transfected with pSUPER-neo (Mock) or pLyn shRNA (shLyn) for 24 h and then exposed to PBS or 5 μM $A\beta_{1-42}$ for 36 h. Cells which had apoptotic fragmented nuclei characterized by EtHD were considered as dead cells (*left*). Bars represent mean ± SD (n = 3). Cell extracts were prepared and immunoblotted with p-Lyn (Y397), Lyn and β-actin antibodies (*right*). $^{**}P < 0.005$.

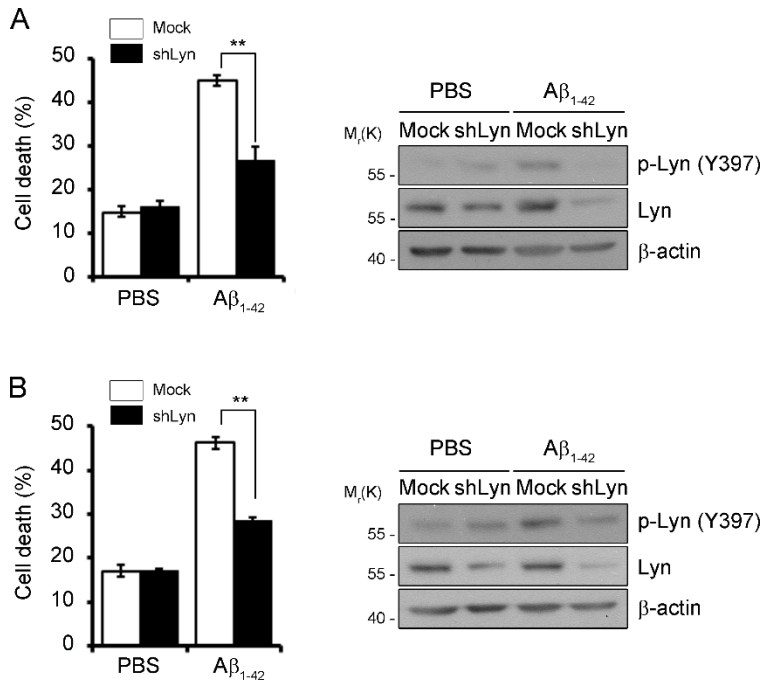
A
Mock
shLyn
**
Cell death (%)
50
40
30
20
10
0
PBS
Aβ1-42
PBS
Aβ1-42
Mr(K)
Mock shLyn Mock shLyn
55 -
55 -
40 -
p-Lyn (Y397)
Lyn
β-actin
B
Mock
shLyn
**
Cell death (%)
50
40
30
20
10
0
PBS
Aβ1-42
PBS
Aβ1-42
Mr(K)
Mock shLyn Mock shLyn
55 -
55 -
40 -
p-Lyn (Y397)
Lyn
β-actin

Figure II-4. Co-crystal structure of kinase domain of Lyn with KICG2576.

(A) Ribbon representation of the crystal structure of Lyn kinase domain. The N- and C-lobes are colored in green and cyan, respectively. The hinge region is colored in yellow and the activation loop in orange. (B) Hydrogen and hydrophobic interactions between the inhibitor KICG2576 and Lyn kinase domain in the active site. (In collaboration with CrystalGenomics Inc.)

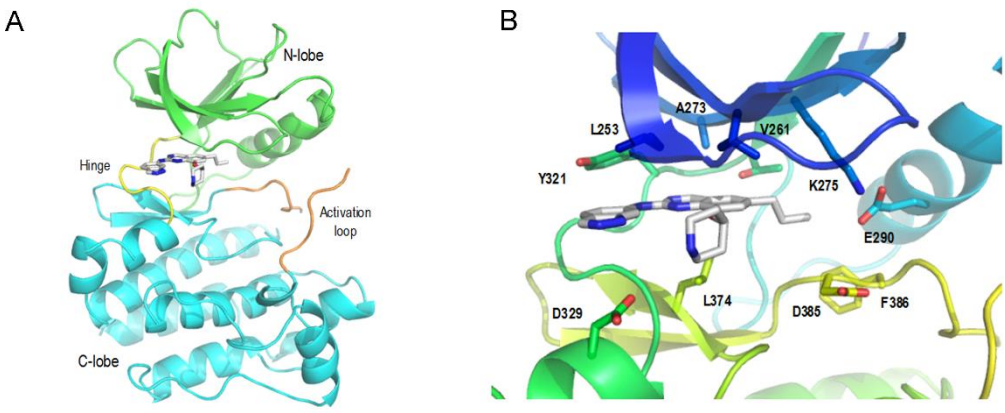
A
N-lobe
Hinge
Activation loop
C-lobe
B
A273
L253
V261
Y321
K275
E290
L374
D329
D385
F386

Figure II-5. Effective inhibition of Lyn by KICG2576.

(A) *In vitro* kinase assay showing dose-dependent inhibition of Lyn kinase activity by KICG2576. HT22 cells were treated with DMSO or the indicated concentrations of KICG2576 or LynK-in#25 (#25, negative control) for 24 h. Cell lysates were subjected to immunoprecipitation assay with pre-immune serum (Pre) or Lyn antibody (Lyn). The immunoprecipitates were incubated with dephosphorylated casein and the reaction mixtures were immunoblotted with p-Tyr (Top, short and long) and Lyn antibodies (middle). Casein was stained with Coomassie (bottom). (B) Inhibition of $A\beta_{1-42}$-induced auto-phosphorylation at tyrosine 397 of Lyn by KICG2576. SH-SY5Y cells were pre-treated with DMSO or 0.5 μM KICG2576 for 2 h and then incubated with PBS or 5 μM $A\beta_{1-42}$ for 12 h. Cell extracts were immunoblottted with p-Lyn (Y397), Lyn and β-actin antibodies.

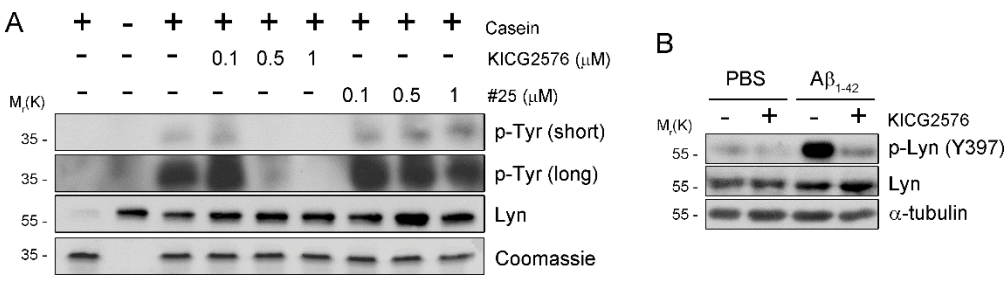
A
Casein
KICG2576 (μM)
#25 (μM)
M_r(K)
35 -
35 -
55 -
35 -
p-Tyr (short)
p-Tyr (long)
Lyn
Coomassie
B
PBS
Aβ1-42
KICG2576
M_r(K)
55 -
55 -
55 -
p-Lyn (Y397)
Lyn
α-tubulin

Figure II-6. Suppression of $A\beta_{1-42}$-evoked cell death by KICG2576.

(A) Protection of Aβ-triggered cell death by KICG2576. HT22 cells were pre-treated with the indicated concentrations of each compound (KICG2576 and #25: LynK-in#25) for 2 h and then exposed to DMSO or 5 μM $A\beta_{1-42}$ for 36 h in the presence of those molecules. Cell death was measured by trypan blue exclusion assay. Bars represent mean ± SD (n = 3). (B) Comparison of KICG2576 to PP1 in aspect with their protective ability against $A\beta_{1-42}$. HT22 cells were pre-treated with the indicated concentrations of pyrazolopyrimidine1 (PP1) and KICG2576 for 2 h and then exposed to DMSO or 5 μM $A\beta_{1-42}$ for 36 h in the presence of those molecules. Cell death was assessed as in (A). Bars represent mean ± SD (n = 3). $^{\#}P < 0.005$ versus PBS with DMSO-treated sample (PBS). $^{**}P < 0.005$, $^{***}P < 0.0005$ versus $A\beta_{1-42}$ with DMSO-treated sample (DMSO). NS; not significant.

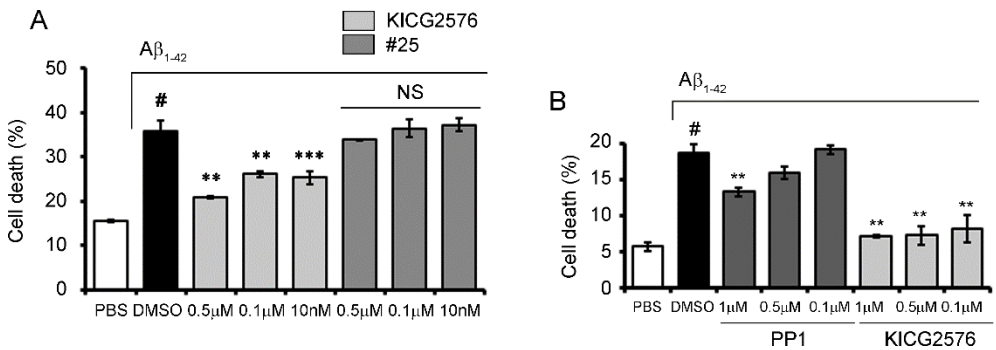
A
KICG2576
#25
Aβ1-42
NS
Cell death (%)
50
40
30
20
10
0
#
**
**
***
PBS DMSO 0.5μM 0.1μM 10nM 0.5μM 0.1μM 10nM
B
Aβ1-42
Cell death (%)
20
15
10
5
0
#
**
**
**
**
PBS DMSO 1μM 0.5μM 0.1μM 1μM 0.5μM 0.1μM
PP1
KICG2576

Figure II-7. Suppression of $A\beta_{1-42}$-induced neuronal death by KICG2576.

Primary cortical neurons at DIV 5 were pre-treated with DMSO or the indicated concentrations of each compounds (KICG2576 and #25: LynK-in#25) for 2 h and then incubated with 5 μM $A\beta_{1-42}$ for 48 h. Cell death was assessed by trypan blue exclusion assay. Results represent mean ± SD (n=3) (*Left*). $^{\#}P < 0.005$ versus PBS with DMSO-treated sample (PBS). $^{*}P < 0.05$, $^{**}P < 0.005$ versus $A\beta_{1-42}$ with DMSO-treated sample (DMSO). Cell lysates were immunoblotted with cleaved caspase-3, p-Lyn (Y397) and α-tubulin antibodies (*right*).

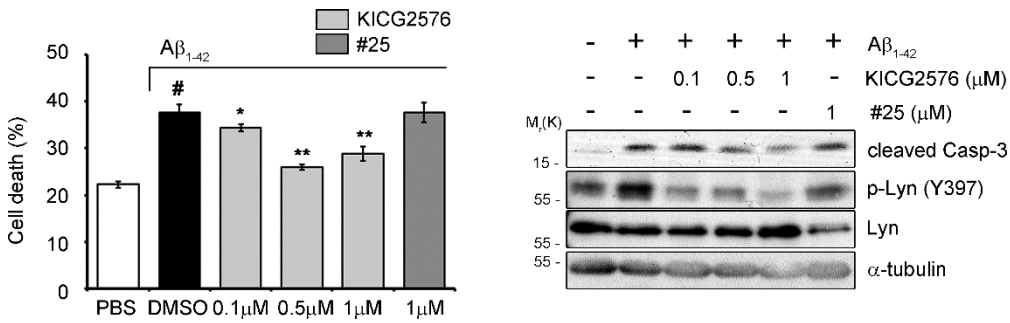
KICG2576
#25
Aβ1-42
Cell death (%)
50
40
30
20
10
0
#
*
**
**
PBS
DMSO
0.1μM
0.5μM
1μM
1μM
- + + + + + Aβ1-42
- - 0.1 0.5 1 - KICG2576 (μM)
- - - - - 1 #25 (μM)
Mr(K)
15 -
55 -
55 -
55 -
cleaved Casp-3
p-Lyn (Y397)
Lyn
α-tubulin

Figure II-8. KICG2576 does not affect apoptosis triggered by TNF-α or etoposide.

HT22 cells were treated with DMSO or 0.5 μM KICG2576 for 2 h and then incubated with 30 ng/ml TNF-α with 10 μg/ml cyclohexamide (CHX) for 6 h or 25 μM etoposide for 12 h. Results represent the mean ± SD (*n*=3).

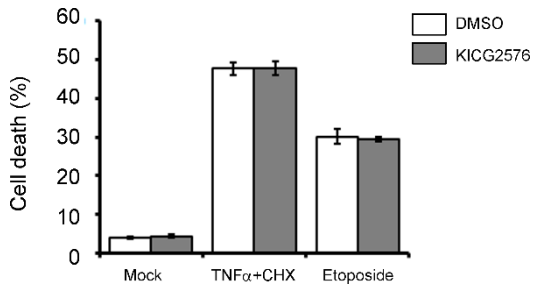
60
50
40
30
20
10
0
Cell death (%)
DMSO
KICG2576
Mock
TNFα+CHX
Etoposide

Figure II-9. Suppression of FcγRIIb-induced cytotoxic signaling by KICG2576.

(A) Inhibition of FcγRIIb-mediated cell death by KICG2576. HT22 cells were incubated with DMSO, 0.5 μM KICG2576 or LynK-in#25 (#25) and transfected with pEGFP-N1 (Mock) or pFcγRIIb-EGFP (FcγRIIb) for 36 h. Cells with apoptotic fragmented nuclei characterized by EtHD were considered as dead cells. Results represent mean ± SD (n = 3). $^{**}P < 0.005$. (B) Suppression of FcγRIIb tyrosine phosphorylation at ITIM by KICG2576. SH-SY5Y cells were pre-treated with the indicated concentrations of KICG2576 or LynK-in#25 for 2 h and transfected with pFcγRIIb-EGFP for additional 24 h. Cell lysates were immunoblotted using p-FcγRIIb, GFP, p-Lyn (Y397), Lyn, and α-tubulin antibodies.

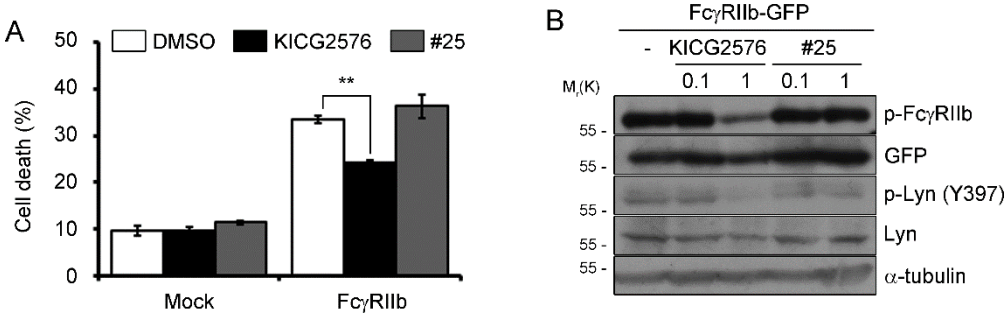
A
DMSO
KICG2576
#25
Cell death (%)
50
40
30
20
10
0
**
Mock
FcγRIIb
B
FcγRIIb-GFP
- KICG2576 #25
0.1 1 0.1 1
M_r(K)
55 -
55 -
55 -
55 -
55 -
p-FcγRIIb
GFP
p-Lyn (Y397)
Lyn
α-tubulin

Figure II-10. KICG2576 prevents intracerebroventricularly injected $A\beta_{1-42}$-induced behavioral alteration.

(A-C) Memory defects initiated by *i.c.v.* $A\beta_{1-42}$ was suppressed by KICG2576 in mice. WT mice (5-week-old; 3-6 mice per group) were *i.c.v.*-injected with PBS or $A\beta_{1-42}$ (410 pm) alone or together with KICG2576 (molar ratio with 1:3). After two and ten days, spatial memory of mice was analyzed using Y-maze test. Graphs represent the reversible memory impairment of *i.c.v*. $A\beta_{1-42}$-injected mice after 22 days in Y-maze test (B). Object recognition memory was reflected by the percentage of time that each group of mice spent exploring a familiar versus a novel object (C). Values represent mean ± SEM of all independent experiments. $*P < 0.05$.

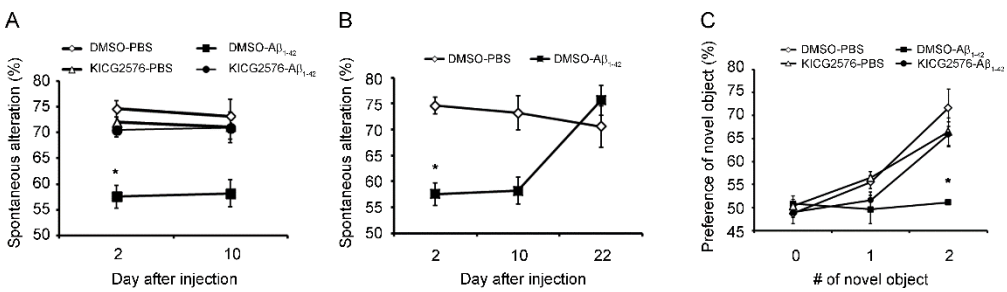
A
DMSO-PBS
DMSO-Aβ1-42
KICG2576-PBS
KICG2576-Aβ1-42
Spontaneous alteration (%)
80
75
70
65
60
55
50
2
10
Day after injection
B
DMSO-PBS
DMSO-Aβ1-42
Spontaneous alteration (%)
80
75
70
65
60
55
50
2
10
22
Day after injection
C
DMSO-PBS
DMSO-Aβ1-2
KICG2576-PBS
KICG2576-Aβ1-42
Preference of novel object (%)
80
75
70
65
60
55
50
45
0
1
2
# of novel object

Figure II-11. Lyn is activated in the hippocampus of AD patients.

(A) Activation of Lyn in the hippocampus of AD patients. Hippocampal lysates from normal individuals and AD patients were immunoblotted using p-Lyn (Y397), Lyn and β-actin antibodies. (B) Graph depicts the densitometric analysis of the blots in upper panel. Bars represent mean ± SD. *$P < 0.05$, NS; not significant.

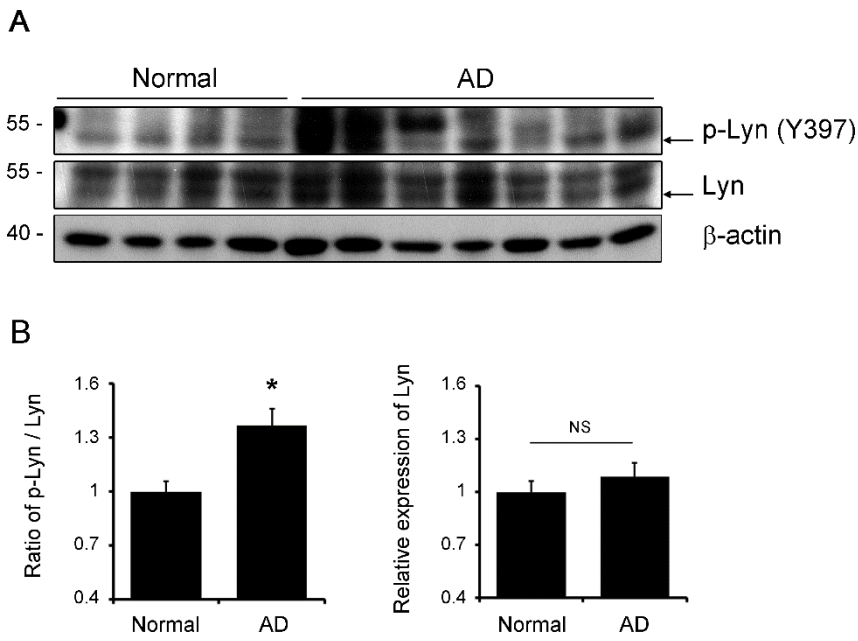
A
Normal
AD
55 -
55 -
40 -
p-Lyn (Y397)
Lyn
β-actin
B
Ratio of p-Lyn / Lyn
1.6
1.3
1
0.7
0.4
*
Normal
AD
Relative expression of Lyn
NS

Figure II-12. KICG2576 modulates expression of inflammatory cytokines by $A\beta_{1-42}$ in BV-2 microglial cells.

BV-2 cells were pre-incubated with DMSO or 0.5 μM KICG2576 (2576) for 4 h and then treated with 2 μM $A\beta_{1-42}$ or 1 μg/ml lipopolysaccharide (LPS) for 6 h. Cell lysates were prepared and subjected to RT-PCR analysis using synthetic primers of MCP-1, TNF-α, CD11b, and β-actin.

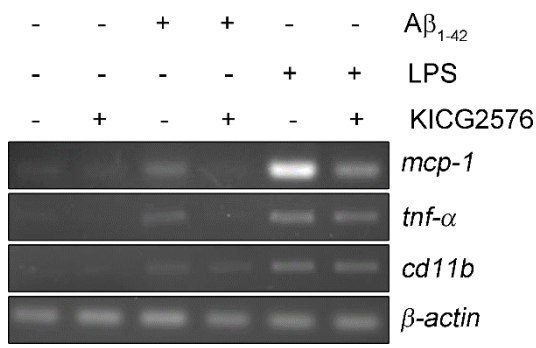
- - + + - - Aβ1-42
- - - - + + LPS
- + - + - + KICG2576
mcp-1
tnf-α
cd11b
β-actin

Table II-1. Crystallographic data collection and refinement statistics of KICG2576-Lyn kinase domain.

Data Collection	Lyn with KICG2576
Space group	R3
Unit cell *a, b, c* (Å), x(°)	128.864, 128.864, 55.123, 120
Resolution range (Å)	50.00-2.55
Observations	45198
Unique reflections	10941
Completeness (%)	98.3 (93.5)
Data redundancy	4.10 (2.60)
R_{sym}[1] (%)	7.4 (43.8)
I/σ (I)	19.8 (1.75)
Refinement	
Resolution range	50-2.6
R_{cryst}[2] (%)	23.1
R_{free}[3] (%)	29.4
Number of all atoms	2133
R.m.s.d.[4] bond lengths (Å)	0.0088
R.m.s.d.[4] bond angles (Å)	1.331

Values in parentheses are for highest-resolution shell. The data were obtained using one crystal.

[1] $R_{sym} = \sum_h \sum_i |\mathbf{I}_{h,i} - \langle \mathbf{I}_{h,i} \rangle| / \sum_h \sum_i \sum_{h,i}$ for the intensity of (**I**) of *i* observations of reflection *h*.

[2] $R_{cryst} = \sum |\mathbf{F}_{obs} - \mathbf{F}_{calc}| / \sum |\mathbf{F}_{obs}|$, where $\mathbf{F}_{obs}$ and $\mathbf{F}_{calc}$ are the observed and calculated structure factors. respectively.

[3] R_{free} = R-factor calculated using 5% of the reflections data chosen randomly and omitted from the start of refinement.

[4] Root-mean-square deviations from ideal geometry.

Discussion

Though signaling cascades mediated by tyrosine kinase have been studied for a long time, their contribution in the pathogenesis of AD is not clear. However, their role is thought to be critical in AD pathogenesis in that several tyrosine kinase inhibitors, including Gleevec and STI571, have been reported to be beneficial to AD pathology (Cancino et al., 2008; Dhawan et al., 2012; Lonskaya et al., 2013; Netzer et al., 2003). Here I report that Lyn, a member of SFK, is involved in the pathogenesis of AD by regulating $A\beta_{1-42}$-FcγRIIb pathway.

Although several receptors about $A\beta_{1-42}$ such as receptor for advanced glycosylation end products (RAGE) and cellular prion protein (PRNP) have been isolated and their contributions to $A\beta_{1-42}$-neurotoxicity are well-established, there are no therapeutic approaches using molecular targets based on their downstream pathway (Lauren et al., 2009; Yan et al., 1996). Moreover, limitation of RAGE inhibition for AD therapy confirmed by ineffective result of clinical trial about PF-04494700, an oral inhibitor of RAGE, suggests the need for novel targets of drug development (Sabbagh et al., 2011). Even though KICG2576 has much room for improvement about accessibility across blood-brain barrier (BBB) and selectivity, our data imply that blockade of $A\beta_{1-42}$-

FcγRIIb signaling through Lyn inhibition can be a good alternative for the attempt to AD therapeutics.

While Lyn is known to mediate signaling cascades initiated by several immunoreceptors and inflammation signal in immune cells, increasing evidences suggest that Lyn also plays a crucial role in neuroinflammation which is an important feature of AD pathology. In the brain, Lyn delivers $A\beta_{1-42}$-initiated inflammatory signaling in microglia and activates NF-κB pathway to produce cytokines, leading to exacerbate the symptoms of AD (Querfurth and LaFerla, 2010; Stewart et al., 2010). Consistently, I also confirmed that induction of inflammatory cytokines by $A\beta_{1-42}$ was reduced under treatment of KICG2576 in BV-2 microglia cells (Figure II-12). Moreover, I first identified the neural role of Lyn in neurodegenerative disease in this study. Though I concentrated the effect of $A\beta_{1-42}$-induced Lyn activation in aspect of neuronal death, there are enough possibilities of relevance of Lyn to other neuronal malfunctions involved in AD. Follow-up studies about the specific events encouraged by Lyn activation will provide an elaborated view of neurodegenerative mechanisms.

Fyn, a member of SFK, is highly homologous to Lyn and much of its function overlaps with Lyn in that functional complementation is attained by Fyn in Lyn-deficient mice (Odom et al., 2004). Recent study shows that Fyn is required for

$A\beta_{1-42}$ neurotoxicity mainly through the excitotoxicity mediated by NMDA receptor (Um et al., 2012). Because all members of SFK share common regulatory mechanism which determines the phosphorylation status of C-terminal regulatory domain, it is plausible that both Lyn and Fyn are activated by $A\beta_{1-42}$. In contrast to complementary function in immune cells, however, it appears that Fyn and Lyn are differently activated during $A\beta_{1-42}$ toxicity in neuronal cells. Fyn is transiently activated within 1 h after $A\beta_{1-42}$ treatment, whereas the activation of Lyn lasts for 36 h (Um et al., 2012). Considering that the expression and phosphorylation of FcγRIIb are induced by $A\beta_{1-42}$ for more than 24 h in neuronal cells (Kam et al., 2013), the prolonged activation of Lyn may potentiate $A\beta_{1-42}$ neurotoxicity through FcγRIIb.

Since kinase domains of individual SFK family members are highly conserved, it is difficult to develop a selective inhibitor of them. Actually, PP1 and PP2, other commercial inhibitors of SFK, prohibit not only Lyn but also all SFKs at the concentration over 10 μM (Summy et al., 2005). However, both compounds have some "off-target" kinases at these concentrations. In this study, I characterized KICG2576, a highly efficient inhibitor of Lyn by combining structure-based drug design and high-throughput screening (HTS). Fortunately, I discovered that KICG2576 effectively inhibits $A\beta_{1-42}$-neurotoxicity at sub-micromolar concentrations on the contrary to PP1 (Figure II-6B). High

efficiency of KICG2576 in low concentration is advantageous in that non-selective inhibition of other kinases like p38 and MEK1 provoked by micromolar usage of PP1 can be avoided (Bain et al., 2003). However, I cannot exclude the cross-reactivity of KICG2576 with other SFKs. Thus, it is required to further develop more specific Lyn inhibitor, though this study shows that Lyn is required for $A\beta_{1-42}$-neurotoxicity *in vitro* and *in vivo*, and provide a potential of new target for drug development,

I isolated KICG2576 as a novel inhibitor of Lyn. KICG2576 effectively inhibits Lyn activity *in vitro* and in cells. However, KICG2576 exhibits low accessibility of BBB. That is why I tried to analyze the effect of KICG2576 on $A\beta_{1-42}$-neurotoxicity *in vivo* using *i.c.v*. injection assay as the second best try. Because I found positive effect of brain-injected KICG2576 in several behavior tests, it is necessary to characterize derivatives of KICG2576 which exhibit more hydrophobicity and lower molecular weight to acquire improved BBB entrance.

In conclusion, I demonstrate that Lyn is implicated in the pathogenesis of AD by mediating $A\beta_{1-42}$-FcγRIIb signaling. In addition, I provide insight of Lyn inhibition as an alternative AD therapeutic development.

Materials and methods

Reagents

Synthetic human $A\beta_{1-42}$ peptide (Sigma-Aldrich®, MO, U.S.A.), dephosphorylated casein (Sigma-Aldrich®), PP1 (Calbiochem®, Darmstadt, Germany), and sodium orthovanadate (Na_3VO_4: Sigma-Aldrich®) were purchased.

Plasmid construction

The cDNA of human FcγRIIb variant 2 was subcloned into pEGFP-N1 (Clontech, CA, U.S.A.) (pFcγRIIb-EGFP). FcγRIIb-ΔC, ΔITIM, and ΔCyto deletion mutants were generated by PCR and the PCR products were inserted into pEGFP-N1 (pFcγRIIb ΔC-EGFP, pFcγRIIb ΔITIM-EGFP, and pFcγRIIb ΔCtyo-EGFP, respectively). FcγRIIb Y273F mutant was generated by site-directed mutagenesis. To make shRNA construct of Lyn (pLyn shRNA), oligonucleotides containing gene-specific sequences (5′- GGG AAG TCT GGA TGG GTT A-3′) were annealed and ligated into *Bgl*II and *Hin*dIII sites of pSUPER.neo (OligoEngine, WA, U.S.A.). The C-terminal segment (human Lyn kinase, residues 239–512) containing the kinase domain was inserted into pFastBacHTa vector (Invitrogen) to generate pFastBacHTa-hLyn.

Preparation of $A\beta_{1-42}$

Synthetic human $A\beta_{1-42}$ peptide was dissolved in DMSO at 2.2 mM and further diluted in PBS at 250 μM. Diluted $A\beta_{1-42}$ was incubated at 4 °C for 48 h and then stored at -70 °C until use. Naturally secreted $A\beta_{1-42}$ was acquired as described (Kam et al., 2013). Briefly, Chinese hamster ovary cells stably expressing human APP_{751} with Val717Phe mutation, provided kindly by Dr. D. J. Selkoe (Harvard Medical School), were grown to approximately ~90 % confluence. Then, cells were washed with PBS and further cultured for ~16 h in serum-free DMEM. The conditioned media were collected and centrifugated at 1000 g to remove cell debris. Supernatants were concentrated ~10-fold using YM-3 Centriprep filters (Millipore).

Cell culture and DNA transfection

B103 rat neuroblastoma cells, HT22 mouse hippocampal cells, SH-SY5Y human neuroblastoma cells, CHO Chinese hamster ovary cells, and BV-2 mouse microglial cells were cultured in Dulbecco's modified eagle medium (DMEM; Hyclone®, UT, U.S.A.) replenished with 10 % (v/v) fetal bovine serum (FBS; Hyclone®). Mouse cortical primary neurons were cultured as described

previously (Park et al., 2012). Briefly, mouse brain cortical tissue from embryonic day 16 was isolated and triturated using Trypsin-EDTA (Gibco®, NY, U.S.A.). Cortical neurons were placed on the poly-L-Lysine (Sigma-Aldrich®)-coated culture plates and maintained in Neurobasal medium (Gibco®) supplemented with 2 % B-27 (Invitrogen™, CA, U.S.A.) and 0.5 mM L-glutamine (Invitrogen™). B103, HT22, and SH-SY5Y cells were transfected with appropriate DNA using Polyfect reagent (Qiagen, CA, U.S.A.) according to the manufacturer's protocol.

Reverse transcription-PCR

Total RNAs were purified from $A\beta_{1-42}$ or LPS-stimulated BV-2 cells using TRI reagent® (MRC Inc., OH, U.S.A.) according to the manufacturer's instruction. Cytokine RNAs were identified by PCR with cytokine-specific synthetic primers after synthesis of cDNA with M-MLV reverse transcriptase (Enzynomics™, Daejeon, South Korea). The sequences used for PCR are as follows; MCP-1, sense 5'- CCT GCT GTT CAC AGT TGC C - 3', and antisense 5′-TGA GGT GGT TGT GGA AAA GG-3′; TNF-α, sense 5′-TTC TGT CTA CTG AAC TTC GGG GTG ATC GGT CC-3′, and antisense 5′-GTA TGA GAT AGC AAA TCG GCT GAC GGT GTG GG -3′; CD11b, sense 5′-CAG ATC AAC AAT GTG ACC GTA TGG G-3′, and antisense 5′-CAT CAT GTC CTT

GTA CTG CCG CTT G-3′; β-actin, sense 5′-ATG GGG AAG GTG AAG GTC GGA-3′, and antisense 5′-CCA TGA CGA ACA TGG GGG CAT-3′.

Western blotting and antibodies

The following antibodies were used for western blot analysis; p-Lyn (1645-5), and p-FcγRIIb (2308-1) (Epitomics, Inc. CA, U.S.A.), Lyn (sc-15), GFP (sc-8334), and β-actin (sc-47778) (Santa Cruz biotechnology, CA, U.S.A.), FcγRIIb (ab45143: Abcam, MA, U.S.A.), and cleaved caspase-3 (#9661, Cell signaling, MA, U.S.A.). Generally, cell extracts were dissolved with ice-cold RIPA buffer [50 mM Tris-Cl pH 7.5, 30 mM NaCl, 1 % Triton-X100, 0.5 % sodium deoxycholate, 0.1 % sodium dodecyl sulfate (SDS), 1 mM phenylmethylsulfonyl fluoride (PMSF), and 1 mM Na_3VO_4]. After brief centrifugation, the supernatant was subjected to SDS-polyacrylamide gel electrophoresis (PAGE), and transferred to polyvinylidene fluoride (PVDF) membrane using Semi-Dry transfer cell (Bio-Rad, CA, U.S.A.). Blots were blocked by 3 % (w/v) BSA solution in TBS-T [10 mM Tris-Cl pH 8.0, 150 mM NaCl, 0.5 % (v/v) Tween-20] and subjected to western blot analysis. Immunoreactive blots were detected by using chemiluminescence method.

Immunoprecipitation assay

SH-SY5Y cells were lysed with 0.5X RIPA buffer (25 mM Tris-Cl pH 7.5, 15 mM NaCl, 0.5 % Triton-X100, 0.25 % sodium deoxycholate, 0.05 % SDS, 1 mM PMSF, and 1 mM Na_3VO_4). After centrifugation at 12000rpm, the supernatant was incubated with 2 μg of mouse normal IgG or Lyn antibody (sc-15) for overnight at 4 °C. After adding 30 μl protein G bead (GE Healthcare), mixtures were incubated for additional 2 h at 4 °C. Proteins bound to Protein G bead were pulled down by centrifugation after three times of washes and analyzed by western blotting.

Cell death assessment

Cell death rates were determined as described previously (Oh et al., 2012), In brief, cells were exposed to various stimuli and cell death was assessed by counting cells showing apoptotic fractured nucleic characterized by ethidium homodimer-1 (Molecular Probes, OR, USA) under a fluorescence microscope (Olympus, Tokyo, Japan). In other way, dead cells were counted after staining with 2 % trypan blue under a microscope.

***In vitro* kinase assay**

In vitro kinase assay of Lyn was conducted as depicted previously (Young et al., 2003). Briefly, HT22 cells were solubilized with 0.5 X RIPA buffer. After centrifugation at 12000rpm, the supernatant was subjected to immunoprecipitation assay using pre-immune serum or Lyn antibody (sc-15). The immunoprecipitates were then mixed with dephosphorylated casein (1 μg/μl) in kinase assay buffer (20 mM Tris-Cl pH 7.5, 10 mM $MgCl_2$, 1 mM ATP, 1 mM Na_3VO_4) and incubated for 15 min at 30 °C. Reaction was quenched by adding 5X non-reducing SDS sample buffer [60 mM Tris-Cl pH 7.5, 2 % SDS, 25 % (v/v) glycerol] and mixtures were subjected to SDS-PAGE. The blots were analyzed with western blotting using p-Tyr (PY69, Santa Cruz biotechnology) and Lyn (sc-15) antibodies or stained with coomassie blue for casein.

Protein expression and purification of Lyn kinase domain

DH10Bac competent cells were transformed with the pFastBacHTa-hLyn to prepare the recombinant bacmid according to the instruction for Bac-to-Bac baculovirus expression systems (Invitrogen^{TM}). Sf21 (*Spodoptera frugiperda*) insect cells were transfected with the recombinant bacmid containing pFastBacHTa-hLyn using Cellfectin reagent (Invitrogen^{TM}) in medium A (Grace's insect cell culture medium, TNM-FH and antibiotic–antimycotic

reagent). The insect cells were grown at 27.5 °C and the baculovirus were harvested at 72 h after transfection. For protein production, High Five (*Trichopulsia ni*) insect cells were infected with baculovirus, incubated in medium B (HyClone® SFX-Insect MP and antibiotic–antimycotic reagent) for 48 h at 27.5 °C, harvested by centrifugation, and then frozen at -70 °C until purification.

Purification was carried out at 4 °C unless otherwise stated and details of purification are described as follows. Frozen cells were thawed and suspended in buffer A [50 mM Tris-HCl pH 7.5, 5 % (v/v) glycerol, 200 mM NaCl, 2 mM DTT] containing 1 mM PMSF and complete protease inhibitors mixture (Roche Applied Sciences). Cells were disrupted by sonication and then cell lysate was then centrifuged at 35,000*g* for 1 h. The supernatant was filtered and loaded on a 5 ml Ni-NTA column (Histrap HP, GE healthcare) pre-equilibrated with buffer A. After washing the column with buffer A and again with the buffer A containing 20 mM imidazole, proteins were eluted with buffer A containing linear gradient of imidazole (20-500 mM). Lyn-containing fractions were pooled and treated with TEV protease overnight to cleave the His6 tag. Lyn kinase proteins were concentrated to 5ml and loaded on a gel filtration column (HiLoad 16/60 Superdex 75 prep grade, GE healthcare) pre-equilibrated with buffer B (50 mM Tris-HCl, pH 8.0, 100 mM NaCl, 2 mM DTT). Lyn-containing

fractions were pooled and loaded on anion-exchange column (Mono Q, GE Healthcare) followed by elution with a linear gradient of 500 mM NaCl in buffer C. Purified Lyn proteins were concentrated to 9 mg/ml for crystallization.

Crystallization and data collection

Lyn kinase protein (1 µl) was mixed with same volume of reservoir solution (23% PEG3350, 0.1 M NaCl and 0.1 M HEPES pH 7.5). Apo crystals of Lyn kinase domain were grown at 4 °C by vapor diffusion using the hanging-drop method. The complex crystals of the proteins with inhibitors were obtained by soaking the apo crystals in the reservoir solution with 1 mM inhibitor solution for 24 h. Prior to X-ray data collection, the crystals were transferred to the cryoprotectant solution for a few seconds and frozen in a stream of liquid nitrogen at 100K. The X-ray diffraction data was collected at 4A beam line of Pohang Light Source (PLS) and processed and scaled using HKL2000 (Otwinowski and Minor, 1997). A diffraction data of a crystal belongs to the rhombohedral space group R3 with one molecule per asymmetric unit.

Structure determination and refinement

The structure of Lyn was solved by molecular replacement using kinase domain

of Lyn (PDB code: 2ZV7) as an initial model. Refinement of the structure was carried out with the program CNS (Brunger et al., 1998) and manual model building was performed using the program QUANTA [Accelrys, Inc (San Diego, USA)]. Subsequent rounds of model adjustment, simulated annealing, and thermal parameter refinement were performed. A *Fo-Fc* electron density corresponding to the inhibitor was shown clearly after a full domain model of Lyn was built. Position of the inhibitor was determined based on *Fo-Fc* map. Quality of the refined structure was validated by using PROCHECK (Laskowski et al., 1993). Crystallographic data collection and refinement statistics are summarized in Table II-1.

Intracerebroventricular (*i.c.v*) injection of $A\beta_{1-42}$ and behavior tests

Intracerebroventricular injection of $A\beta_{1-42}$ and Y-maze task were performed as described previously (Yan et al., 2004). Novel object recognition task was examined as described (Tang et al., 1999). $A\beta_{1-42}$ (2 μg) was administrated into *i.c.v.* region of 5-week-old mouse using Hamilton microliter #702 syringe (Hamilton, NV, U.S.A.) equipped with 26-gauge needle. These tests were accomplished in accordance with the regulations of the Animal Care and Use Committee of Seoul National University.

Statistical analysis

Data are expressed as mean ± SD or SEM as indicated. Differences between two means were analyzed by Student's t-test.

References

Bain, J., MacLauchlan, H., Elliott, M., Cohen, P. (2003). The specificities of protein kinase inhibitors: an update. Biochem. J. *371*, 199-204.

Bertram, L., Lill, C. M., Tanzi, R. E. (2010).The genetics of Alzheimer's disease: back to the future. Neuron *68*, 270-281.

Bolland, S., Ravetch, J.V. (2000). Spontaneous autoimmune disease in FcγRIIb-deficient mice results from strain-specific epistasis. Immunity *13*, 277-285.

Brunger, A. T., Adams, P. D., Clore, G. M., DeLano, W. L., Gros, P., Grosse-Kunstleve, R. W., Jiang, J. S., Kuszewski, J., Nilges, M., Pannu, N. S., Read, R. J., Rice, L. M., Simonson, T., Warren, G. L. (1998). Crystallography & NMR system: a new software suite for macromolecular structure determination. Acta Cryst. D Biol. Crystallogr. *54*, 905-921.

Cancino, G. I., Toledo, E. M., Leal, N. R., Hernandez, D. E., Yevenes, L. F., Inestrosa, N. C., Alvarez, A. R. (2008). STI571 prevents apoptosis, tau phosphorylation and behavioural impairments induced by Alzheimer's beta-amyloid deposits. Brain *131*, 2425-2442.

Carter, R. H., Park, D. J., Rhee, S. G., Fearon, D. T. (1991). Tyrosine phosphorylation of phospholipase C induced by membrane immunoglobulin in B lymphocytes. Proc. Natl. Acad. Sci. U.S.A. *88*, 2745-2749.

Chan, V. W., Lowell, C. A., DeFrance, A. L. (1998). Defective negative regulation of antigen receptor signaling in Lyn-deficient B lymphocytes. Curr. Biol. *8*, 545-553.

Dhawan, G., Floden, A. M., and Combs, C. K. (2012). Amyloid-beta oligomers stimulate microglia through a tyrosine kinase dependent mechanism. Neurobiol. Aging *33*, 2247-2261.

Haass, C., and Selkoe, D. J. (2007). Soluble protein oligomers in neurodegeneration: lessons from the Alzheimer's amyloid beta-peptide. Nat. Rev. Mol. Cell. Biol. *8*, 101-112.

Hardy, J., and Selkoe, D. J. (2002). The amyloid hypothesis of Alzheimer's disease: progress and problems on the road to therapeutics. Science *297*, 353-356.

Hibbs, M. L., Tarlinton, D. M., Armes, J., Grail, D., Hodgson, G., Maglitto, R., Stacker, S. A., Dunn, A. R. (1995). Multiple defects in the immune system of Lyn-deficient mice, culminating in autoimmune disease. Cell *83*, 301-311.

Hirao, A., Hamaguchi, I., Suda, T., Yamaguchi, N. (1997). Translocation of the Csk homologous kinase (Chk/Hyl) controls activity of CD36-anchored Lyn tyrosine kinase in thrombin-stimulated platelets. EMBO. J. *16*, 2342-2351.

Jacob, A., Cooney, D., Tridandapani, S., Kelley, T., Coggeshall, K. M. (1999). FcγRIIb modulation of surface immunoglobulin-induced Akt activation in murine B cells. J. Biol. Chem. *274*, 13704-13710.

Kam, T. I., Song, S., Gwon, Y., Park, H., Yan, J. J., Im, I., Choi, J. W., Choi, T. Y., Kim, J., Song, D. K., Takai, T., Kim, Y. C., Kim, K. S., Choi, S. Y., Choi, S., Klein, W. L., Yuan, J., Jung, Y. K. (2013). FcγRIIb mediates amyloid-β neurotoxicity and memory impairment in Alzheimer's disease. J. Clin. Invest. *123*, 2791-2802.

Laskowski, R. A., MacArthur, M. W., Moss, D. S. & Thornton, J. M. (1993). PROCHECK: a program to check the stereochemical quality of protein structures. J. Appl. Crystallogr. *26*, 283-291.

Lauren, J., Gimbel, D. A., Nygaard, H. B., Gilbert, J. W., Strittmatter, S. M. (2009). Cellular prion protein mediates impairment of synaptic plasticity by amyloid-beta. Nature *26*, 1128-1132.

Lesne, S., Koh, M. T., Kotilinek, L., Kayed, R., Glabe, C. G., Yang, A., Gallagher, M., Ashe, K. H. (2006). A specific amyloid-beta protein assembly in the brain impairs memory. Nature *440*, 352-357.

Lonskaya, I., Hebron, M. L., Desforges, N. M., Franjie, A., Moussa, C. E. (2013). Tyrosine kinase inhibition increases functional parkin-Beclin-1 interaction and

enhances amyloid clearance and cognitive performance. EMBO. Mol. Med. *5*, 1247-1262.

Netzer, W. J., Dou, F., Cai, D., Veach, D., Jeans, S., Li, Y., Bornmann, W. G., Clarkson, B., Xu, H., Greengard, P. (2003). Gleevec inhibits beta-amyloid production but not Notch cleavage. Proc. Natl. Acad. Sci. U.S.A. *100*, 12444-12449.

Nimmerjahn, F., Ravetch, J, V. (2008). Fcγ receptors as regulators of immune responses. Nat. Rev. Immunol. *8*, 34-47.

O'Brien, R. J., and Wong, P. C. (2011). Amyloid precursor protein processing and Alzheimer's disease. Annu. Rev. Neurosci. *34*, 185-204.

Odom, S., Gomez, G., Kovarova, M., Furumoto, Y., Ryan, J. J., Wright, H.V., Gonzalez-Espinosa, C., Hibbs, M. L., Harder, K. W., Rivera, J. (2004). Negative regulation of immunoglobulin E-dependent allergic responses by Lyn kinase. J. Exp. Med. *199*, 1491-1502.

Oh, Y., Jeon, Y. J., Hong, G. S., Kim, I., Woo, H. N., Jung, Y. K. (2012). Regulation in the targeting of TRAIL receptor 1 to cell surface via GODZ for TRAIL sensitivity in tumor cells. Cell Death Differ. *19*, 1196-1207.

Ono, M., Bolland, S., Tempst, P., Ravetch, J. V. (1996). Role of the inositol phosphatase SHIP in negative regulation of the immune system by the receptor

FcγRIIb. Nature *383*, 263-266.

Otwinowski Z., Minor W. (1997). Processing of X-ray diffraction data collected in oscillation mode. Methods Enzymol. *276*, 307-326.

Park, H., Kam, T. I., Kim, Y., Choi, H., Gwon, Y., Kim, C., Koh, J. Y., Jung, Y. K. (2012). Neuropathogenic role of adenylate kinase-1 in Aβ-mediated tau phosphorylation via AMPK and GSK3β. Hum. Mol. Genet. *21*, 2725-2737.

Podlisny, M. B., Walsh, D. M., Amarante, P., Ostaszewski, B. L., Stimson, E. R., Maggio, J. E., Teplow, D. B., Selkoe, D. J. (1998). Oligomerization of endogenous and synthetic amyloid beta-protein at nanomolar levels in cell culture and stabilization of monomer by Congo red. Biochemistry *37*, 3602–3611.

Querfurth, H. W., LaFerla, F. M. (2010). Alzheimer;s disease. N. Engl. J. Med. *28*, 329-344.

Reinhard, C., Hébert, S., S., De Strooper, B. (2005). The amyloid-beta precursor protein: integrating structure with biological function. EMBO. J. *24*, 3996-4006.

Roychaudhuri, R., Yang, M., Hoshi, M. M., and Teplow, D. B. (2009). Amyloid beta-protein assembly and Alzheimer's disease. J. Biol. Chem. *284*, 4749-4753.

Sabbagh, M. N., Agro, A., Bell, J., Aisen, P. S., Schweizer, E., Galasko, D.

(2011). PF-04494700, an oral inhibitor of receptor for advanced glycation end products (RAGE), in Alzheimer disease. Alzheimer. Dis. Assoc. Disord. *25*, 206-212.

Shankar, G. M., Li, S., Mehta, T. H., Garcia-Munoz, A., Shepardson, N. E., Smith, I., Brett, F. M., Farrell, M. A., Rowan, M. J., Lemere, C. A., Regan, C. M., Walsh, D. M., Sabatini, B. L., and Selkoe, D. J. (2008). Amyloid-beta protein dimmers isolated directly from Alzheimer's brains impair synaptic plasticity and memory. Nat. Med. *14*, 837-842.

Song, S., Lee, H., Kam, T. I., Tai, M. L., Lee, J. Y., Noh, J. Y., Shim, S. M., Seo, S. J., Kong, Y. Y., Nakagawa, T., Chung, C. W., Choi, D. Y., Oubrahim, H., Jung, Y. K. (2008). E2-25K/Hip-2 regulates caspase-12 in ER stress-mediated Aβ neurotoxicity. J. Cell Biol. *182*, 675-684.

Stewart, C. R., Stuart, L. M., Wilkinson, K., van Gils, J. M., Deng, J., Halle, A., Rayner, K. J., Boyer, L., Zhong, R., Frazier, W. A., Lacy-Hulbert, A., El Khoury, J., Golenbock, D. T., Moore, K. J. (2010). CD36 ligands promote sterile inflammation through assembly of a Toll-like receptor 4 and 6 heterodimer. Nat. Immunol. *11*, 155-161.

Summy, J. M., Trevino, J. G., Lesslie, D. P., Baker, C. H., Chakespeare, W. C., Wang, Y., Sundaramoorthi, R., Metcalf, C. A. 3rd, Keats, J. A., Sawyer, T. K.,

Gallick, G. E. (2005). AP23846, a novel and highly potent Src family kinase inhibitor, reduces vascular endothelial growth factor and interleukin-8 expression in human solid tumor cell lines and abrogates downstream angiogenic processes. Mol. Cancer. Ther. *4*, 1900-1911.

Tang, Y. P., Shimizu, E. Dube, G. R., Rampon, C., Kerchner, G. A., Zhuo, M., Liu, G., Tsien, J. Z. (1999). Genetic enhancement of learning and memory in mice. Nature *401*, 63-69.

Um, J. W., Nygaard, H. B., Heiss, J. K., Kostylev, M. A., Stagi, M., Vortmeyer, A., Wisniewski, T., Gunther, E. C., Strittmatter, S. M. (2012). Alzheimer amyloid-beta oligomer bound to postsynaptic prion protein activates Fyn to impair neurons. Nat. Neurosci. *15*, 1227-1235.

Walsh, D. M., Klyubin, I., Faddeeva, J. V., Cullen, W. K., Anwyl, R., Wolfe, M. S., Rowan, M. J., and Selkoe, D. J. (2002). Naturally secreted oligomers of amyloid beta protein potently inhibit hippocampal long-term potentiation *in vivo*. Nature *416*, 535-539.

Xu, Y., Harder, K. W., Huntington, N. D., Hibbs, M. L., Tarlington, D. M. (2005). Lyn tyrosine kinase: accentuating the positive and the negative. Immunity *22*, 9-18.

Yan, S. D., Chen, X., Fu, J., Chen, M., Zhu, H., Roher, A., Slattery, T., Zhao, L.,

Nagashima, M., Morser, J., Migheli, A., Nawroth, P., Stern, D., Schmidt, A. M. (1996). RAGE and amyloid-beta peptide neurotoxicity in Alzheimer's disease. Nature *22*, 685-691.

Yan, J. J., Kim, D. H., Moon, Y. S., Jung, J. S., Ahn, E. M., Baek, N. I., Song, D. K. (2004). Protection against beta-amyloid peptide-induced memory impairment with long-term administration of extract of *Angelica gigas* or decursinol in mice. Prog. Neuropsychopharmacol. Biol. Psychiatry *28*, 25-30.

Young, R. M., Holowka, D., Baird, B. (2003). A lipid raft environment enhances Lyn kinase activity by protecting the active site tyrosine from dephosphorylation. J. Biol. Chem. *278*, 20746-20752.

국문초록

아밀로이드 베타는 알츠하이머병의 병리적 특징인 세포외 노인성 플라크의 주 성분이며 다양한 경로를 통하여 신경세포에 독성을 야기한다. 몇몇 막 단백질이 아밀로이드 베타에 결합하여 신경독성회로를 유도하는 수용체로써 보고되어 왔다. FcγRIIb 는 아밀로이드 베타 올리고머의 수용체로써 작용한다. FcγRIIb 의 유전적 제거를 통하여 아밀로이드 베타 올리고머에 의해 유도되는 신경세포 사멸과 LTP 저하가 감소되며 PDAPP 알츠하이머병 생쥐 모델에서의 기억 감소 역시 복구시킨다. 최근에는 아밀로이드 베타-FcγRIIb 결합을 통한 Phosphoinositide 대사 변화가 타우 단백질의 과인산화와 3x Tg-알츠하이머병 생쥐 모델에서의 기억 감소에 기능한다고 보고되었다. 본 연구에서는 아밀로이드 베타의 신경내 유입을 통한 FcγRIIb 의 새로운 병리적 기능을 밝혔다. 또한 FcγRIIb 의 인산화를 야기하는 Lyn 의 역할 및 가상 스크리닝을 통해 발굴한 잠재적 Lyn 저해제의 효과를 제시하였다.

세포내 아밀로이드 베타는 초기 알츠하이머병 환자의 뇌에서 발견된다. 세포내 아밀로이드 베타를 보이는 몇몇 알츠하이머병 생쥐 모델에서는 심지어 세포외 아밀로이드 침전이 없음에도 기억 감소를 보이기도 한다. 나아가 병리적 아밀로이드 베타의 신경세포간 전파가 신경세포내의 아밀로이드 베타의 축적과 연관되어 있다. 하지만 신경세포내 아밀로이드 베타의 축적과 인접한 신경세포로의 전파에 연관된 분자적 기작은 밝혀지지 않았다. 본 논문의 첫 장에서는 FcγRIIb2 이형이 병리적 아밀로이드 베타의 신경세포내 유입 및 신경세포간 전파에 작용하는 기능을 밝혔다. 아밀로이드 베타 올리고머의 신경세포내 유입이 야생형 생쥐의 신경세포에 비해 FcγRIIb 녹아웃 생쥐의 신경세포에서 감소되어 있다. 3x Tg-알츠하이머 병 생쥐 모델에서의 신경세포내 아밀로이드 베타 및 수용성 아밀로이드 베타가 FcγRIIb의 기능 제거에 의해 감소되었다. 나아가 FcγRIIb의 아밀로이드 베타 유입이 불가능한 돌연변이체를 전뇌특이적으로 발현하였을 때 3x Tg-알츠하이머 병 생쥐 모델에서의 기억 감소가 완화되었다. 신경세포에서 FcγRIIb 전사 이형 2 (FcγRIIb2)의 증대된 발현이 아밀로이드 베타의 유입에 연관되어 있다. 기능성 스크리닝을 통해

동정한 TOM1은 FcγRIIb2에 결합하며 FcγRIIb2에 의한 아밀로이드 베타의 유입을 저해한다. FcγRIIb2를 통한 FcγRIIb의 유입 가속화는 세포질 및 미토콘드리아에서의 아밀로이드 베타를 축적시키며 신경 독성을 야기한다. 마지막으로 서로 연결된 신경세포간의 아밀로이드 베타의 전파가 FcγRIIb2의 제거를 통해 저해됨을 미세역학 기구를 통하여 확인하였다. 이는 세포내 아밀로이드 베타를 조절함으로써 알츠하이머병의 발병에 기능하는 FcγRIIb2 전사 이형의 새로운 기능을 밝힌 것이다.

Lyn은 Src-연관 타이로신 인산화 효소 중 하나로 밝혀졌으며 FcγRIIb를 포함하는 면역 복합체에 결합하는 단백질을 인산화함으로써 면역세포를 저해하는 기능이 보고되었다. 하지만 신경세포에서의 아밀로이드 베타-FcγRIIb 신호체계에서의 연관성은 밝혀지지 않았다. 본 논문의 두 번째 장에서는 Lyn이 FcγRIIb 를 인산화함으로써 아밀로이드 베타에 의한 신경 독성 과정 중에서 기능함을 밝혔다. 아밀로이드 베타 올리고머에 의해 Lyn이 활성화되며 나아가 FcγRIIb 의 타이로신 인산화가 이루어진다. 아밀로이드 베타에 의한 FcγRIIb의 인산화와 신경세포 독성은 Lyn의 감소를 통하여 저해된다. ATP 경쟁적으로 작용하는 Lyn의 잠재적

저해제로써 저분자물질인 KICG2576을 가상 스크리닝을 통하여 동정하였다. Lyn의 인산화효소 도메인의 두 엽 사이의 틈과 KICG2576간의 결합을 공결정 구조를 통하여 확인하였다. 아밀로이드 베타에 의한 FcγRIIb 의 인산화가 KICG2576에 의하여 감소되는 동시에 아밀로이드 베타와 FcγRIIb 에 의한 신경세포 사멸 역시 KICG2576을 통하여 완화되었다. 아밀로이드 베타의 주입에 의한 기억 감소가 KICG2576의 뇌실내 주입을 통하여 개선되었음을 Y자형 미로와 신규물체인식 실험을 통해 확인하였다. 마지막으로 Lyn의 활성이 알츠하이머병 환자의 뇌에서 증가되어 있음을 확인하였다. 정리하자면, Lyn은 아밀로이드 베타에 의한 신경 독성 과정에서 기능하며 본 연구를 통해 알츠하이머병의 발병 과정에서 아밀로이드 베타- FcγRIIb 신경 독성 체계에 대한 이해를 넓힐 수 있었다.

주요어: 알츠하이머병, 아밀로이드 베타, 세포내 아밀로이드 베타, 병리적 단백질의 전파, FcγRIIb2, TOM1, Lyn

학번: 2009-20322